Development and Application of a new Long Path Absorption Photometer (LOPAP) Instrument for the Sensitive Detection of NO$_2$

by
Guillermo Harold Villena Tapia

Wuppertal, May 2012

8]Y¨8]ggYffhUhcb¨_Ubb¨k]Y¨Zc`[hn]h]Yfhk YfXYb.

i fb.bVb.XY.\Vn.(*, !&$%($%&$!%$%' , !(
O\hd.#bVb!fYgc`j]b["XY#ifb#fYgc`jYf'd`3ifb1ifbı ' 5bVbı ' 5XYı ' 5\nı ' 5(*, !&$%($%&$!%$%' , !(O.

To Karen and Emilia

and

To my Parents

Acknowledgements

I would like to express my sincere thanks to Prof. Dr. Peter Wiesen for the opportunity of doing this PhD in his research group and for the support and supervision of this work. Also I would like to thank him the opportunity to participate in different field campaigns, summer schools and workshops around the world.

I want express to special gratitude to PD Dr. Jörg Kleffmann for his scientific supervision, suggestions, constructive criticisms, patience and his tremendous support in all the aspects involved in writing a thesis.

I am grateful to Dr. Ralph Kurtenbach for introducing me to the NO_x analysis techniques and his constant support during my work.

My special thanks to Dr. Iustinian Bejan for his friendship, suggestions and help. I would also like to thank him for his assistance and job during those memorable smog chamber campaigns in the Halle.

Special thanks to Robin Brüning, the "Lord of the stripping coils".

I wish to thank all my colleagues, technical staff and secretary of the Physical Chemistry department family. Special thanks to Dr. Anita Niedojadlo, Ana Mangas and Sebastian Laufs for their friendship, encouragement, help and the great time spent together.

I am deeply grateful to Prof. Dr. Eduardo Lissi and Prof. Dr. María Angélica Rubio for trusting me and encourage me to do my doctoral studies in Wuppertal.

Last but not least, I am grateful to my beloved wife, Karen, for her support and patience during these years. I would like also to thank to my wonderful daughter, Emilia, for bringing me so much happiness to my life and remember me that life is not only science. I would also like to thank my parents, Sole and Guillermo, and my sister Maureen for the continuous support that they have provided me through my entire life.

I finish with a special thank to God.

Contents

List of Figures

1   Abstract

A compact and simple instrument for the sensitive detection of NO_2 in the atmosphere has been developed. NO_2 is sampled in a stripping coil by a selective chemical reaction, converted into a highly absorbing dye, which is detected by long path absorption in a liquid core waveguide. Several interferences were quantified in the laboratory, which so far can all be neglected. The significant interferences against HONO and O_3 were suppressed by using an upstream HONO/O_3-scrubber. The instrument has a detection limit of 2 pptv, an accuracy of 10 % and a precision of 0.5 % for 3 min time resolution. Thus, the new NO_2-LOPAP technique is more sensitive than known commercial NO_2 instruments. The new analyzer is much simpler to apply than other highly sensitive and selective NO_2 methods, e.g. LIF, DOAS, pulsed CRDS or REMPI methods. The new instrument allows an absolute calibration that can be easily performed with liquid nitrite standards, which is a significant advantage over other NO_2 measurement techniques, for which NO_2 calibration gas mixtures are typically necessary. The new instrument has been validated against the chemiluminescence technique during an urban field campaign and against the FTIR technique in a smog chamber under complex photosmog conditions. The data sets exhibit high correlation and excellent agreement.

The instrument was used at an urban field site and direct NO_2 emissions, from engine combustion, were determined. A NO_2/NO_x ratio of (12 ± 1) % was determined, a ratio much higher than 10 years ago. This is explained by high NO_2 emissions from modern diesel vehicles and an increasing diesel vehicle fraction. The ratio is lower than that determined by using a chemiluminescence instrument, which is explained by interferences.

The new NO_2-LOPAP was also used in laboratory studies on the photolysis of nitroaromatic species. In contrast to a recent study on this topic, in which a luminol NO_2 instrument was used, a significant formation of NO_2 was observed besides formation of nitrous acid (HONO). Both applications demonstrate that the use of selective NO_2 instruments is of paramount importance for the quantification and interpretation of NO_2 sources in the atmosphere.

2   Introduction

The atmosphere is a complex photochemical system that surrounds our earth and plays an important role because it affects the environment where we live. The most abundant components close to the Earth´s surface are: nitrogen (N_2) (~78 %), oxygen (O_2) (~21 %), argon (Ar) (~0.9%), and carbon dioxide (CO_2) (~0.04%)[a], which, with the exception of the latter, have very long lifetimes and therefore their concentrations remain almost constant (Brasseur et al., 1999). On the other hand, the concentrations of minor constituents (trace gases), such as ozone (O_3), total reactive nitrogen compounds (NO_y), volatile organic compounds (VOC), and many others, which sum account for only 0.004 % of dry air mass, are changing. These trace gases play a significant role in the chemistry of the atmosphere, determining for example the oxidizing capacity of the atmosphere (Monks, 2005).

Of all the nitrogen present in the atmosphere, N_2 accounts for more than 99.99 %, and nitrous oxide (N_2O) on average constitutes 99 % of the rest (Wallace and Hobbes, 2006). However, in spite of being trace gases, the rest of the nitrogen compounds, i.e. ammonia (NH_3), reactive nitrogen oxides (NO_y), nitrogen oxides ($NO_x = NO + NO_2$), nitric acid (HNO_3), nitrous acid (HONO), the nitrate radical (NO_3), dinitrogen pentoxide (N_2O_5), peroxynitric acid (HNO_4), peroxyacetyl nitrate (PAN), organic nitrates, etc. are very important in atmospheric chemistry. For example, NH_3 is the only basic gas in the atmosphere and nitrogen oxides are of crucial importance for the photochemical formation of ozone in the troposphere and for the formation of acid rain (Seinfeld and Pandis, 2006; Finlayson-Pitts and Pitts, 2000).

2.1   Nitrogen Oxides (NO_x) in the Atmosphere

2.1.1   Tropospheric Chemistry of NO_x

NO and NO_2 are very important species in both stratosphere and troposphere. In the troposphere, NO_2 plays a central role in the formation of ozone (O_3). In an atmosphere

---

[a]   The specified relative abundances in [%] refer to dry air. Since the water content of the atmosphere can vary between 0-3 % the numbers given above also show some variability.

containing only NO, NO$_2$, sunlight and air, i.e. without the presence of organics, the reactions controlling the concentration of O$_3$ are:

(R 1)   NO$_2$ + hv ($\lambda \leq$ 420 nm) $\longrightarrow$ NO + O(^{3}P)

(R 2)   O(^{3}P) + O$_2$ + M $\longrightarrow$ O$_3$ + M

(R 3)   O$_3$ + NO $\longrightarrow$ NO$_2$ + O$_2$.
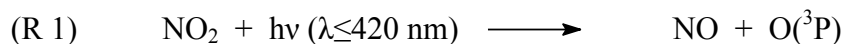
Reactions (R 1) - (R 3) lead to a photo-stationary state between O$_3$, NO, and NO$_2$ and were first proposed by Leighton (1961). This relationship can be expressed by:

$$\text{(Eq. 1)} \qquad \frac{[NO]}{[NO_2]} = \frac{J_{NO_2}}{k_{O_3+NO} \times [O_3]}$$

Where J_{NO_2} denotes the photolysis frequency of NO$_2$ and k_{O_3+NO} denotes the rate constant for the reaction of O$_3$ with NO. The reaction cycle formed by (R 1) - (R 3) does not lead to a net formation of O$_3$. However, in the presence of organic compounds, a net production of O$_3$ is achieved due to the formation of NO$_2$ in the presence of HO$_2$ (hydroperoxyradicals) and/or RO$_2$ (alkylperoxyradicals) through the following reaction:

(R 4)   HO$_2$/RO$_2$ + NO $\longrightarrow$ OH/RO + NO$_2$.

By reaction (R 4) NO$_2$ is formed from NO without a loss of O$_3$ by reaction (R 3). Thus, the subsequent photolysis of NO$_2$ (R 1) leads to net production of O$_3$ through (R 2) (Seinfeld and Pandis, 2006; Finlayson-Pitts and Pitts, 2000; Holloway and Wayne, 2010).

NO$_2$ affects the oxidation capacity of the atmosphere through its direct participation in the formation of O$_3$ and nitrous acid (HONO), which through their photolysis are major sources of the OH radical, the detergent of the atmosphere (see Fig. 1).

A complete picture of the different processes in which NO$_2$ is involved is shown in Fig. 2, where it can be observed that by its reaction with the OH radical, NO$_2$ also limits radical concentrations in the polluted atmosphere. NO$_2$ also contributes to acid precipitation and formation of other atmospheric oxidants such as the nitrate radical, NO$_3$ (Crutzen, 1979; Finlayson-Pitts and Pitts, 2000; Seinfeld and Pandis, 2006).
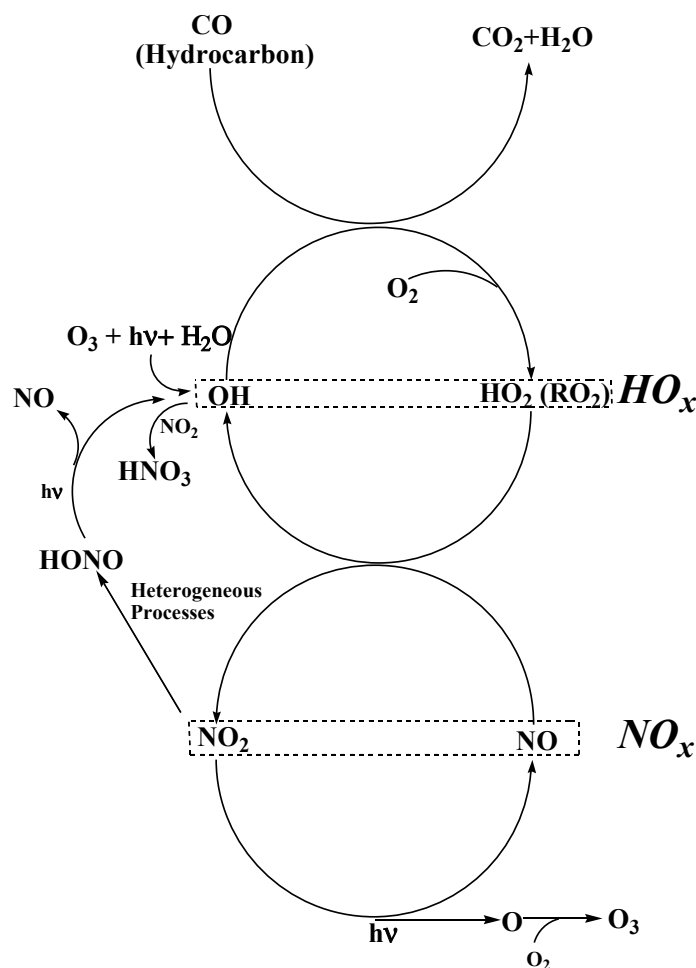
Fig. 1:   Ozone formation in the troposphere (HO_x-NO_x cycles) (Platt and Stutz, 2008).

NO_2 is also involved in the formation of peroxyacyl nitrates (PANs, $RC(O)OONO_2$), also known as peroxycarboxylic nitric anhydrides (Roberts, 2007), which are typical photochemical secondary pollutants and are part of organic nitrates formed in the atmosphere. The most abundant organic nitrate in the atmosphere is peroxyacetyl nitrate (PAN), which is formed through reactions (R 5)-(R 7) (Finlayson and Pitts, 2000):

(R 5) $CH_3CHO + OH$ $\longrightarrow$ $CH_3CO\bullet + H_2O$,

(R 6) $CH_3CO\bullet + O_2 + M$ $\longrightarrow$ $CH_3C(O)OO\bullet + M$,

(R 7) $CH_3C(O)OO\bullet + NO_2 + M$ $\rightleftharpoons$ $CH_3C(O)OONO_2 + M$,

where $CH_3CO\bullet$ is an acetyl radical and $CH_3C(O)OO\bullet$ is a peroxyacetyl radical whose general formula is $RC(O)OO\bullet$. The concentration of PAN is controlled by thermal decomposition,

which is strongly temperature dependent (Roberts and Bertman, 1992). Thus, PAN can provide an effective sink of NO_x at cold temperatures and high solar zenith angles. Its lifetime is long enough at low temperatures so that it can be transported long distances (depending on meteorological conditions) before decomposing to release NO_2, which can participate in O_3 formation in remote regions far away from the original source of NO_x (EPA, 2008). In Fig. 2, the many interactions of NO_2 in the troposphere are depicted.
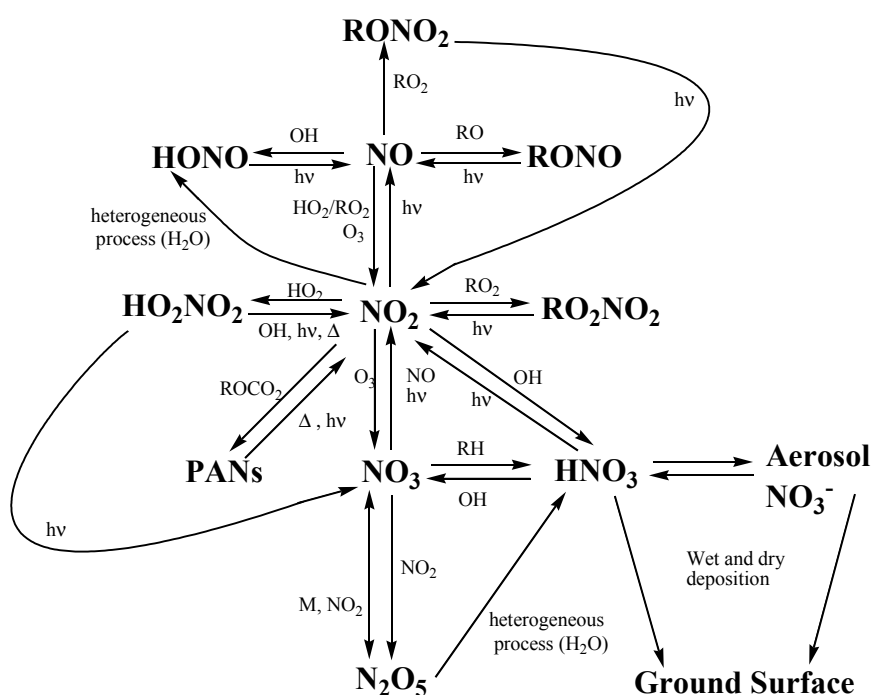
Fig. 2: Schematic diagram of reactive nitrogen compounds in the troposphere. Adapted from Brasseur et. al., 1999; Warneck, 2000; Möller, 2010.

The range of NO_2 concentrations varies from few pptv in remote areas to more than 100 ppbv in polluted regions (Finlayson-Pitts and Pitts, 2000). Thus, for example, Elshorbany et al. (2009), informed diurnal profiles of NO_2 with peaks of $\sim$ 100 ppbv during the day in the framework of a field campaign carried out in Santiago de Chile in 2005. On the other hand concentrations as low as ~2 pptv were reported by Jones et al. (2011) during a CHABLIS field campaign in coastal Antarctica in 2004-2005.

2.1.2   Sources of Nitrogen Oxides

Nitrogen oxides are important trace species that are emitted into the atmosphere from both, natural and anthropogenic sources, the latter being dominated by fossil fuel combustion and industrial processes (see Tab. 1) (IPCC, 2007). In Europe road transport reaches 40 % of the anthropogenic emissions of NO_x (Vestreng et al., 2009 and references therein), which are mainly emitted as NO and only a smaller portion as NO_2 (5-25 % average NO_2/NO_x, Carslaw and Beevers, 2005a).

Tab. 1:   Global sources (TgN yr^{-1}) of NO_x (taken from IPCC 2007)

Source	Emissions [TgN/yr]
Anthropogenic sources	
Fossil fuel combustion & industrial processes	25.6
Agriculture	1.6
Biomass and biofuel burning	5.9
Atmospheric deposition	0.3
Natural sources	
Soils under natural vegetation	7.3
Lightning	1.1-6.4
Total sources	**42-47**

2.1.3   Formation of NO_x in Combustion Processes

NO_x can be formed in combustion of fossil fuels by three main processes: *thermal-NO* and *prompt-NO* mechanisms, which produce NO_x by the high temperature oxidation of elemental nitrogen present in the combustion air, and finally the *fuel-NO* mechanism where NO is formed from nitrogen chemically bound in certain fuels (Dean and Bozzelli, 2000; AQEG, 2004).

2.1.3.1 Thermal NO Mechanism (Zeldovich NO):

This process involves the oxidation of atmospheric N_2 by O_2 at high temperature and pressure, through the following mechanism proposed by Zeldovich et al. in 1946 (Flanagan and Seinfeld, 1988):

(R 8) $O_2 + M$ $\rightleftharpoons$ $2O + M$

(R 9) $N_2 + O$ $\rightleftharpoons$ $NO + N$

(R 10) $N + O_2$ $\rightleftharpoons$ $NO + O$

(R 11) $N + OH$ $\rightleftharpoons$ $NO + H$

The name "thermal" is used, because reaction (R 9) has a very high activation energy due to the strong triple bond in the N_2 molecule and is only fast when the temperature is sufficiently high (>2000 K) to break the triple bond and also, as consequence of this high temperature, the concentration of oxygen atoms in the flame is very high (Lissianski et al., 2000; Dean and Bozzelli, 2000; Warnatz et al., 2006). Thus, reaction (R 9) is the rate limiting step in the mechanism and due to the energy requirements and the presence of O atoms *thermal NO* is formed mostly in the flame regions with highest temperatures and under fuel-lean conditions.

2.1.3.2 Prompt NO Mechanisms (Fenimore NO):

This process is closely related to the formation of the CH radical in fuel rich zone. This mechanism was first described by Fenimore in 1971 (Eckert and Rakowski, 2012) who measured nitric oxide in a flame front where the concentration of hydrocarbon radicals is larger. The mechanism is initiated by the reaction of CH radicals with N_2:

(R 12) $CH + N_2$ $\rightleftharpoons$ $HCN + N$

the nitrogen atom (N) formed can produce an NO molecule through reactions (R 10) and (R 11), while hydrocyanic acid (HCN) can lead to a new NO molecule through a series of radical reactions, where for example isocyanate radical (NCO), cyanonitrene diradical (NCN) and imidogen (NH) are formed (see Fig. 3 for more details; Miller and Bowman, 1989; Dean and Bozzelli, 2000; Warnatz et al., 2006; Eckert and Rakowski, 2012).

Under lean flame conditions the amount of NO formed by the prompt NO mechanism is small compared with the amount formed by the thermal NO due to the lower abundance of CH

radicals in the flame. However, it makes an important contribution under fuel-rich conditions when higher concentrations of hydrocarbon radical species like CH are present (AQEG, 2004).

Fig. 3:   Reaction path diagram illustrating the major steps in prompt NO formation and conversion of fuel nitrogen to NO. The bold lines represent the most important reaction paths (adapted from Miller and Bowman, 1989; Sutton and Fleming, 2008).

2.1.3.3   *Fuel-Bound Nitrogen NO Mechanism:*

The conversion of fuel-bound nitrogen to NO is mainly observed in coal combustion, which contains 0.5 - 2 % nitrogen by weight, chemically bound in large heterocyclic compounds, with pyridine and pyrrole-type structures and aromatic amines (AQEG, 2004 and references therein). Fuel NO can reach 50 % of the NO production in coal combustion (McAllister et al., 2011). When the coal is heated, some of the nitrogen compounds are released into the gas phase and small nitrogen compounds such as hydrocyanic acid (HCN), cyano radicals (CN) and ammonia (NH_3) (Miller and Bowman, 1989; AQEG, 2004) are formed. The further

conversion of these species takes place through the reaction with small gas-phase radicals (O, OH, H) in accordance with mechanisms indicated in Fig. 3.

However, this mechanism does not play any role in engine combustion, because fuels for internal combustion engines contain negligible amounts of nitrogen, for example diesel has less than 0.05 % nitrogen (AQEG, 2004).

2.1.3.4 Formation of NO_2 in Combustion:

Generally is assumed that only 5 % of the NO_x released from combustion exhaust is in the form of NO_2. However, despite this low ratio, it is important to understand the mechanism of formation and removal of NO_2 in the engine. In the low temperatures regions of the flame (between 600-1000 K), and under fuel-lean conditions, NO_2 is formed through the following reaction:

(R 13) $\qquad HO_2 + NO \quad \rightleftharpoons \quad NO_2 + OH.$
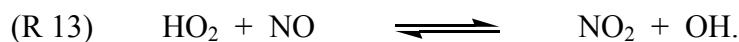
Since the rate of this reaction depends on the HO_2 concentration, NO_2 formation is sensitive to reactions forming and removing HO_2. At higher temperatures HO_2 dissociates quickly into H atoms and O_2, and the higher prevailing concentrations of H, O, and OH lead to more rapid NO_2 loss by:

(R 14) $\qquad NO_2 + O \quad \rightleftharpoons \quad NO + O_2$

(R 15) $\qquad NO_2 + H \quad \rightleftharpoons \quad NO + OH$

(R 16) $\qquad NO_2 + OH \quad \rightleftharpoons \quad NO + HO_2.$

Hence, in combustion systems that are well-mixed, i.e. spark-ignition engines (gasoline engines); most of the NO_x remains as NO. However, in diesel engines, where the fuel is injected to the cylinder just before combustion starts, there is a nonuniform burned gas temperature and composition due to the nonuniform fuel distribution during combustion, and there are cooler regions in the cylinder, which quench the conversion of NO_2 back to NO (Heywood, 1988; AQEG, 2004). As a consequence diesel engines emit more NO_2 than gasoline engines.

In addition, the use of oxidation catalysts in diesel engines also increases the content of NO_2 in the exhaust gas (Wurzenberger and Tatschl, 2012).

2.1.4   Control of NO$_x$ Emissions from Combustion

As the main source of NO$_x$ emission, are coming from road transport (Vestreng et al., 2009) the methods given in this section focus on those control techniques related with internal combustion engines, which use either diesel or gasoline.

Control of NO$_x$ emissions can be performed using two strategies: the first one is controlling the combustion conditions in the engine and the second one is with post combustion treatment.

2.1.4.1   *Combustion Modification:*

The aim is to reduce NO$_x$ emissions, where they are formed. In the case of low-nitrogen fuels (diesel, gasoline and natural gas), the thermal NO production is the main mechanism for NO$_x$ formation and the control is done by reducing the temperature of the combustion and the residence time. Thus, control over the combustion entails manipulating the mixing of fuel and air in order to affect the temperature and fuel/air ratio in the engine (Lissianski et al., 2000).

2.1.4.2   *Post Combustion Treatment*

Post combustion treatments are based on the application of different control techniques to the exhaust gases that are coming from the engine itself.

One of the techniques used in is the so-called *"exhaust gas recirculation" (EGR)* in which a fraction of the exhaust gas is recycled through a control valve from the exhaust to the engine intake system, where it is mixed with fresh fuel-air mixture. The effect of this recirculation is to reduce the peak flame temperature and as a consequence the rate of NO formation is also reduced (thermal NO) due to EGR gases act as a diluent (AQEG, 2004).

Three-way catalyst promotes the oxidation of carbon monoxide (CO) and hydrocarbons (HC) to CO_2 and H_2O, and simultaneously, nitrogen oxide (NO) are reduced to N_2. The surface where the catalytic process takes place contains platinum (Pt), palladium (Pd) and rodhium (Rh) with some alumina as a supported material (Heywood, 1988; AQEG, 2004). This kind of catalytic converter is efficient under fuel/air ratios close to the stoichiometric conditions, i.e. for vehicles with gasoline engines. In the case of diesel engines "diesel oxidation catalyst" is used, which oxidizes carbon monoxide and unburned hydrocarbons, and oxidizes nitrogen monoxide (NO) to nitrogen dioxide (NO$_2$) (Wurzenberger and Tatschl, 2012).

Selective catalytic reduction (SCR) systems are used in diesel vehicles for NO$_x$ reduction. The principle is based on the injection of urea ((NH_2)$_2$CO) into the exhaust, upstream of the

catalyst bed layers, where N_2 is produced. The most common catalyst used is vanadium pentoxide (V_2O_5) supported on titanium dioxide (TiO_2) (Schnelle and Brown, 2002; AQEG, 2004). Reactions involved are:

(R 17) $(NH_2)_2CO + H_2O \rightleftharpoons 2\,NH_3 + CO_2$

(R 18) $4\,NO + 4\,NH_3 + O_2 \rightleftharpoons 4\,N_2 + 6\,H_2O$

(R 19) $2\,NO_2 + 4\,NH_3 + O_2 \rightleftharpoons 3\,N_2 + 6\,H_2O.$
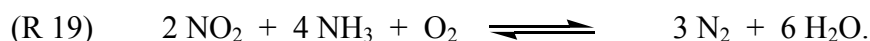
2.1.5   Health Effects and Legislative Frameworks for NO_2

The health effects of a specific pollutant are studied by epidemiologic, human clinical, and animal toxicological investigations. It has been shown in such studies that NO_2 has health impacts on both, short term and long-term exposures of the population.

2.1.5.1   Effects of Short Term Exposure

Epidemiologic evidence that NO_2 is associated with adverse effects on the respiratory system, has been supported by animal toxicologic and human clinical studies, which has been carried out within the range of maximum ambient concentrations observed in epidemiologic studies (100-300 ppbv). The observed effects are related with an increase of the risk of susceptibility to viral and bacterial infections, airway hyperresponsiveness, lung functions decrements, inflammation, and aggravation of asthma effects after NO_2 exposures (EPA, 2008; and references therein).

The evidences of cardiovascular and mortality effects of short terms exposure are weak and can not be used for inferring a relationship with NO_2. Thus, as an example, Peters et al. (2000) found that association of ventricular arrhythmias with other pollutants are similar or even stronger than with NO_2.

2.1.5.2   Effects of Long Term Exposure

Long term exposure to NO_2 is associated to deficits in lung function growth, which reduce maximum lung size and subsequently this fact may increase the risk in adulthood for chronic respiratory disease (Gauderman et al., 2004; Oftedal et al., 2008).

Nyberg et al. (2000) and Nafstad et al. (2003) have shown, through epidemiologic studies, that there is a positive association between long term NO_2 exposure and incidence of lung

cancer. However, animal toxicological studies have not provided clear evidence that NO_2 act directly as a carcinogen (EPA, 2008). But even though there is no direct evidence that NO_2 is a carcinogen, NO_2 is precursor of nitrous acid (HONO) which either can form carcinogenic nitrosamines (Pitts et al., 1978) or DNA-DNA cross-links (Harwood et al., 2000).

It is important to note that it is difficult to separate NO_2 health effects from other pollutants such as particulate matter or any other pollutant not measured (Samoli et al., 2006; Delfino et al., 2008; Mol et al., 2008). In addition, the instrumentation used in all these health studies may be affected by the non-selective detection of NO_2 for the techniques applied, which may lead to wrong conclusions (Spicer et al., 2001; Brunekreef, 2001; Van Strien et al., 2004; Jarvis et al., 2005).

Based on these health effects, the European Union (EU), during the last two decades set different legislative frameworks in order to assess and manage air quality and to control the pollutants released in vehicle exhaust, e.g. *EU Directives 96/62/EC, 98/69/EC, 99/96/EC* and *99/30/EC (First Daughter Directive)*. European NO_x emissions linked to road transport have strongly decreased during the last 20 years by approximately 40 % (Williams and Carslaw, 2011) due to the introduction of the three-way catalyst at the beginning of the 1990s (AQEG, 2004). However, unexpectedly, in many European cities NO_2 is not showing the same tendency, either NO_2 levels are constant or even show a small increase (EEA, 2007; Vestreng et al., 2009; Carslaw et al., 2011a). EU Directive *99/30/EC* set two limits on ambient concentration of NO_2, which must be achieved since 2010: an annual mean limit of 40 $\mu g/m^3$ and an hourly limit of 200 $\mu g/m^3$ that must not be exceeded more than 18 hours a year (Carslaw et al., 2007). However, for European urban network stations it has been difficult to meet the annual mean limit value for NO_2 (Carslaw et al., 2007; Carslaw et al., 2011a). The reasons for this NO_2 behaviour can be explained in terms of secondary formation in the atmosphere and by increasing primary NO_2 emissions particularly close to roads where exceedances of the annual mean limit value of NO_2 are more probably (Carslaw, 2005; Carslaw et al., 2011b). The former can be explained in terms of the increase of the background level of O_3 (Wang et al., 2009), which reacts with NO emitted to the atmosphere mainly from combustion processes related to road transport. The latter is due to increasing number of diesel cars and the introduction of new exhaust technologies, which oxidize a portion of NO to NO_2 in order to promote the oxidation of soot collected on the particle filter (Grice et al., 2009). Due to this increase of primary NO_2 emissions many studies have been focused on its impact on air quality in the urban environment (Carslaw and Beevers, 2004;

2005a; 2005b; Carslaw, 2005; AQEG, 2007; Carslaw et al., 2007; Carslaw and Carslaw, 2007; Jenkin et al., 2008; Alvarez et al., 2008; Keuken et al., 2009; Kurtenbach et al., 2009; 2012).

2.2   Measurement Methods

Due to its importance in atmospheric chemistry and air quality, many direct or indirect techniques have been developed for measuring NO_2 in the laboratory and/or in the field. In this section some of the techniques used for NO_2 measurements will be described.

2.2.1   Spectroscopic Methods

2.2.1.1 Differential Optical Absorption Spectroscopy (DOAS)

The differential optical absorption spectrometer (DOAS) technique was pioneered, in the late 1970s, by Platt and Perner and until now has been used in many field campaigns for the measurements of different molecules, among them NO_2 (e.g. Platt et al., 1979; Biermann et al., 1988; Harder et al., 1997; Dunlea et al., 2007). The technique is based on the absorption of electromagnetic radiation, by trace gases and can be expressed by the Lambert-Beer Law:

(Eq. 2) $I(\lambda) = I_0(\lambda) \times \exp(-L \times \sigma(\lambda) \times c)$,

where $I_0(\lambda)$ corresponds to the initial intensity emitted by a source of radiation (natural or artificial), $I(\lambda)$ is the intensity of the radiation after passing through the air with an optical path length L, where the molecules to be measured are present at the concentration c; $\sigma(\lambda)$ denotes the absorption cross section of the molecule to be measured, which depends on the wavelength λ.

However, because of the wide range of both, gases and particles that are present in ambient air, which lead to light scattering (Rayleigh and Mie) and absorption, it is difficult to measure the original unattenuated atmospheric spectrum I_0. Thus, the so-called *differential absorption* is used, where I'_0 is calculated based on measuring the difference between the absorbance at some wavelength, where the species of interest has a sufficiently narrow absorption peak, and another wavelength on either side of the peak. (Eq. 2) can be rewritten as:

(Eq. 3) $\ln\left(I'_0(\lambda)/I(\lambda)\right) = L \times \sum_{i=1}^{n} \sigma'_i(\lambda) \times c_i$,

where the absorption is summed over all species i and $\sigma'_i(\lambda)$ corresponds to the differential absorption cross section (Finlayson-Pitts and Pitts, 2000; Platt, 1994; Plane and Smith, 1995; Plane and Saiz-Lopez, 2006). The main advantages of this system are its ability to detect absolute trace gas concentrations without calibration if the absorption cross sections and the optical path length are known (Stutz and Platt, 1997) and its capability to allow simultaneous detection of multiple absorbing species (Gherman et al., 2008). However, since the absorbance is integrated over long and open paths, interpretation of DOAS data becomes difficult when the air masses are inhomogeneous and rapidly changing (Osthoff et al., 2006). Several detection limits have been reported, however they will depend on the path length and the absorption cross section used. Detection limits as low as 55 pptv have been reported for 5 min integration time (Harder et al., 1997).

2.2.1.2 *Cavity Ring-Down Spectroscopy (CRDS)*

Cavity Ring Down Spectroscopy covers those absorption techniques that use high-finesse cavities, i.e. stable optical resonators with high reflectivity mirrors to achieve long sample absorption path lengths and high sensitivities (Brown, 2003; Langridge et al., 2008). Different schemes have been used including Cavity Ring Down Spectroscopy (CRDS) (Mazurenka et al., 2003; Hargrove et al., 2006; Osthoff et al., 2006; Fuchs et al., 2009; 2010), Cavity Enhanced Absorption Spectroscopy (CEAS) (Langridge et al., 2008), Incoherent Broad Band Cavity Enhanced Absorption Spectroscopy (IBBCEAS) (Gherman et al., 2008; Wu et al., 2009; Fuchs et al., 2010), and Cavity Attenuated Phase shift Spectroscopy (CAPS) (Kebabian et al., 2005; 2008).

In CRDS in particular, the absorption path length of a pulsed laser through an absorbing sample is made very long by trapping the pulse between the mirrors of a high-finesse (low-loss) optical cavity containing the sample. Instead of measuring the total intensity of the light exiting the cavity, the decay time is determined by measuring the time dependence of the light leaking out of the cavity. The decay time inversely depends on absorption of the sample (Berden et al., 2000). The effective absorption path length can be several kilometres, so very small concentrations of chemical species can be detected, being limited mainly by the cavity mirror reflectivity and scattering losses. With this technique only a small gas volume is required due to small diameters of CRDS cells of only a few millimetres to centimetres. (Vasudev et al., 1999).

Instruments based on cavity ring-down spectroscopy and related techniques have the advantage of both long effective path lengths and a compact sample volume for in situ sampling (Osthoff et al., 2006). However, they have not yet reached detection limits for NO_2 like those obtained with Tunable Diode Laser Absorption Spectroscopy (TDLAS) and chemiluminescence techniques. For example, Gherman et al. (2008) obtained a detection limit of 300 pptv for 10 min integration with IBBCEAS, while Fuchs et al. (2010) reported a detection limit of 80 pptv for 10 seconds with a CRDS instrument.

2.2.1.3 *Laser Induced Fluorescence (LIF)*

Laser induced fluorescence (LIF) is a direct spectroscopic technique where the molecules of interest are selectively excited to one of their molecular transitions, using a narrow band laser. The number of fluorescence photons detected is then proportional to the atmospheric trace gas concentration (Thornton et al., 2000). LIF is based on fluorescence assay by gas expansion (FAGE) and the excitation of the target molecule with the second harmonic of a Nd:YAG laser at 532 nm (in the case of NO_2). The low pressure in the gas expansion leads to reduction of collisional quenching and to increasing fluorescence times of the molecule of interest (George and O´Brien, 1991; Matsumi et al., 2001). The shortcomings of the FAGE technique are the low signals for the lower trace gas concentrations obtained due to the pressure reduction in the cell and the use of fixed frequency laser sources which may lead to interferences of molecules that absorb at the same wavelength than NO_2 (Fong and Brune, 1997). These difficulties were overcome using a high resolution tunable dye laser, exciting the NO_2 sample at two wavelengths alternatively around 564 nm, corresponding to the peak and bottom positions of the absorption cross-section spectrum of NO_2, avoiding the interference of fluorescent species other than NO_2, reaching a detection limit of ca. 1 ppbv in 10 s (Fong and Brune, 1997; Matsumoto et al., 2001). During the last ten years, several light sources have been tested and several field campaigns have been carried out using LIF instruments (Thornton et al., 2000; 2003; Matsumoto et al., 2001; 2006; Dari-Salisburgo et al., 2009; Fuchs et al., 2010) reaching good sensitivities as good as 10 pptv/10 s (Day et al., 2002). However, LIF requires complex systems and highly skilled operators (Schiff, 1992).

2.2.1.4 *Resonance Enhanced MultiPhoton Ionization-Mass Spectrometry (REMPI-MS)*

Resonance enhanced multiphoton ionization is a technique that so far is in developing state and combines laser spectroscopy with mass spectrometry. A laser-induced process is used to

produce the ions, which are needed for mass spectrometry, where the resonant intermediate states formed in the first step, enhance the ionization process. McKeachie et al. (2001) used a two-color method for the selective detection of NO_2, i.e. the wavelengths involved in the different steps were not the same. Detection limit as low as 5 pptv has been reached by Garnica et al. (2000) and 20 pptv by McKeachie et al. (2001), the difference between the system is that the latter used tunable broad-bandwidth laser radiation for the detection of NO_2. The main disadvantage of this technique is the cost of the complex system components together with the difficulties to deploy the instrument in the field.

2.2.1.5 *Fourier Transform Infrared Spectroscopy (FTIR)*

Another possibility for the detection of NO_2 is Fourier Transform Infrared Spectroscopy (FTIR), which is an optical technique based on infrared absorption by the gas molecules due to vibrational-rotational transitions (Fried and Richter, 2006). Infrared light is absorbed only when the electric dipole moment of a molecule changes. The pattern of these absorptions for a molecule, i.e. the IR spectrum, is generally unique for a particular compound. Since the spectral absorbance is directly proportional to the amount of sample present (Lambert Beer´s Law), IR spectra can also be used to make quantitative determinations of the amount of individual components in a sample mixture (McKelvy, 2000).

A major advantage of the FTIR technique is its ability for multicomponent analysis of gaseous samples. On the other hand, FTIR cannot always provide the high resolution required to avoid interference between species, particularly at wavelengths where the ubiquitous water vapour and carbon dioxide have their maximum absorptions. In addition, the sensitivity of the FTIR technique is frequently insufficient to measure most species in relatively clean air (Schiff et al., 1994). Even using very long optical path lengths, detection limits for NO_2 only in the low ppbv range have been reached (Mentel et al., 1996).

The FTIR technique has been used for NO_2 detection in smog chambers studies (Mentel et al., 1996; Ramazan et al., 2004); as well as in atmospheric monitoring with an open-path configuration (Burling et al., 2010).

2.2.1.6 *Tunable Diode Laser Absorption Spectroscopy (TDLAS)*

Another technique used for NO_2 detection, based on infrared absorption, is tunable diode laser spectrometry which has much higher optical resolution and sensitivity than FTIR (Schiff, 1992). The difference to FTIR is the use of a tunable diode laser of very narrow line-width,

which allows NO_2 detection at specific rotational-vibrational transition. The composition of the laser determines the frequency of the emitted radiation. In the middle infrared region, lead salts alloyed with group IV-VI elements, e.g. tin (Sn), tellurium (Te), sulphur (S) and selenium (Se) are generally used (Schiff et al., 1994). Tuning of the emitted wavelength can be done by either changing the temperature or the forward current of the diode (Schiff, 1992; Finlayson-Pitts and Pitts, 2000). Open long path (Nelson et al., 1998; Jimenez et al., 2000) and long path multipass absorption cells (Gregory et al., 1990; Schiff et al., 1990; Fehsenfeld et al., 1990; Li et al., 2004; Horii et al., 2004; Herndon et al., 2004; Dunlea et al., 2007) have been used as configuration in order to permit a sensitive detection. The former can only be applied to small molecules such as CO, NO_2, N_2O, NH_3, CH_2O, and other small-molecule hydrocarbons (Nelson et al., 1998), since at atmospheric pressure the rotational and vibrational lines get broader and the identification of specific lines is more difficult. In the case of TDLAS systems with absorption cells it is important to remark that they operate at reduced pressures in order to minimize rotational line broadening, decreasing the sensitivity and, at the same time, decrease the probability of interferences between atmospheric gases (Schiff et al., 1983; Schiff, 1992). Detection limits as low as 30 pptv/min have been reached for NO_2 (Li et al., 2004).

2.2.2 Chemiluminescence Methods

2.2.2.1 *Luminol Chemiluminescence*

A commonly used technique for the detection of NO_2 in the atmosphere is the luminol-chemiluminescence method, which employs the reaction between NO_2 and an alkaline solution of luminol resulting in light emission (Wendel et al., 1983). In this technique, the air sampled is drawn through the instrument by a vacuum pump and flows across a fabric wick that is saturated with a specially formulated luminol (5-amino-2,3-dihydro-1,4-phthalazine-dione) solution. When NO_2 encounters the wick, the luminol is oxidized leading to an excited aromatic species that produces chemiluminescence (in the region of 465 nm) (R 20). A photomultiplier tube (PMT) measures the light intensity and converts it into a signal which is proportional to the concentration of NO_2.

(R 20)
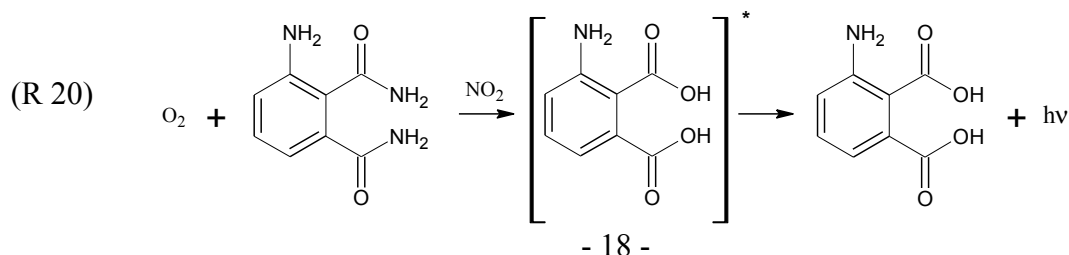
This technique is direct, but it is non-specific for NO_2 because ozone and peroxyacylnitrates (PANs) are also detected (Fehsenfeld et al., 1990). Another disadvantage of this technique is the non-linear response below a few ppbv (Kelly et al., 1990) and at high NO_2 levels. In addition, ppmv levels of NO and hydrocarbons lead to quenching of the excited aromatic species and to reduced sensitivity against NO_2 (Kleffmann et al., 2004; Bejan et al., 2006b).

2.2.2.2 *NO based Chemiluminescence Techniques*

The most widely used chemiluminescence technique is based on the gas phase reaction between NO and O_3 forming an electronically excited molecule of NO_2^* that emits light, which is proportional to the NO concentration.

(R 21) $NO + O_3 \longrightarrow NO_2^* + O_2$

(R 22) $NO_2^* \longrightarrow NO_2 + h\nu$

(R 23) $NO_2^* + M \longrightarrow NO_2 + M$

To detect also NO_2, either heated (300-350 °C) molybdenum (Mo) surfaces (Fontjin et al., 1970; Ridley and Howlett, 1974) or photolytic NO_2 converters (Kley and McFarland, 1980) are applied.

a) *Thermal Converters*

The reduction of NO_2 to NO by heated Mo converters (R 24) followed by ozone reaction is the reference method recommended by the US EPA (Demerjian, 2000) and by the European legislation (European Standard, EN 14211, 2005):

(R 24) $Mo + 3\ NO_2 \longrightarrow MoO_3 + 3\ NO,$
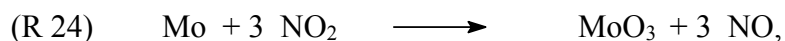
but is affected by significant interferences against other reactive nitrogen species (NO_y) like N_2O_5, HONO, HNO_3, PAN, etc., which are also reduced to NO (Winer et al., 1974; Dunlea et al., 2007).

As an example of these interferences, Fig. 4a shows the campaign averaged diurnal profiles of NO_2 obtained by DOAS and a chemiluminescence instrument with molybdenum converter (TELEDYNE MO) from a two week field campaign in 2005 in Santiago de Chile (Elshorbany et al., 2009). There is a clear difference between the results from both instruments with lower concentrations of the DOAS compared to the chemiluminescence instrument. While during the night, both data sets differ by only ~5-10 ppbv, the chemiluminescence instrument shows

positive interferences of up to ~25 ppbv during daytime. On a relative basis, NO_2 is overestimated by up to a factor of four during daytime (see Fig. 4a). Interestingly, the difference between both instruments correlates quite well with the concentration of ozone (see Fig. 4a and b). Ozone may be used here as an indicator for the photo-chemical activity of the atmosphere. Since most NO_y species, such as nitric acid (HNO_3), peroxyacetyl nitrate (PAN), and organic nitrates ($RONO_2$), are photo-chemically formed during daytime and since all NO_y species, which enter the molybdenum converter, are quantitatively measured by this technique (Winer et al., 1974; Steinbacher et al., 2006; Dunlea et al., 2007), the observed differences are due to NO_y interferences of the chemiluminescence instrument. PAN and HONO were the only measured NO_y species during the campaign. Subtraction of their concentrations from the observed interference (see "corr. NO_2-interference", Fig. 4b) showed that the night-time differences of both instruments could be mainly attributed to interference of the chemiluminescence instrument by HONO. However, during daytime there were still significant, not quantified NO_y-interferences, which correlated well with the concentration of ozone (see Fig. 4b).
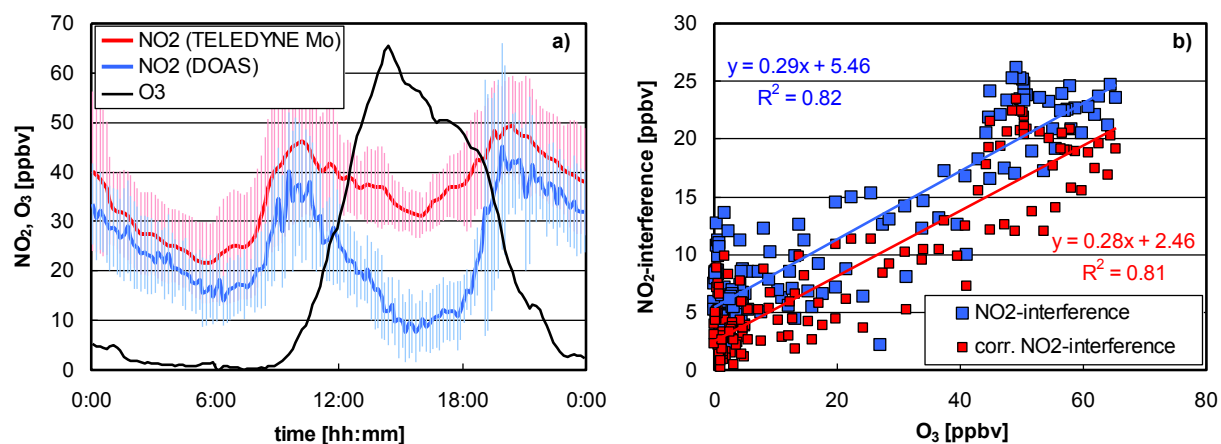
Fig. 4: a) Campaign averaged NO_2 and O_3 diurnal profiles in Santiago de Chile, 2005 (Elshorbany et al., 2009). The error bars show the 1σ error of the average of all 10 min NO_2 data. The spectroscopic DOAS technique was used as a reference in this campaign. b) Correlation of the NO_2-interference of the chemiluminescence instrument, i.e. difference NO_2 (TELEDYNE Mo) - NO_2 (DOAS), with the ozone concentration. In addition, the NO_2-interference, which was corrected for the HONO and PAN interferences of the chemiluminescence instrument, is also shown ("corr. NO_2-interference").

b) Photolytic Converters

The conversion of NO_2 into NO by photolytic converters, for which either Xenon lamps or UV emitting diodes ("blue light converters") are used (R 25), are much more selective, although positive interferences by photolysis of HONO for the Xenon lamp converter instruments (Rohrer et al., 2005) and negative interferences in the presence of hydrocarbons have been reported (Kurtenbach et al., 2001; Kleffmann et al., 2001; Bejan et al., 2006b; Villena et al., 2012).

$$(R\ 25) \qquad NO_2\ +\ h\upsilon \qquad \longrightarrow \qquad NO\ +\ O(^3P)$$
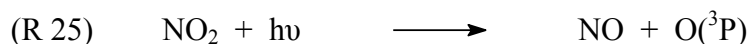
As an example of these negative interferences, Fig. 5 shows the diurnal variation of NO and NO_2 concentrations in the Kiesberg tunnel during a campaign in 1999 (Kurtenbach et al., 2001), in which a chemiluminescence instrument with photolytic NO_2 converter (ECO) was compared with a DOAS instrument.
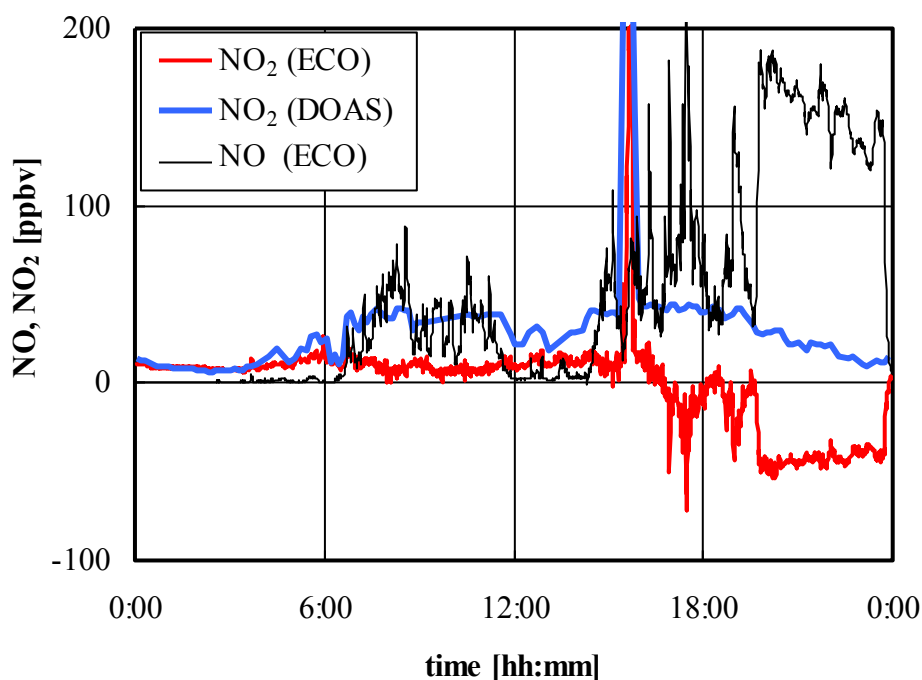
Fig. 5: NO_2 diurnal profiles measured with DOAS and a chemiluminescence instrument with photolytic NO_2 converter (ECO) in a tunnel study (Kurtenbach et al., 2001).

Both NO_2 data sets exhibit excellent agreement for measurements at low pollution levels during night-time (see Fig. 5 0:00-4:00 LT). However, with the onset of elevated volumes of traffic through the tunnel, the NO_2 measurements of the ECO instrument exhibited strong

negative interferences. Remarkable are the artificial negative concentrations measured by the ECO-Physics instrument during the early night at high pollution levels as indicated by the high NO concentrations also shown in Fig. 5.

In addition to the negative interferences, photolytic converter instruments exhibit non linear response for high NO_2 and O_3 levels caused by the reaction NO with O_3 in the converter. Finally, all NO/O_3 chemiluminescence instruments show a negative H_2O interference by quenching of the excited NO_2^* during the NO detection.

2.2.3 NO_2 Detection using Griess-Saltzman-type Reagents

During the 1960s and 1970s, one of the most used analytical methods for the determination of NO_2 was the colorimetric detection using the Griess-Saltzman reagent, where a dye compound is formed and the color intensity, which is directly proportional to the NO_2 concentration, is measured in a photometer.

Peter Griess discovered diazo compounds in 1858 and this was the starting point of the chemistry of azodyes (Ivanov, 2004). Based on his experience with azo compounds, Griess proposed in 1879 the use of sulphanilic acid, α-naphthylamine, in a sulphuric acid solution (H_2SO_4) for identification of nitrites (NO_2^-) in water, through the formation of an azodye compound (Griess, 1879). In 1889, Lajos Ilosvay did the first modification to the method, changing sulphuric acid by acetic acid (CH_3COOH) for the preparation of the reactants, being the reaction much faster and sensitive (Treadwell and Hall, 1955). Since then this reagent is also commonly known as Griess-Ilosvay reagent. Thus, the diazotization of sulphanilic acid by the available nitrite in the absorbing solution, using α-naphthylamine as a coupling agent, continued throughout the years being used just for nitrite determination.

The first time that Griess-Ilosvay reagent was used for a quantitative determination of nitrogen oxide was in a work published by Bennett in 1929, in the framework of impurities determination of nitrous oxide used for anaesthesia. In that opportunity NO_2 was first absorbed in a sodium hydroxide (NaOH) solution and the nitrite formed was mixed with the Griess-Ilosvay reagent. The first published method for the use of the combined Griess-Ilosvay reagent as both absorbent and reactant for the determination of NO_2 in air was the British method in 1939 (Jacobs, 1960). During the same year, Bratton and Marshall (1939) introduced the use of N-(1-naphthyl)-ethylenediamine dihydrochloride (NEDA) for the determination of sulphanilamide in blood samples, due to NEDA produced a greater reproducibility and rapidity of coupling, also the sensitivity was increased and the azodye

formed remained stable for a longer time. In 1941, Shinn was the first to make use of sulphanilamide and the coupling agent NEDA, as a means of determining nitrites.

In 1943, Patty and Petty did the first field campaign, specifically in an industrial area, and used for the first time the Griess-Ilosvay reagent for the determination of NO_2 as NO_2^-. A 50 ml glass syringe was used as a container for the reagents, sampling unit, reaction vessel and color comparator tube. However, the useful sampling range was from 1 to 500 ppmv (Patty and Petty, 1943).

In 1954 Saltzman published a work where he investigated several reagents and reported that a mixture of sulphanilic acid (5 g/l), NEDA (0.02g/l) and CH_3COOH (140 g/l) was the most sensitive and gave the best results with respect to the absorption of NO_2. Color development was reached within 15 min, and it was stated that the reagent was specific for NO_2 and did not absorb NO. The absorbance was measured at 550 nm and a nitrite equivalent of nitrogen dioxide (Saltzman factor), i. e. the moles on NO_2 required to give a color intensity equivalent to that produced by one mole of sodium nitrite ($NaNO_2$), of 0.72 was observed, which was in disagreement with the value of 0.57 found by Patty and Petty (1943). The method had a sensitivity of a few ppbv with an air flow of 0.4 liter min^{-1} and 10 ml of the reagent mixture.

Thomas (1956) developed an apparatus for continuous determination of NO_2 and NO using the mixture of Griess-Ilosvay reagent recommended by Saltzman, which was later known as Griess-Saltzman reagent, forgetting completely the work by Ilosvay. The instrument had two special absorbers, one absorber measured the nitrogen dioxide alone and the other measured nitrogen dioxide and nitric oxide after the latter was oxidised to NO_2 by potassium permanganate, ozone or chloride dioxide. The response time of the instrument was ~20 min.

Since then, many modifications were done to the Griess-Saltzman reagent. Jacobs and Hochheiser (1958) used the reagent along with an absorption solution of NaOH in order to reduce NO_2 to NO_2^- which was later reacted with sulphanilamide and NEDA in acid media to form the azodye. Inspite of its low collection efficiency (~35 %) (Purdue et al., 1972), NO interference (Hauser and Shy, 1972) and its long sampling period (24-hr), the Griess-Saltzman method was used as a reference method for NO_2 determination by the Environmental Protection Agency (EPA) until the end of the 1970s when it was replaced by chemiluminescence methods.

Saltzman itself modified the reagent two times. The first modification was the reduction of CH_3COOH to 50 ml and the increase of NEDA to 0.05 g/l. The objective was to reduce economic cost and the color development time (Saltzman, 1960). The second modification

was to increase the concentration of NEDA to 0.1 g/l because he observed that the color was developed faster in comparison with the first modification. Also a wetting agent (Kodak photo flow) was incorporated in order to facilitate the free movement of air bubbles (Saltzman and Mendenhall, 1964).

Lyshkow (1965) used a modified Griess–Saltzman reagent that consisted of NEDA 0.05 g/l, 2-naphtol 3,6 disulphonic acid disodium salt 0.05 g/l (promoter), sulphanilamide 1.5 g/l, tartaric acid 15 g/l and Kodak photoflow 0.25 ml/l (used as wetting agent). The time resolution and the detection limit of the instrument were 15 min (Margeson and Fuerst, 1975) and 10 ppbv, respectively (Baumgardner et al., 1975; Margeson et al., 1976). This version of the Griess-type reagent was among those tentative techniques studied by EPA in order to replace the reference method (Jacobs-Hochheiser method) used during the 1970s (Margeson and Fuerst, 1975). However, due to the divergent values of the Saltzman factor (0.57-1) (Huygen and Lanting, 1975), its relative long response time (15 min) and its negative ozone interferences, this technique was not chosen as a reference method.

However, the Griess-Saltzman method is still used in developing countries (Goyal, 2003; Raheem et al., 2009).

2.3   Multiphase Reactions

In the LOPAP instrument developed in the present study, NO_2 from the gas phase is taken up by a liquid solution and converted into a dye by a chemical reaction in the liquid phase. Such reactions are termed "multiphase reactions". This type of reaction is also of importance in the atmosphere, e.g. for the transformation of halogen reservoir species into ozone destroying species on polar stratospheric clouds during winter in the stratosphere (Seinfeld and Pandis, 2006). The detailed understanding of the different steps and rate limiting parameters of these heterogeneous multiphase reactions is of paramount importance, both to describe atmospheric processes but also to optimize the LOPAP instrument in the present study.

Heterogeneous reaction systems are characterized by the fact that their reactants are in different states of aggregation, e.g. in gas and liquid phases. The reactants react only when they reach and overcome the interface. In practice, heterogeneous chemistry involves a number of processes that determine the overall rate of transport and chemical conversion between the gas and condensed phases. The processes involved are shown in Fig. 6 and include gas diffusion of the reactant to the surface, mass accommodation and evaporation at

the interface, diffusion of the solvated specie into the bulk phase and chemical reaction in the condensed phase or at the interface itself (Kolb et al., 1995; Molina et al., 1996; Finlayson-Pitts and Pitts, 2000).
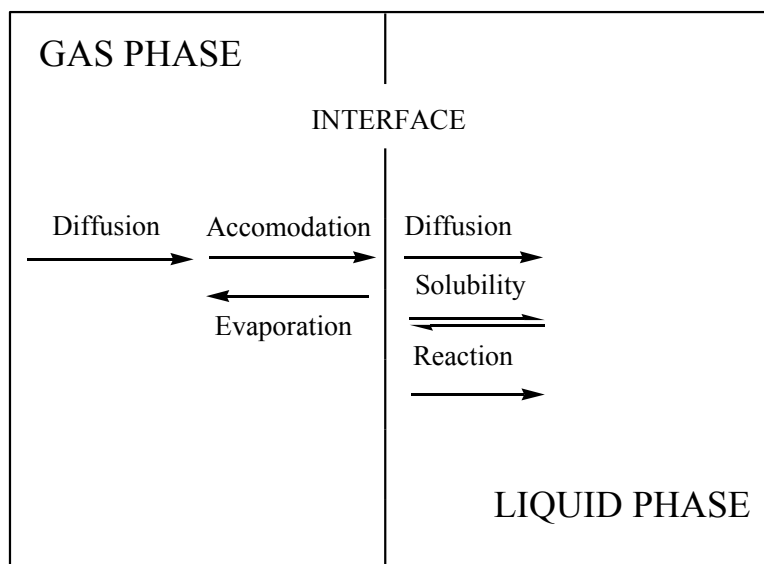
Fig. 6: Schematic diagram of transport and conversion processes that determine the net uptake of gaseous species by the condensed phase (adapted from Molina et al., 1996).

An understanding about heterogeneous multiphase reactions can be met only if the kinetics of the reaction and the limiting steps are known.

An approach based on a resistance model, which is a simplified representation (see Fig. 7), provides a broad framework to determine the different transport and kinetic processes involved (Kolb et al, 1995; Molina et al., 1996). In the model it is assumed that the overall uptake process can be divided in sub-steps and every sub-step can be considered analogous to an electrical resistance, which may be combined in series or parallel to obtain the rate of the overall heterogeneous process (Kolb et al., 1995; Molina et al., 1996; Fogg, 2003). In Fig. 7 and (Eq. 4) the resistances $1/\gamma_g$ and $1/\alpha$ represent the effect of gas-phase diffusion and surface accommodation, respectively, and $1/\gamma_{rxn}$ and $1/\gamma_{sol}$ are associated with liquid solubility and reaction in the liquid phase, respectively. Thus, the overall resistance model can be expressed as:

(Eq. 4) $$\frac{1}{\gamma_{meas}} = \frac{1}{\gamma_g} + \frac{1}{\alpha} + \frac{1}{(\gamma_{rxn} + \gamma_{sol})}.$$
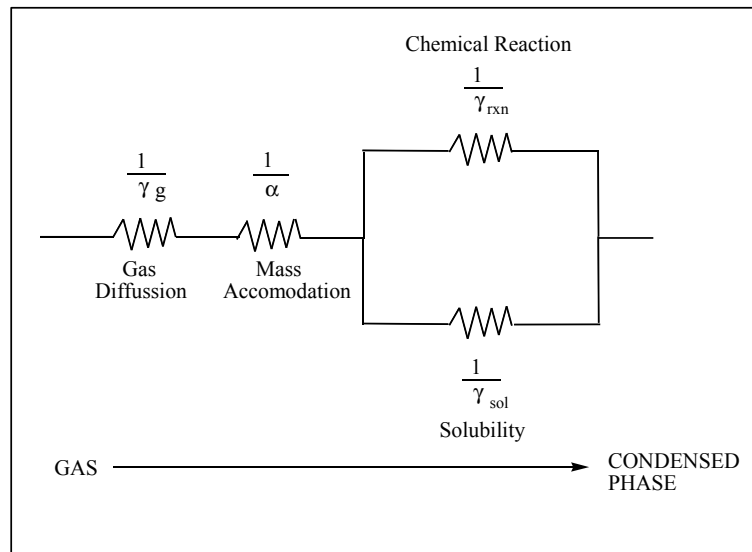
Fig. 7:   Electric circuit resistance model representing transport and conversion processes in heterogeneous processes (adapted from Kolb et al., 1995; Molina et al., 1996; Finlayson-Pitts and Pitts, 2000).

The mass accommodation, α, defines the probability at which molecules cross the interface, in one direction, from the gas to the condensed phase and is defined as (Fogg, 2003):

(Eq. 5) $$\alpha = \frac{number\ of\ gas\ molecules\ absorbed\ by\ the\ condensed\ phase}{number\ of\ gas\ molecule\ collisions\ with\ condensed\ surface}.$$

α can vary between 0 and 1 (Kolb et al., 1995; Fogg, 2003). In contrast, the measured uptake coefficient combines all limiting steps shown in Fig. 7 and is defined as:

(Eq. 6) $$\gamma_{meas} = \frac{number\ of\ reactive\ collisions}{number\ of\ gas\ molecule\ collisions},$$ (Kolb et al., 1995).

2.4   Aim of the Study

Caused by the non-selective detection of NO_2 in most commercial instruments, the development of a simple instrument for reliable NO_2 measurements is of high importance. Accordingly, in the present study a new NO_2-LOPAP instrument (Long Path Absorption Photometer), which is based on the Griess-Saltzman reaction (Saltzman, 1954) is described. The instrument is designed to be easy to use, sensitive and compact for continuously measuring of NO_2 under all experimental conditions both, in the atmosphere but also in laboratory and in smog chamber studies.

For the development of the instrument the uptake of NO_2 by the Saltzman reaction should be optimized by varying different system parameters and based on the studied dependencies the multiphase system should be described. In addition, the homogeneous liquid phase reaction of NO_2 with NEDA used in the Saltzman reagent should be determined for the first time. The instrument should be validated both in the atmosphere and in a smog chamber under complex conditions, for which also problems of commercial chemiluminescence should be investigated and described in detail.

After optimizing and validating the instrument, NO_2 should be measured in different environments, i.e. in the urban atmosphere and in a smog chamber, to investigate different atmospheric relevant topics related to NO_2 by an instrument, which is free of interferences. The study of direct NO_2 vehicle emissions and its impact on the EU NO_2 limit values and NO_2 formation during the photolysis of nitroaromatic species were chosen as examples to demonstrate the applicability of the new instrument.

3 Experimental Section

3.1 The NO$_2$-LOPAP Instrument

The NO$_2$-LOPAP prototype instrument consists of two separate units. (1) The external sampling unit, which is directly situated at the sampling site (i.e. in the atmosphere) and thus avoiding the use of any sampling lines. (2) The detection unit (19'' instrument) where the azodye, which is formed in the sampling unit, is detected using long path absorption. The system is furthermore designed as a two-channel system for correction of possible interferences (Fig. 8).
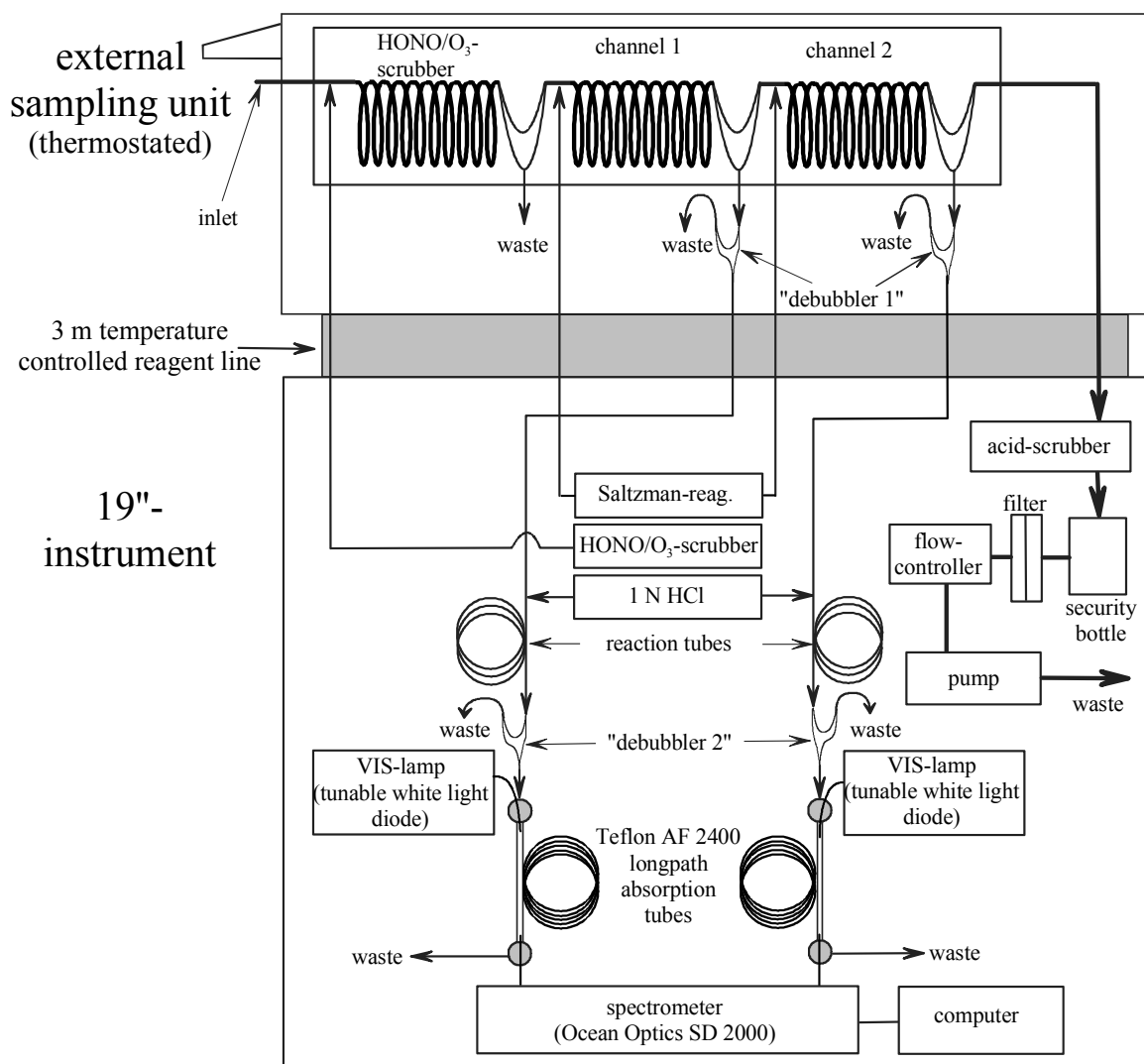
Fig. 8: Schematic setup of the NO$_2$-LOPAP instrument.

3.1.1 Sampling Unit

In the external sampling unit three stripping coils are used in series. In the first coil ("HONO/O$_3$-scrubber": 24 turns; 35 mm average turn diameter; 1.6 mm inner tube diameter), interfering HONO and O$_3$ are removed from the air stream without significant uptake of NO$_2$. This separation from NO$_2$ is made with a stripping solution that contains 10 g/l sulphanilamide, 0.6 g/l potassium indigo-trisulphonate in 158 g/l acetic acid, in which HONO and ozone are quantitatively removed. Ozone efficiently reacts with Indigo (Bader and Hoigné, 1981):

(R 26)
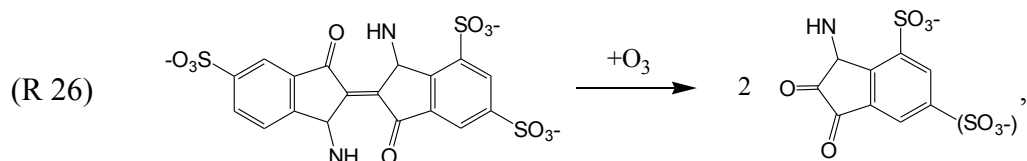
while HONO is transformed into a diazonium salt:

(R 27) $HONO + H^+ \rightleftharpoons NO^+ + H_2O$

(R 28)
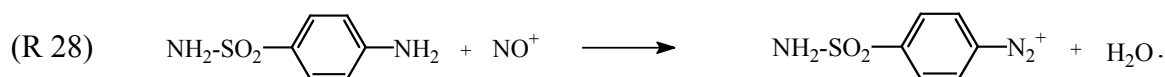
Besides HONO and O$_3$, 4 % of the NO$_2$ is also collected in this scrubber solution, which is corrected in the data evaluation. Through this HONO/O$_3$-scrubber the known HONO (Milani and Dasgupta, 2001) and ozone interferences (Adema, 1979) by the Griess-Saltzman reaction are suppressed.

NO$_2$ and other potential interferences are collected in the second stripping-coil (Channel 1), while potential interferences are measured in the third coil (Channel 2). Both coils have similar dimension than the HONO/O$_3$-scrubber. The gas phase is sucked with a membrane pump through the stripping-coils, a security flask with electrical control, a Teflon membrane filter and a mass flow controller. The gas flow through the stripping-coils is 0.5 l/min. As sampling solution a modified Griess-Saltzman reagent (N-(1-naphthyl)ethylenediamine dihydrochloride (NEDA) 1 g/l, sulphanilamide 7 g/l, 84 g/l acetic acid, 3 g/l NH$_3$ 25 %, pH = 3) is used. By the reaction of NO$_2$ with the sampling solution an intensive coloured azodye is formed (Saltzman, 1954), the mechanism of which is not completely understood. It was postulated that NO$_2$ first reacts with water (Saltzman, 1954):

(R 29) $2\,NO_2 + H_2O \longrightarrow HONO + HNO_3$ (or NO_3^-).

The formed HONO further reacts according to reactions (R 27) and (R 28) forming the diazonium salt, which reacts with NEDA forming an intensively coloured azodye:

(R 30)
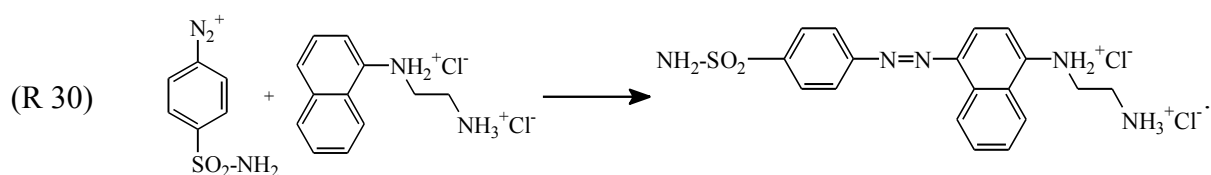
Based on reaction (R 29) a maximum dye yield of 50 % is expected, which is however observed only for very high concentrations of NO_2 in the higher ppmv-range; whereas at atmospheric concentrations yields near 100 % have been measured (Huygens and Lanting, 1975). The yield of the overall reaction (amount of dye / NO_2 absorbed) is expressed in the literature as so-called "Saltzman factor" (Huygens and Lanting, 1975). The high Saltzman factor and the observed dependency of the sampling efficiency on the NEDA concentration and the pH (see sections 4.1.1.1 and 4.1.1.2) shows that at low NO_2 concentrations reaction (R 29) is of minor importance. Instead, it is proposed here that NO_2 oxidizes partly deprotonated NEDA leading to quantitative formation of HONO:

(R 31) NO_2 + NEDA $\longrightarrow$ HONO + products.

Analogue redox reactions in the liquid phase are also known for other organic compounds, such as phenols and alkenes (Alfassi et al., 1986; Pryor and Lightsey, 1981). Instead of reaction (R 31), Saltzman originally postulated a reaction of NO_2 with sulphanilamide (Saltzman, 1954). However this can be ruled out based on the results obtained with the HONO-LOPAP instrument (Heland et al., 2001; Kleffmann et al., 2002). With this instrument no significant reaction between the sampling solution containing 10 g/l sulphanilamide and NO_2 could be observed.

The thermostated stripping coils (15 ^{o}C), which are connected to the detection unit through an isolated reagent line are located in the external sampling unit directly at the sampling site. Thus, line effects, for example heterogeneous reactions of NO_2 or the gas phase reaction between NO and O_3, can be neglected.

3.1.2   Detection Unit (19'' Instrument)

After the transfer of the sampling reagent from the external sampling unit to the instrument, the sampling solution is mixed with 1 N HCl (ratio 1:1) in order to convert all HONO, originating from reaction (R 31), into NO^+, reaction (R 27). Furthermore, the addition of HCl,

increases the refraction index of the solution and in consequence increases the light intensity in the absorption tubes. Finally, NEDA precipitates slowly with time on the surface of the absorption tubes, which leads to a reduction of the measured light intensity. This is also reduced by the addition of HCl.

A downstream reaction volume (1.6/0.8 o.d./i.d. mm Teflon tube) with residence time ≥1 min guarantees a quantitative formation of the dye. Before entering the detection unit, potential air bubbles are separated from the sampling solution ("debubbler 2", see Fig. 8), since bubbles would deteriorate the stability of the light signal. The detection unit is basically composed of a special flexible Teflon tube (DuPont, Teflon AF 2400; 0.6 mm i.D.; 0.8 mm o.d.; variable length, here: 1.4 m and 2.4 m used). Visible light (LUXEON, warm white LED, Typ: LXHL-MWGC) is focused into the tubing via fibre optics. With the refractive index of the tubing material being lower (n_{AF2400}: ~1.29) than that of the solution of the dye, the light - depending on the angle of incidence - undergoes multiple total reflection on the inner walls of the tubing and stays inside the liquid for absorption (Yao et al., 1998). The intensity of the diodes can be regulated without change of the spectral distribution (pulsed power supply unit: QUMA Elektronik & Analytik GmbH). On the opposite end of this so-called liquid core waveguide, LCW, the light is collected again by a glass fibre and detected with a two channel grating mini-spectrometer using a diode array detector (Ocean Optics, SD 2000). The absorption spectra of both channels averaged over a variable time interval are stored on a mini computer for later analysis. In addition, the absorption of the azodye can be continuously monitored for variable absorption wavelengths (see section 3.1.3).

A two channel system is used for the quantification of possible interferences. With this arrangement, two stripping coils are connected in series (see Fig. 8). In Channel 1, NO_2 is almost quantitatively taken up (97 % sampling efficiency) as well as potentially interfering compounds, whereas in Channel 2 - under the assumption of a low uptake of the interferences - only the interferences are collected. NO_2 concentrations can be calculated from the difference between both channels considering the sampling efficiency of NO_2 in Channel 1.

3.1.3   Data Evaluation

To be independent from intensity fluctuations, which are caused by e.g. temperature changes and/or bubbles of air entering the tubing, no so-called background (I_0) spectra without absorption of the dye are used for data evaluation. Instead, the logarithm of the ratio of two

intensities taken at different wavelengths in the same measured spectrum is a more stable and robust measure of the azodye concentration. These two intensities are taken (a) at the absorption maximum near 544 nm or a neighbouring wavelength, I_{abs}, and (b) at a wavelength where no azodye absorption occurs, I_{ref}, e.g. at λ_{ref} of 650 nm. Knowing that I_{ref} is directly proportional to the background intensity I_0 at the absorption wavelength, λ_{abs}, the logarithm of (I_{ref}/I_0) becomes a linear measure of the concentration c according to Lambert-Beers law:

(Eq. 7) $$ABS = \log\left(I_{ref}\middle/I_{abs}\right) = k_\lambda \times l \times c + \log\left(I_{ref}\middle/I_0\right).$$

Where l denotes the absorption path length and k_λ is the absorption coefficient of the azodye, which is ca. 5×10^4 l mol^{-1} cm^{-1} at 544 nm (Grasshoff et al., 1983). The intercept of equation (Eq. 7) depends mainly on the chosen absorption and reference wavelengths and may show variations, which are due to different purities of the reagents. Accordingly, zero air measurements have to be performed regularly during the operation of the instrument and a calibration of the two channels with a liquid nitrite standard is mandatory when the reagents have been renewed.

3.2   Other Instruments

3.2.1   FTIR-Spectrometer Nicolet Nexus

The FTIR used for the photosmog experiments (see section 4.5.2), is a Nicolet Nexus that is equipped with a liquid nitrogen cooled (77 K) mercury-cadmium-tellurium (MCT) detector. The instrument is coupled to the photoreactor via a mirror system using KBr windows located in one of the end flages. A white-type mirror system, with a base path length of (5.91 ± 0.01) m, mounted inside the reactor, is used for multiple-reflection of the infrared beam within the reactor volume before it reaches the detector. The total optical path length of the system is (487 ± 1) m, which is reached through 82 traverses of the beam (Bejan, 2006a).

3.2.2   10 l White Type Multiple Reflection Cell

During the experiments in section 5.2, the concentrations of 2-nitro-toluene were determined with a FTIR spectrometer Nicolet Nexus (see above) which was coupled to a 10 l White type multiple reflection cell operated at a total optical path length of 32.8 m. The optical cell was connected to the exit of the photoreactor (see Fig. 9). IR spectra were recorded at a spectral resolution of 1 cm^{-1} using the FTIR mentioned before.
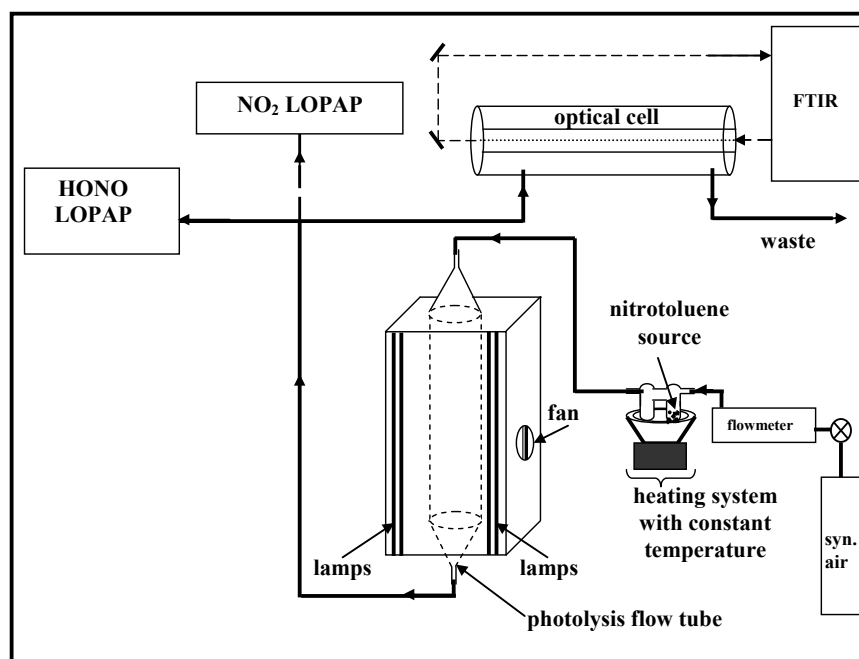
Fig. 9   Experimental set up of the flow tube experiments with 2-Nitro-Toluene (see section 5.2).

3.2.3   ECO-Physics CLD 770 Al ppt/PLC 760

The NO_x instrument "CLD 770 Al ppt" distributed by ECO Physics GmbH (hereafter: *ECO*), detects NO by means of the chemiluminescence technique (see (R 21) - (R 23), section 2.2.2.2). For measurement of NO the sample gas is drawn directly into the O_3 reaction chamber, whereas for the measurement of NO_x the sample gas is routed first to a photolytic converter (PLC 760) operated with a Xenon lamp (300 W, 320-420 nm) for selective NO_2 conversion by reaction (R 25) and is then drawn into the O_3 reaction chamber. The NO and NO_x measurements are made sequentially. For the shortest full measurement cycle time of 30 s, the ECO has a DL for NO_2 of ~0.1 ppbv.

3.2.4   Ansyco AC31M with "Blue-Light" and Mo Converter

The Ansyco AC31M (hereafter: *Ansyco blue light*) is a combined NO/NO_x instrument, which has two channels, i.e. two parallel reaction chambers, one for NO and one for NO_x measurements, where the sample gas is mixed with O_3 (internally generated) to produce chemiluminescence. The only difference between Ansyco blue light and the standard model Ansyco AC31M is the converter; the molybdenum converter was replaced by a home made

"blue light converter". In this converter NO_2 is photolysed by reaction (R 25) using 6 UV LEDs at 395 ± 10 nm with a converter efficiency of 52 %. The instrument has a higher time response of 10 s compared to the ECO instrument, but is much less sensitive with a DL for NO_2 of only 1-2 ppbv. In the case of Ansyco with Mo converter, a DL of 0.6 ppbv was determined during the campaign.

3.2.5   LMA3D

In the Unisearch LMA3D instrument (hereafter: *Luminol*) the sample air is sucked by a pump across a wick that is continuously flushed with a specially formulated luminol (5-amino-2,3-dihydro-1,4-phthalazinedione) solution. When NO_2 encounters the wick, the oxidation of luminol by NO_2 in the presence of O_2 produces chemiluminescence in the region of 425 nm. A photo-multiplier tube (PMT) measures the light produced and converts it into an electrical signal, which is almost linearly correlated with the NO_2 concentration. The instrument shows a high time response of a few seconds and is very sensitive with a DL of 0.2 ppbv.

3.2.6   Ansyco O3 41M

The measurement principle of Ansyco O3 41M is based on the absorption of the ozone molecule (O_3) in the UV range. The UV spectrum of the O_3 molecule has its maximum at 254 nm, wavelength that is generated in the instrument with low pressure mercury (Hg) lamp, which has a strong emission line at 253.7 nm that also coincides with the maximum spectral sensitivity of the detector, a vacuum UV cesium-tellurid (Cs-Te) diode. An ozone-free air flow is created by an ozone-specific scrubber in order to obtain a reference air, which is compared with the ambient air. The concentration of O_3 is determined by the straightforward Lambert-Beer absorption equation, which depends on the well known absorption cross section of the molecule of O_3.

3.2.7   HONO-LOPAP

The HONO-LOPAP instrument (QUMA Elektronik & Analytik) is a very sensitive technique for the detection of HONO and is described in detail elsewhere (Kleffmann et al., 2002). HONO determination is based in the same principle used for NO_2 detection developed in this Thesis. Briefly, HONO is sampled in a stripping coil by a fast chemical reaction and converted into an azodye, which is photometrically detected by long path absorption. The

instrument can reach a detection limit of 0.2 pptv for a response time of 7 min (Kleffmann et al., 2008).

3.3   1080 *l* Quartz-Glass Photoreactor

The smog chamber experiments described in section 4.5.2 were carried out in a quartz glass reactor. In Fig. 10 a scheme of the photoreactor used is shown. The reactor consists of two quartz tubes with an inner diameter of 47 cm and a wall thickness of 5 mm. Silicone rubber rings are used for all the glass connections as well as for metal-metal connections. The tubes are joined together by an enamelled flange ring and the ends are capped with two enamelled aluminium flanges. The reactor has a total length of 6.2 m (see Fig. 10). Around the chamber there are two different types of lamps installed (32 each) in order to ensure uniform intensity distribution within the chamber. For the range 320-480 nm are used fluorescent lamps (Philips TL05-40W, VIS lamps) with a maximum intensity at 360 nm. For the UV range, low-pressure mercury lamps (Philips TUV-40W) are used, which have an emission maximum at 254 nm (see Barnes et al., 1994; Bejan, 2006a).
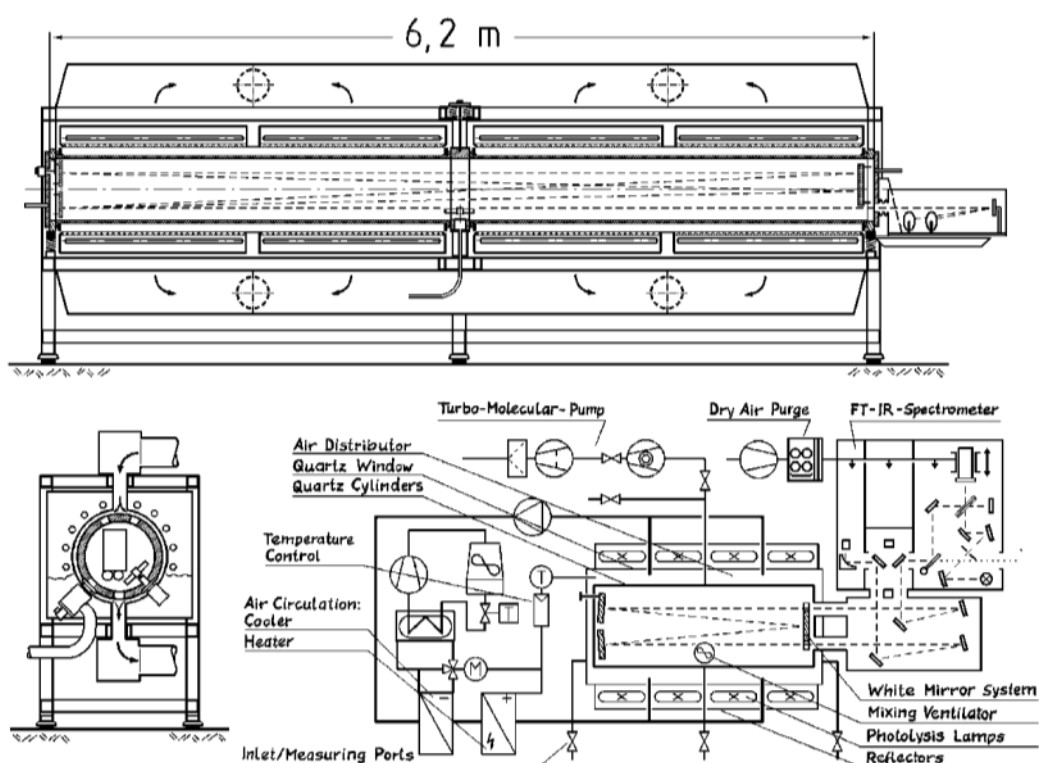
Fig. 10:   Schematic diagram of the 1080 l quartz glass photoreactor with FTIR facility.

The reactor can be evacuated by a turbo molecular pump (Leybold-Heraeus PT 450 C) backed by a Leybold D65B double stage rotary vacuum pump reaching an end vacuum of 10^{-3} mbar. Around the reactor there are aluminium sheets that protect the reactor and at the same time they act as reflectors. Between the lamps and the quartz reactor a ventilation duct is located where the air can be recycled as a heat carrier. By hot and cold air generators installed in the air duct, the reactor can be thermostated among 283-313 K with a precision of ± 1 K. The capacity of the cold air generator is regulated in order to allow the increase of the temperature inside the reactor only by 1°C during the course of one experiment with full intensity of the lamps (Spittler, 2001). The temperature is monitored by three PT-100 sensors, which are located in both extremes of the reactor and in the middle. For homogeneous mixing, the reactor contains three fans. Different types of inlets are mounted on the end and middle flanges for the introduction of chemicals and gases. Optionally, the inlets can be heated to facilitate the addition of solid compounds into the chamber (Bejan, 2006a). In the present experiments, the NO_x monitors were connected to a sampling port at the middle flange of the reactor.

3.4   Atmospheric Field Sites

3.4.1   Intercomparison Campaign (BUW)

An intercomparison campaign was carried out during the period March 10-13, 2007 at the balcony of the 5th level of the main campus of the University of Wuppertal. The instrument chosen for intercomparison was ECO-Physics model AL 770 ppt / PLC 760. Both instruments, LOPAP and ECO-Physics were taking air from the balcony through a 2 meters PFA Teflon sampling line (4 mm i.d.) which was attached to a particle filter at the beginning of it.

3.4.2   NO$_2$-Emission Campaign (B7, Loher Kreuz)

The site of the intercomparison was the Friedrich-Engels-Allee, Wuppertal in a monitoring station in the middle of two lanes of a busy street, one of them in direction west-east and the other in the opposite way (see Fig. 11).
The sample gas was taken at a height of about 3.5 m above the container through a central sampling line, which is made of an approximately 5 cm diameter glass tube to which the different instrument were connected by 4 mm i.d. PFA Teflon sampling lines. The calibration

of the instruments was performed using diluted mixtures from commercial calibration gas mixtures of 10.7 ppmv $\pm$ 2% NO in N_2 and 7.85 $\pm$ 0.5 ppmv NO_2 in synthetic air (SA). These bottles were diluted with synthetic air using mass flow meters and needle valves for the nitrogen oxides and flow controllers for the synthetic air.

Fig. 11: Different views of the monitoring station at the Friedrich-Engels-Allee in Wuppertal.

4   Results and Discussion

4.1   Instrument Parameters Optimization

4.1.1   Sampling Reagents

Originally, bubblers are used for the detection of NO_2 with the Griess-Saltzman reagent, which however can not be used for continuous detection of NO_2. Instead a stripping coil is used in the present instrument, for which, however, the gas-liquid contact time is much shorter. Thus, to obtain a high sampling efficiency of NO_2 and a high Saltzman factor, a modified sampling reagent has to be used. In the present study, the sampling efficiency is defined as the proportion of NO_2 incorporated in the second stripping coil (Channel 1) with respect to the total quantity of NO_2 entering the coil. The Saltzman factor is calculated based on the proportion of the generated amount of dye with respect to the quantity of NO_2 absorbed. A high sampling efficiency is required for a correction of possible interferences using the two channel system. A low Saltzman factor causes a production of NO as a co-product that should be avoided for a possible future extension of the instrument for NO detection. Thus, both factors need to be as high as possible. For the optimization of the instrument several dependencies of the sampling reagent were investigated.

4.1.1.1   Variation of the pH

The pH of the sampling solution leads to a strong variation of the sampling efficiency as well as of the Saltzman factor (see Fig. 12). The sampling efficiency increases up to pH = 3, gets constant up to pH = 7 and reaches 100 % at higher pH. This can be explained by the reaction of NO_2 with NEDA (R 31) for which the deprotonated form of NEDA reacts faster than the protonated form. This effect was also observed in the reaction of NO_2 with phenols in the liquid phase (Ammann et al., 2005), for which the phenolate anion reacts much faster at high pH, compared to the phenol form at lower pH. Thus, the two steps in the sampling efficiency can be explained by the neutralization of the two $-NH_3^+$ groups of NEDA. The Saltzman factor increases strongly up to pH = 4, however starts to decline at higher pH. Based on the pH dependency, a pH of 3 - 4 is recommended, for which both the sampling efficiency and the Saltzman factor are high. Higher pH leads to a higher sampling efficiency but to a lower Saltzman factor. In addition, stronger interferences against PANs are expected with increasing pH (Frenzel et al., 2000) and therefore should be avoided.
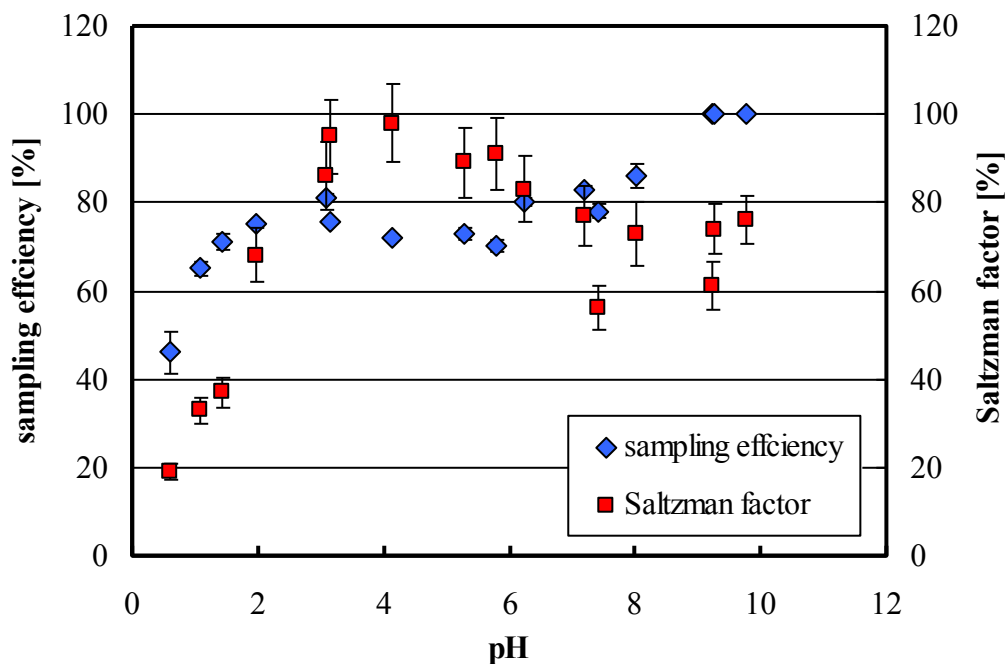
Fig. 12: Variation of the sampling efficiency and the Saltzman factor with the pH. Griess-Saltzman reagent: 1 g/l NEDA, 5 g/l sulphanilamide, 7.2 g/l HCl was used here instead of acetic acid, pH adjusted by the addition of NH_3. Air flow = 1000 ml/min, liquid flow = 0.27 ml/min.

4.1.1.2 Variation of the NEDA Concentration

Increasing NEDA concentration leads to a strong increase of the sampling efficiency, reaching 100 % for high NEDA concentrations (Fig. 13). From the strong NEDA dependence, it is proposed that NO_2 is directly reacting with NEDA, reaction (R 31), whereas the reactions with water (R 29) and sulphanilamide can be neglected. However, at the same time, a decrease of the Saltzman factor is observed. Parallel measurements with a NO chemiluminescence instrument demonstrated an undesirable formation of NO as a co-product. Caused by the NEDA and pH dependencies observed for the Saltzman factor, it is proposed that NO^+ formed by reactions (R 31) and (R 27) can also react with NEDA to generate nitrogen monoxide (NO):

(R 32) NO^+ + NEDA $\longrightarrow$ NO + products.

Based on the undesirable NO formation and the possible future extension of the instrument for NO detection, the NEDA concentration should not be too high and is limited here to ≤1 g/l.
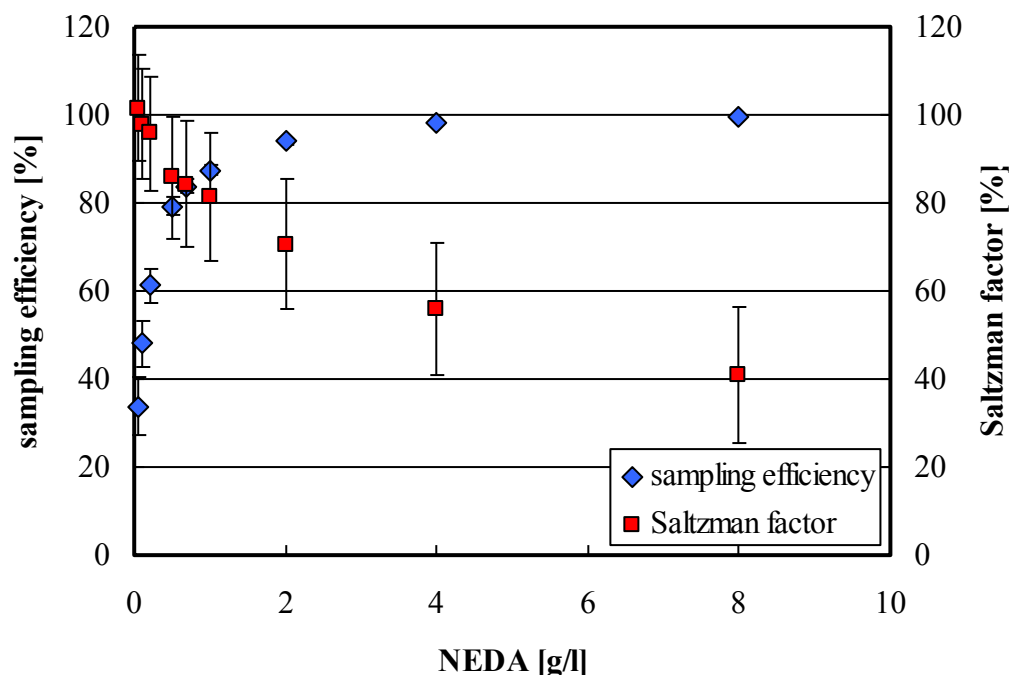
Fig. 13:   Variation of the sampling efficiency and the Saltzman factor with the NEDA concentration. Griess-Saltzman reagent: 7 g/l sulphanilamide, 84 g/l acetic acid, pH=3, adjusted with NH$_3$. Air flow = 650 ml/min, liquid flow = 0.35 ml/min.

4.1.1.3 Variation of the Sulphanilamide Concentration

Whereas the concentration of sulphanilamide has almost no effect on the sampling efficiency of NO$_2$, an increasing Saltzman factor is observed for increasing sulphanilamide concentration (Fig. 14). This behaviour can be explained by a NEDA limited uptake of NO$_2$ by reaction (R 31), and a sulphanilamide limited further conversion of HONO into the diazonium salt via reactions (R 27) and (R 28). It is proposed that the relative high pH used leads to slow kinetics of reactions (R 27) and (R 28) and thus, the low Saltzman factor can be explained by the secondary reaction (R 32). With increasing sulphanilamide concentration, the rate of reaction (R 28) increases and parallel reaction (R 32) becomes of minor importance. Caused by the maximum solubility of sulphanilamide in water, only concentrations up to 7.5 g/l were studied here. However, the solubility can be increased by the addition of higher concentrations of acetic acid. In the present study 7 g/l sulphanilamide in 84 g/l acetic acid is finally used.

The optimized composition of the Griess-Saltzman solution is summarized in Tab. 2.
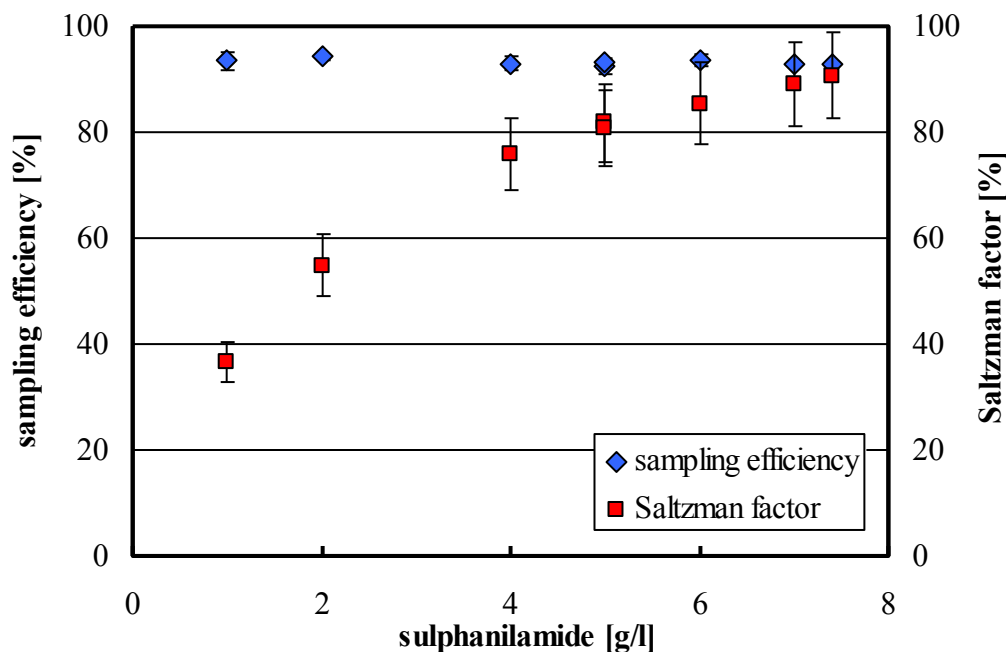
Fig. 14: Variation of the sampling efficiency and the Saltzman factor with the sulphanilamide concentration. Griess-Saltzman Reagent: 1.6 g/l NEDA, pH = 3, adjusted with NH_3. Air flow = 1000 ml/min, liquid flow = 0.2 ml/min.

Tab. 2: Optimized composition of the Griess-Saltzman reagent (pH = 3).

Reagent	conc. [g/l]
N-(1-naphtyl)ethylenediamine dihydrochloride (NEDA)	1
sulphanilamide	7
acetic acid	84
NH_3 (25 %)	3

4.1.2 Improvement of the Sampling Conditions

4.1.2.1 Length of the Stripping-Coil

Stripping coils with different lengths were used (10, 20, 25 turns, 22 mm average turn diameter, 2.4 mm i.d.), which were similar to those used in the previous HONO- and HNO_3-LOPAP instruments (Kleffmann et al., 2002; Kleffmann et al., 2007). Due to the slow uptake of NO_2 only the longest coil could be used for NO_2. Furthermore, because high NEDA concentrations were not applied (see section 4.1.1.2), the maximum sampling efficiency obtained with the longest coil was only 95 %. In addition, caused by the low gas flow applied, a high volume of the sampling reagent accumulated in the stripping coil leading to a lower time resolution of the

instrument. Thus, a new coil with smaller inner diameter, higher surface to volume (S/V) ratio and higher gas velocity was used in order to improve the sampling efficiency and time resolution. This new coil with 24 turns, 35 mm average turn diameter and 1.6 mm inner diameter, increases the sampling efficiency to 97 % and leads to a better time resolution.

4.1.2.2 *Variation of the Sampling Temperature*

The temperature was varied in the range 5 - 20 °C. Only a small increase of the sampling efficiency and a minor decrease of the Saltzman factor were observed with increasing temperature (Fig. 15). For practical reasons a sampling temperature of 15 °C was chosen to avoid condensation of water in the gas line to the instrument.
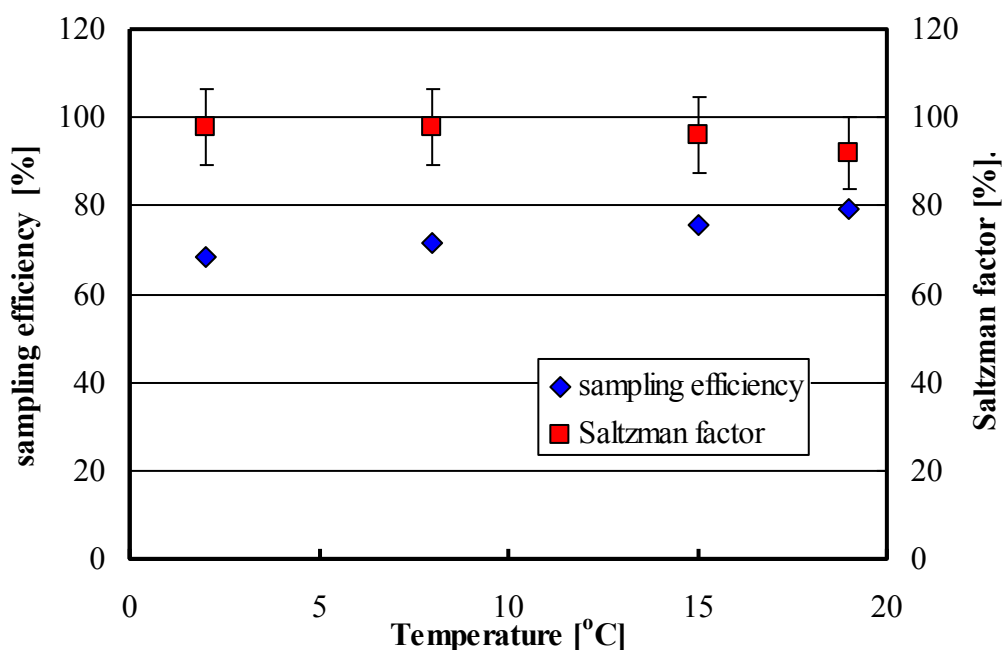
Fig. 15:   Variation of the sampling efficiency and the Saltzman factor with the temperature of the stripping coil. Griess-Saltzman Reagent: 1 g/l NEDA, 5 g/l Sulphanilamide, pH = 3, adjusted with NH_3. Air flow = 1000 ml/min, liquid flow = 0.2 ml/min.

4.1.2.3 *Variation of the Liquid Flow*

The variation of the liquid flow has only a slight effect on the sampling efficiency and the Saltzman factor for values >0.1 ml/min (see Fig. 16). This can be explained by a surface limited uptake of NO_2 by which the fast reaction (R 31) ($k_{NO_2+NEDA}= (3.6 \pm 1.6) \times 10^6$ $M^{-1}s^{-1}$) (see section 4.2.5) and the low solubility of NO_2 leads to a liquid diffusion limited uptake of NO_2. In contrast, for a limitation of the NO_2 uptake by any slow reaction in the liquid phase the sampling efficiency should increase with increasing liquid flow. Caused by the missing liquid flow

dependency, the time resolution and the sensitivity of the instrument can be varied by the liquid flow without influencing other parameters.
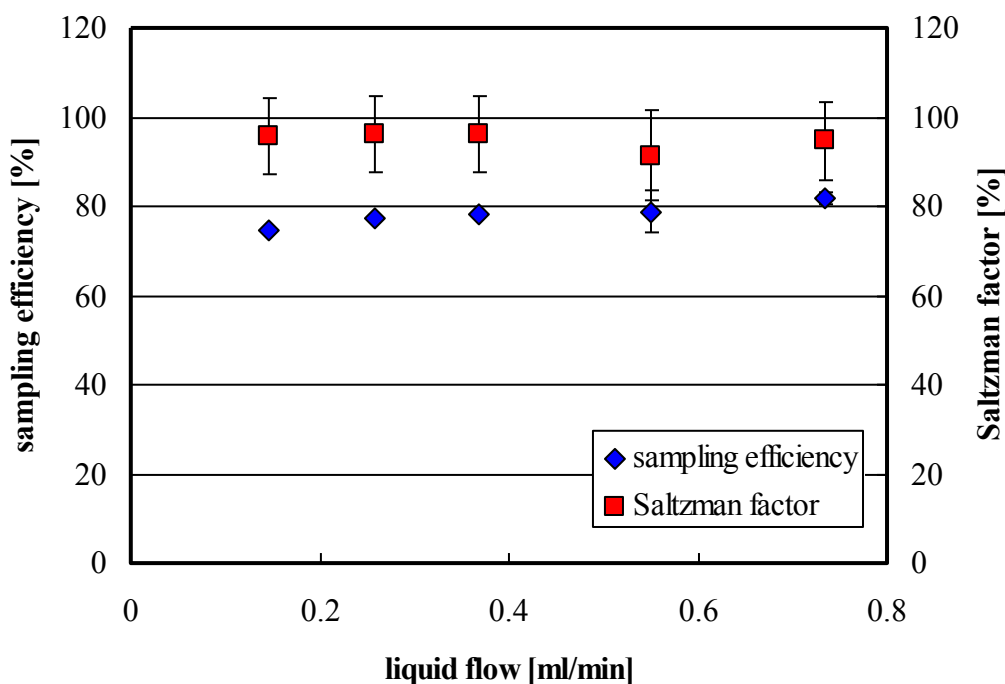
Fig. 16: Variation of the sampling efficiency and the Saltzman factor with the liquid flow. Griess-Saltzman Reagent: 1 g/l NEDA, 5 g/l Sulphanilamide, pH = 3, adjusted with NH_3. Air flow = 1000 ml/min, liquid flow = 0.2 ml/min.

4.1.2.4 Variation of the Gas Flow

The gas flow variation has a strong effect on the sampling efficiency but not on the Saltzman factor. The variation of the sampling efficiency can be well described by a first order uptake kinetics of reaction (R 31), which is expected for a heterogeneous multiphase reaction, which is limited by the low solubility and the liquid phase diffusion of NO_2 (see section 4.2). In contrast, the Saltzman factor is only affected by the slower consecutive chemistry in the liquid phase, which is depending only on the composition of the sampling solution, but not on the gas/liquid contact time (see Fig. 17).

Based on all the observations described up to now, a surface limited NO_2 uptake is proposed, which is improved by increasing the S/V ratio of the stripping coil and increasing the gas/liquid contact time. Thus, a maximum gas flow of only 0.5 l/min is recommended for the used stripping coils (see Tab. 3).
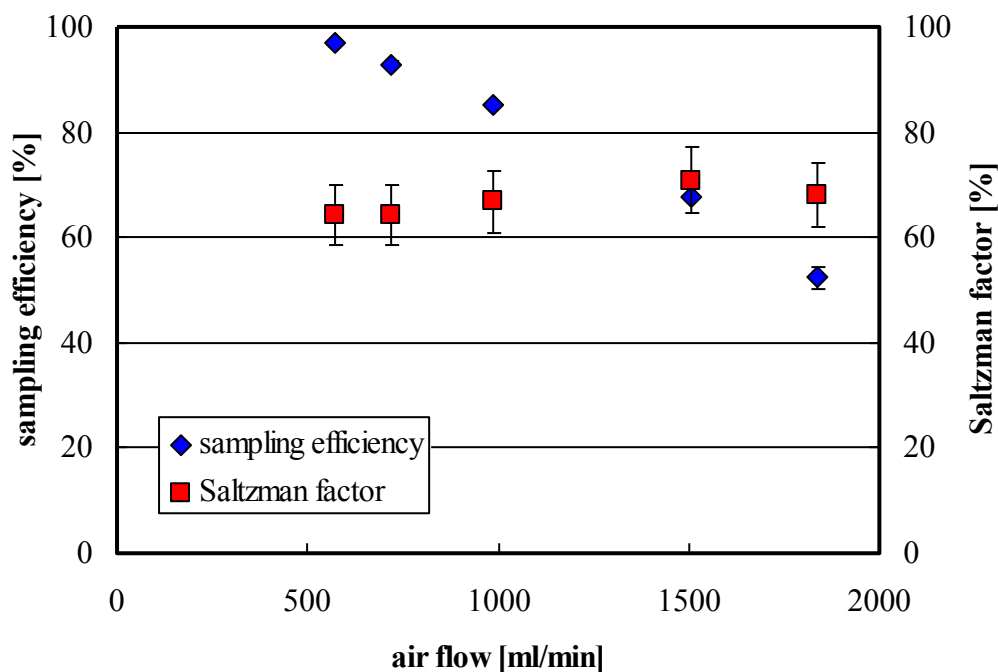
Fig. 17: Variation of the sampling efficiency and the Saltzman factor with the air flow. Griess-Saltzman Reagent: 1.6 g/l NEDA, 5 g/l Sulphanilamide, pH = 3, adjusted with NH₃, liquid flow = 0.2 ml/min.

4.1.3   Instrument Parameters

The detection limit, the response time, i.e. the time the instrument needs to rise from 10 % to 90 % of the full signal and the measurement range of the LOPAP instrument are strongly dependent on several factors such as (a) the sample gas flow rate, (b) the liquid flow rate, and (c) the length of the absorption tubes.

The theoretical sensitivity of the instrument will increase linearly with the gas flow rate and/or the absorption lengths as well as by decreasing the liquid flow rate. In practice, these parameters are limited, e.g. by a decreasing NO_2 sampling efficiency with increasing gas flow rate, so that up to now the air flow is limited to 0.5 l/min. Light intensity as well as time resolution decrease, when the absorption path length is increased, so that a maximum length of 6 m can be used (Kleffmann and Wiesen, 2008). However so far, only optical path lengths of 1.4 and 2.4 m have been applied in the present study. The sensitivity can be increased by decreasing the liquid flow, however, the time resolution of the instrument is then reduced. For the applied liquid flows of the sampling reagent (0.2 - 0.4 ml/min) and the length of the absorption tubes (1.4 - 2.4 m) the time resolution is in the range 3 - 6 min. With an optical path length of 2.4 m and a liquid flow of 0.4 ml/min a time resolution of ~3 min and a detection limit of ~2 pptv is obtained (see Fig. 18

and Fig. 19). The detection limit is defined in the present study as two times the value of the standard deviation of the zero-air signal.

Since the lower limit of the measurement range is set by appropriate values of the above mentioned parameters, the upper limit of the measurement range can also be shifted during the data evaluation by shifting the absorption wavelength (λ_{abs}) during the evaluation of the stored spectra. While highest sensitivity is obtained at the maximum absorption (λ_{abs} = ~540 nm), the measurement range is expanded by more than one order of magnitude by shifting the absorption wavelength into the wings of the absorption band (e.g. λ_{abs} = 600 nm). Thus, with an absorption length of 1.4 m, NO_2 concentrations up to 300 ppbv can be measured.

The precision of the instrument is defined in this study as the minimum detectable change of a measured signal and amounts to approximately ±0.5 % of the measured values and the value the detection limit (Fig. 18). The accuracy is obtained from the sum of all relative errors of ~10 % and the value the detection limit. The instrument parameters of the NO_2-LOPAP are summarized in Tab. 3.

Tab. 3:   Summary of the optimum parameters of the NO_2-LOPAP instrument.

air flow	0.5 l min^{-1}
liquid flow (stripping solution)	0.2 - 0.4 ml min^{-1}
absorption path length	1.4/2.4 m (0.1 - 6 m possible)
range of λ_{abs}	550 - 610 nm
sampling efficiency	97 %
Saltzman factor	95%
measurement range	0.002 - 300 ppbv
time resolution (10-90 %)	≈ 3 - 6 min
precision	±(0.5 % + DL)
accuracy	±(10 % + DL)
detection limit (DL)	2 pptv (3 min time resolution)

With the HONO-LOPAP instrument recently an optical length of 6 m was applied and thus a detection limit of only 0.2 pptv was reached for HONO (Kleffmann and Wiesen, 2008). Since the gas flow used for the NO_2 instrument is ca. a factor of three smaller than that used for the HONO instrument, a minimum NO_2 detection limit <1 pptv can be expected in the future for a time resolution of 8 min.
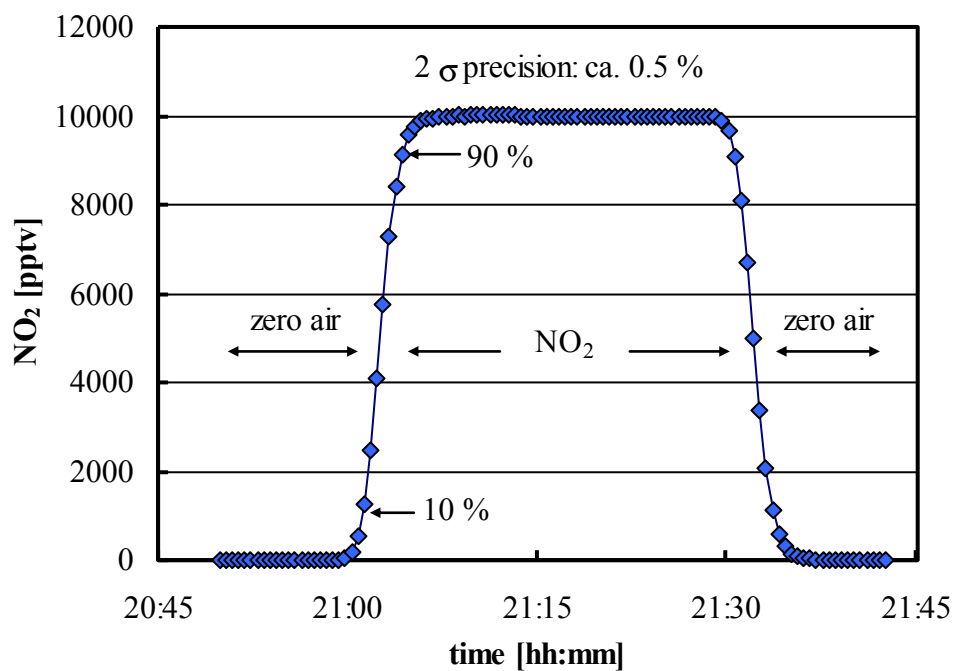
Fig. 18: Time resolution (3 min) and precision (2σ, 0.5 %) of the NO$_2$-LOPAP instrument using recommended sampling solution (see Tab. 1) and instrument parameters (see Tab. 2, liquid flow = 0.35 ml/min).
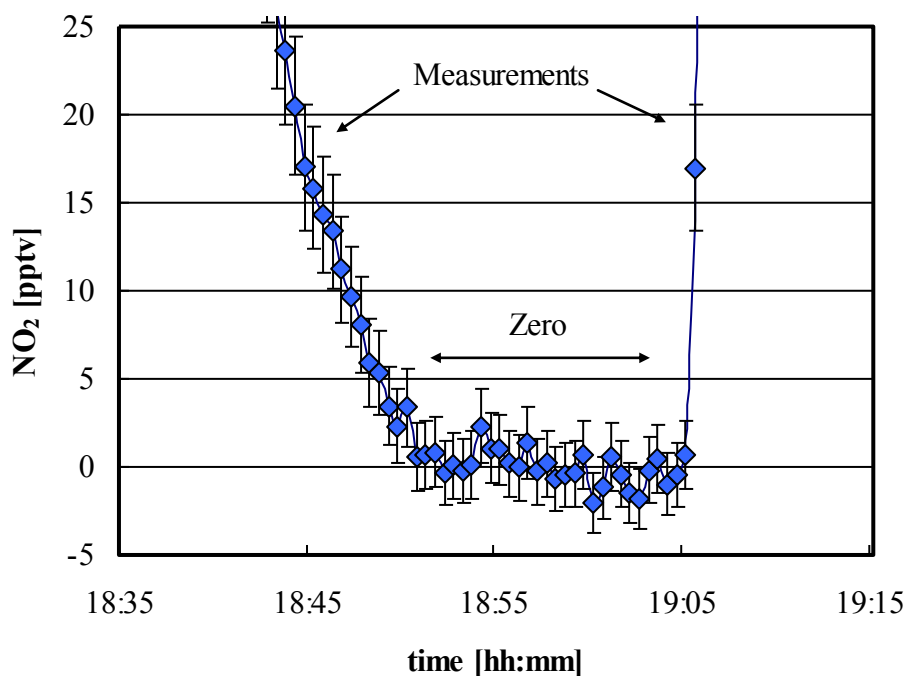
Fig. 19: Determination of the detection limit (DL) using the zero air method. A detection limit, which is defined as twice the standard deviation of the zero air signal, of 2 pptv was determined in the present study.

4.2 Kinetic Study of the Heterogeneous Reaction

In the present study the multiphase reaction between NO_2 and NEDA was used to quantify the gas phase concentrations of NO_2. To better optimize the instrument performance, it is important to fully understand the uptake mechanism and the kinetics of the gas and liquid phase processes involved. Thus, a) the rate limiting steps for the uptake of NO_2 were studied and b) the rate coefficient for the reaction $NO_{2(lq)}$ + $NEDA_{(lq)}$ was quantified.

Under the condition of pseudo-first order, i. e. when the concentration of $NEDA_{(lq)}$ is more than one order of magnitude higher than that of $NO_{2(lq)}$, the change of the NEDA concentration is negligible in comparison to NO_2, and can be assumed as constant. NO_2 reacts with NEDA as:

(R 33) $\qquad NO_2 + NEDA \xrightarrow{\ k''\ } \qquad$ products .

For this second order reaction the following rate equation can be established:

(Eq. 8) $\qquad -\dfrac{d[NO_2]}{dt} = k'' \times [NO_2] \times [NEDA].$

Since *[NEDA] >> [NO₂]*, a pseudo first order rate constant can be defined:

(Eq. 9) $\qquad k' = k'' \times [NEDA].$

Inclusion into the rate equation (Eq. 8) and integration leads to the following concentration-time equation:

(Eq. 10) $\qquad \ln \dfrac{\left[NO_{2(t)}\right]}{\left[NO_{2(t_0)}\right]} = -k' \times t.$

By plotting the natural logarithm of the NO_2 concentration versus the contact time between liquid and gas phase, the pseudo-first order rate constant can be obtained from the slope. The contact time is calculated using the known volume of the stripping coil and the gas flow.

The reactive uptake coefficient (γ_{NO_2}) is the probability of the permanent uptake of NO_2 that hits a liquid surface and is defined as the ratio of the number of reactive collisions to the number of gas kinetic collisions. It is proportional to the pseudo first order rate constant, *k'*, as well as to the surface to volume ratio (*S/V*) of the stripping coil (Eq. 11):

(Eq. 11) $\qquad \gamma_{NO_2} = \dfrac{number\ of\ reactive\ collisions}{number\ of\ gas\ kinetic\ collisions} = \dfrac{4 \times k'}{\bar{v} \times \dfrac{S}{V}},$

where $\bar{v}$ is the mean thermal molecular velocity (for NO_2 = 364 m s^{-1} at 288 K). If the pseudo first order rate constant of the reaction and the surface to volume ratio are known, γ_{NO_2} can be calculated.

The heterogeneous uptake of a gas molecule into the liquid phase can be limited by several consecutive and parallel processes such as gas phase diffusion, mass accommodation (α), high solubility and slow chemical reaction, or low solubility and fast chemical reaction in the liquid phase (see section 2.3). In the following, the different potentially rate limiting steps are discussed in relation to the multiphase reaction of NO_2 studied.

4.2.1 Gas Phase Diffusion and Accommodation Limitations

In a consecutive process, like the one investigated here for the uptake of NO_2 on a liquid surface, the slowest step limits the overall loss of NO_2 from the gas phase. It can be demonstrated that both, gas phase diffusion and mass accommodation of NO_2 with the NEDA solution used here are so fast that they can not act as rate limiting steps. Calculations based on the Conney-Kim-Davis approach explained in Murphy and Fahey (1987) demonstrates that for uptake coefficient smaller than 10^{-4} the gas phase diffusion can not be a limiting step in the stripping coils used, even for the laminar flow conditions assumed. Since the uptake coefficients were typically ca. 10^{-5}, and since turbulent flow condition prevails in a stripping coil, gas phase diffusion limitation can be excluded here.

Mass accommodation (α), (Eq. 5), is typically also no rate limiting step in the heterogeneous uptake of gases on liquid surfaces. Typical values of α vary between 10^{-3} and 1 and are normally much higher than the uptake coefficients for the overall processes (Kolb et al., 1995). Accordingly, in equation (Eq. 4):

(Eq. 4) $\qquad \dfrac{1}{\gamma_{meas}} = \dfrac{1}{\gamma_g} + \dfrac{1}{\alpha} + \dfrac{1}{(\gamma_{rxn} + \gamma_{sol})}$,

the terms for gas phase diffusion and mass accommodation are omitted and only the terms for the solubility of NO_2 in the liquid phase and for the reaction of NO_2 with NEDA remain:

(Eq. 12) $\qquad \dfrac{1}{\gamma} = \dfrac{1}{\gamma_{sol} + \gamma_{rxn}}$ or:

(Eq. 13) $\qquad \gamma = \gamma_{sol} + \gamma_{rxn} = \dfrac{4 \times H \times R \times T \times \sqrt{D}}{\bar{v}} \times \left(\dfrac{1}{\sqrt{\pi \times t}} + \sqrt{k} \right)$.

Two limiting cases are possible, which are explained below.

4.2.2 High Solubility and Slow Chemical Reaction

For a slow chemical reaction in the condensed phase at hypothetically high solubility of NO_2, it is expected, that the liquid phase is homogeneously saturated with NO_2 according to Henry's law (see Fig. 20). In this case, a linear dependency of γ_{NO_2} against the NEDA concentration would be expected due to the homogeneous distribution of NO_2 in the liquid phase. In addition, the uptake coefficient (γ_{NO_2}) would quadratically increase with the thickness of the liquid layer in the stripping coil. At a higher liquid flow, i.e. greater thickness of the liquid layer, the uptake coefficient (γ_{NO_2}) would increases, because more dissolved NO_2 could reacts with an increasing amount of NEDA.
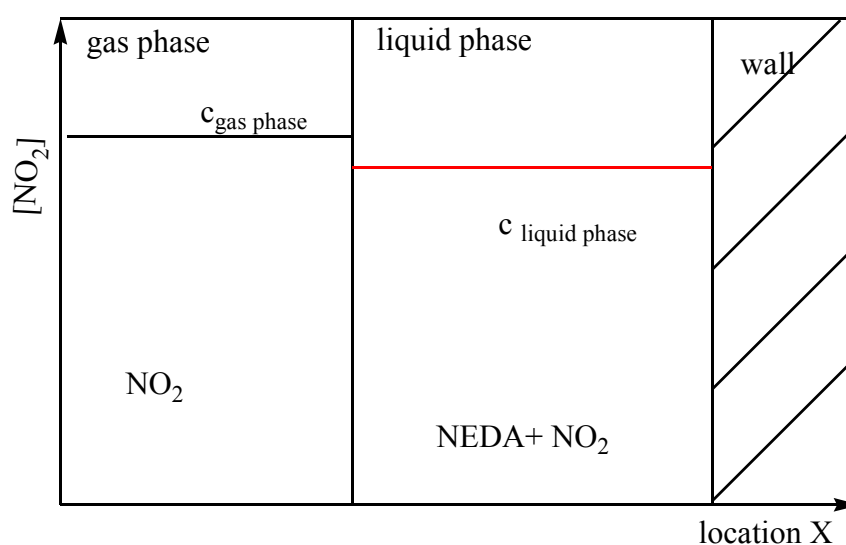
Fig. 20: Schematic illustration of a heterogeneous system, in which the solubility of NO_2 is high and the reaction of NO_2 with NEDA in the liquid phase proceeds slowly. The NO_2 is homogeneously distributed in the condensed phase due to slow consumption reaction (adapted from Peters, 2011).

4.2.3 Low solubility and Fast Chemical Reaction

For a fast chemical reaction of NO_2 in the liquid phase, a concentration gradient of NO_2 is originated due to the diffusion limitation in the liquid phase (see Fig. 21). Thus, not all the NEDA molecules are available for the reaction with dissolved NO_2. The penetration depth or reacto diffusive length, i.e. the distance from the surface, at which the liquid concentration has decreased to 1/e of its Henry's law equilibrium value, decrease with increasing concentration of the reactant NEDA (see Fig. 21).
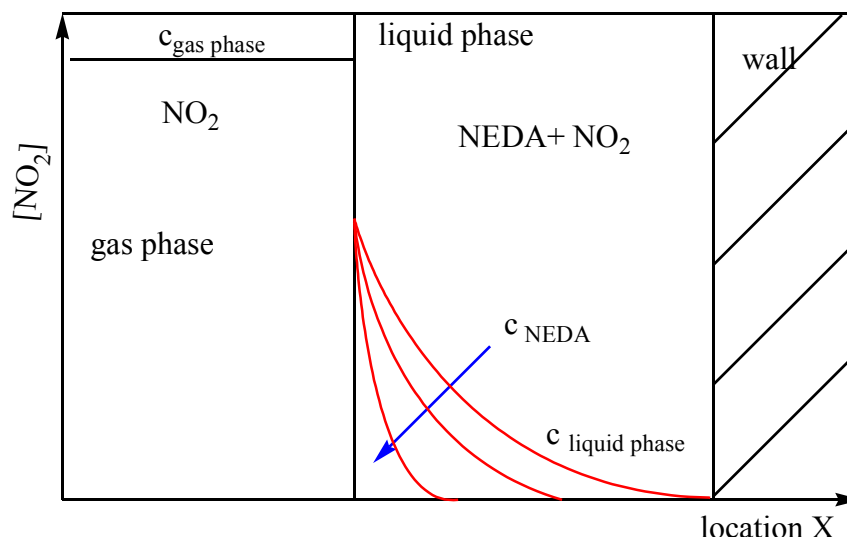
Fig. 21:   Schematic illustration of a fast reaction in the liquid phase at low solubility of NO_2. The concentration gradient of dissolved NO_2 in the liquid phase depends on the concentration of NEDA (adapted from Peters, 2011)

For this limiting case the uptake coefficient (γ_{NO_2}) is a non-linear function of the NEDA concentration in the liquid phase. Caused by the liquid phase diffusion limitation of the uptake and the square root dependence of the average diffusion length with the diffusion time (Einstein-Smoluchowski law) γ_{NO_2} is linearly correlated to the square root of the NEDA concentration:

(Eq. 14) $$\gamma = \frac{4 \times H \times R \times T \times \sqrt{D_{lq}}}{\bar{v}} \times \sqrt{k'' \times [NEDA]}.$$

From the slope of such a plot the second order rate coefficient of the reaction between NO_2 and NEDA can be calculated if the diffusion constant and solubility of NO_2 in the liquid phase are known.

4.2.4   Measurement of the Dependencies

For the determination of the pseudo-first rate constant k' as well as the uptake coefficients, different dependencies were investigated.

4.2.4.1 Air Flow Dependency

When plotting the natural logarithm $[NO_{2(t)}]/[NO_{2(t0)}]$ against the reaction time t according to (Eq. 10), the pseudo-first order rate coefficient, k', is obtained from the negative slope of the linear regression. For higher air flows, i.e. small contact time up to ~0.5 s, the expected linear dependency is observed (see Fig. 22). Thus, a pseudo first order kinetics can be assumed and uptake coefficients of NO_2 on the studied liquid surfaces were calculated from k' according to

(Eq. 11). However, when the air flow decreases, deviation from linearity is evident. This is due to the idealization of the surface to volume ratio, S/V, which was assumed to be independent on the gas flow rate. However, with the change of the gas flow also the surface of the liquid phase is changed. At higher gas flows, the liquid surface is mainly flat, but with smaller flows, ripples are formed on the surface increasing the total surface of the liquid phase. These ripples are caused by the turbulences in the stripping coil and lead to an estimated uncertainty of the surface area of ± 50 %. Therefore, at low gas flows the assumption of a constant surface is no longer possible, resulting in the deviation from linearity in Fig. 22.
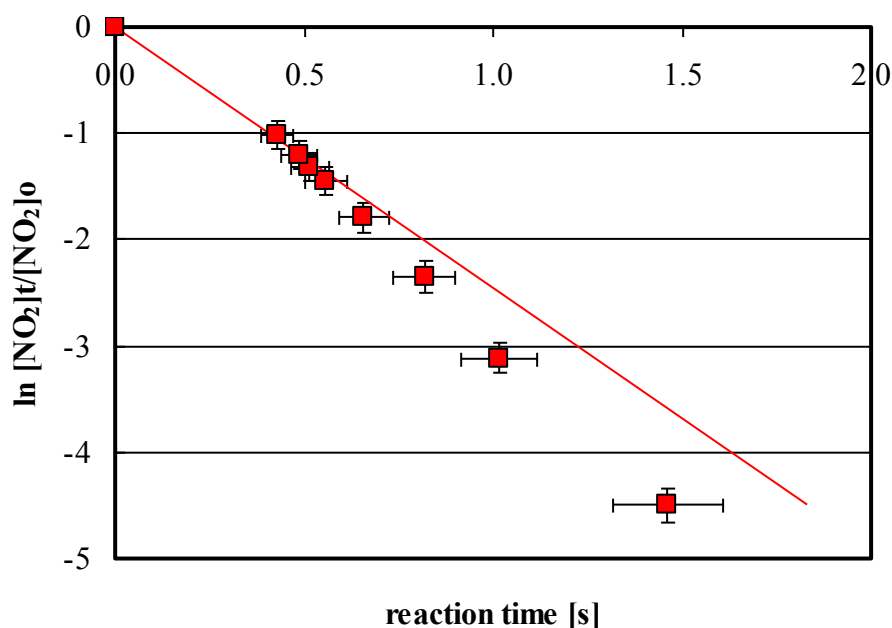
Fig. 22:   Natural logarithm of the ratio of $[NO_{2(t)}]/[NO_{2(t0)}]$ against the reaction time, which was varied by the gas flow rate through the stripping coil.

4.2.4.2 Liquid Flow Rate Dependency

In Fig. 23 the correlation of γ_{NO_2}, calculated from k′ at high gas flow rates (see above), with the liquid flow is shown. Only a small increase of the uptake is observed with increasing liquid flow. In section 4.2, the possible limiting steps of the heterogeneous reactions were discussed. Here a slow reaction and high solubility of NO_2 (see section 4.2.2) should yield a quadratic increase with increasing liquid flow, whereas for a fast reaction and low solubility (see section 4.2.3) the uptake should be independent on the liquid flow. However, neither case 4.2.2 nor case 4.2.3 is observed for all the range of liquid flows investigated. Only for high liquid flow rates almost no dependence of γ_{NO_2} is observed. Thus, case 4.2.3 is assumed here. The slightly curved plot in Fig. 23 is again explained by the variation of the real surface area of the liquid with the liquid flow

rate. Whereas a constant geometric surface of the stripping coil is assumed in the calculations, an increasing surface area with increasing liquid flow is more reasonable, caused by increasing amplitude of the ripples formed in the stripping coil at high liquid flow rate. Thus, the effective available surface will increase together with the calculated uptake coefficient of NO_2. The systematic error arises from the determination of the surface area and is estimated to $\pm50\%$. This high error in the surface area is limiting the overall error of the calculated uptake coefficients. A further evidence for case 4.2.3 is the known low solubility of NO_2 in water ($K_H = (1.6 \pm 0.2) \times 10^{-2}$ M atm^{-1} at 288 K, Squadrito and Postlethwait, 2009).
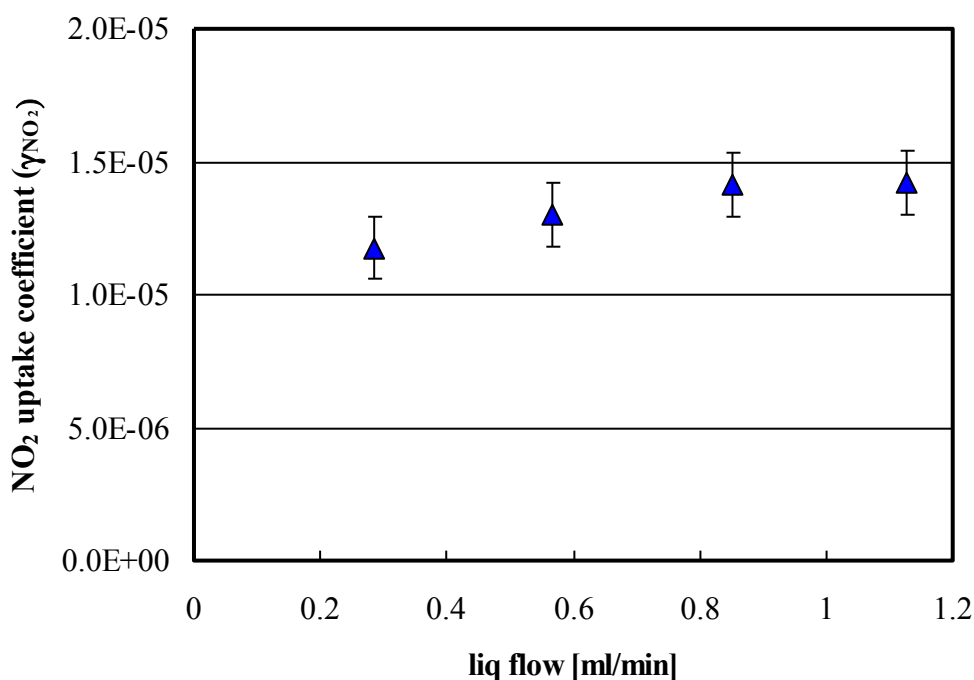
Fig. 23: Variation of NO_2 uptake coefficient with the liquid flow rate.

4.2.4.3 NEDA Concentration Dependency

Fig. 24 shows a plot of uptake coefficient γ_{NO_2} against the concentration of NEDA. The observed non-linear relationship can be explained in terms of the limiting cases discussed in section 4.2. Here a slow reaction and high solubility of NO_2 (see section 4.2.2) should yield a linear correlation between the uptake coefficient and the NEDA concentration, whereas in the case of a fast reaction and low solubility (see section 4.2.3) a linear correlation with the square root of the NEDA concentration is expected. From Fig. 25 the latter can be confirmed, which is in excellent agreement with the conclusion from the last section. From the intercept of the linear regression in Fig. 25 a NO_2 uptake coefficient (γ_{NO_2}) on the used acetic acid/sulphanilamide solution of 7×10^{-7} has been derived, which is higher than the value of $\sim10^{-7}$ reported for the uptake of NO_2 on

pure water by Ammann et al. (2005). The discrepancy can be explained by a very slow reaction of NO_2 with either sulphanilamide or with acetic acid.
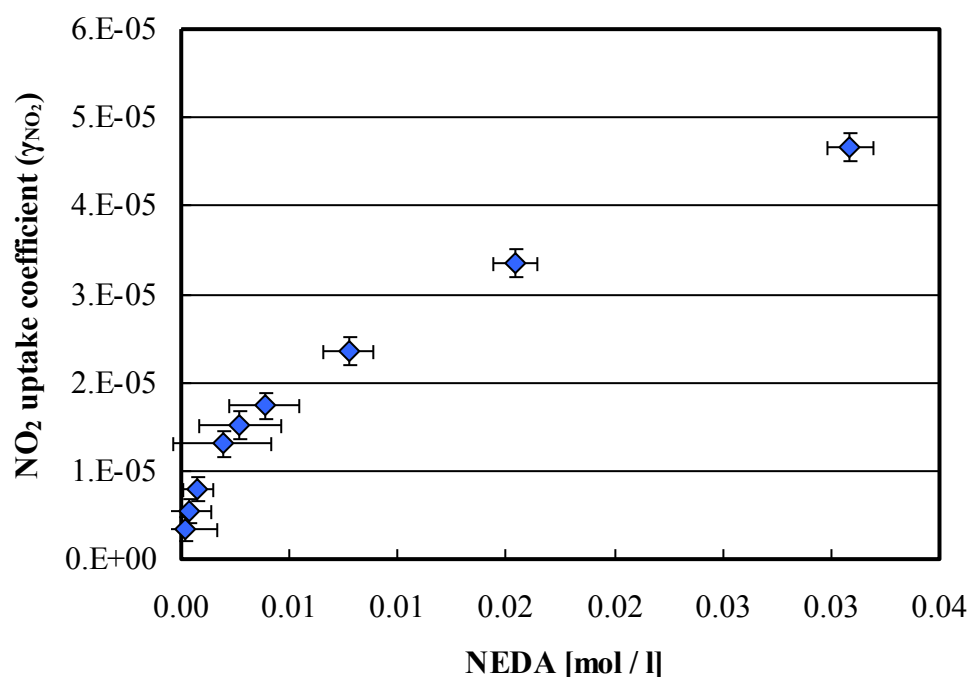
Fig. 24: NO_2 uptake coefficients as a function of [NEDA] at 288 K. Griess-Saltzman Reagent: 7 g/l sulphanilamide, 84 g/l acetic acid, pH = 3, adjusted with NH_3. Air flow = 650 ml/min, liquid flow rate = 0.35 ml/min.
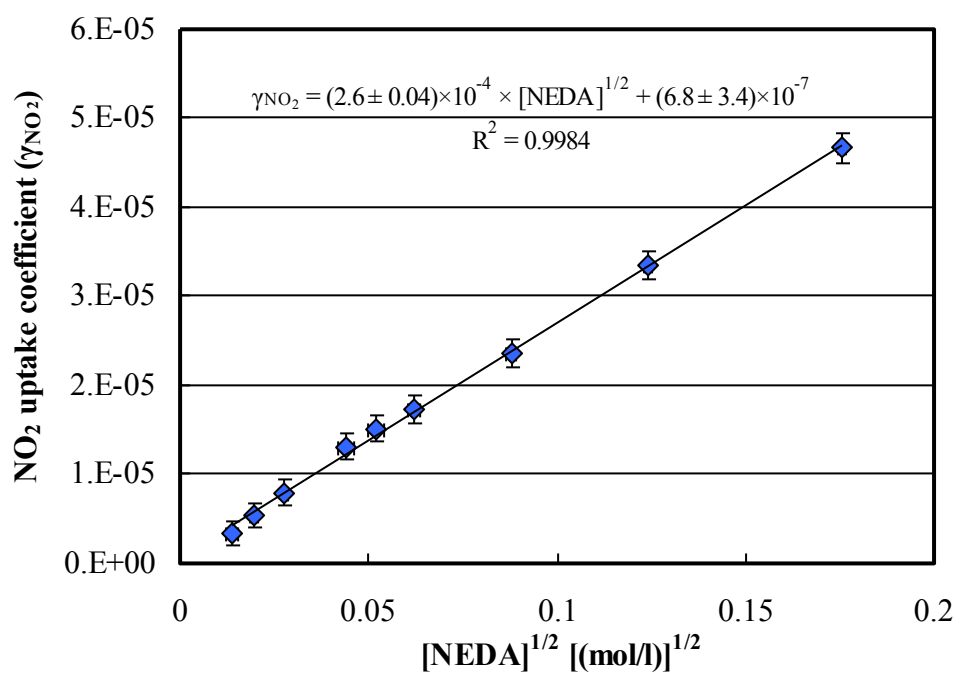
Fig. 25: NO_2 uptake coefficients as a function of $[NEDA]^{1/2}$ at 288 K (same data as in Fig. 24 is shown).

4.2.5 Rate Coefficient of NO₂ + NEDA

The independence of γ_{NO_2} on the liquid flow (see Fig. 23), the linear dependence of γ_{NO_2} with the square root of the NEDA concentration (see Fig. 25) and the known low solubility of NO₂ in water demonstrates that the uptake is limited by liquid phase diffusion for this fast reaction. Similar to the study of Ammann et al. (2005) the second order rate constant k_{NO_2+NEDA} can be calculated from the slope of a plot of γ_{NO_2} against $[NEDA]^{1/2}$ according to equation (Eq. 15):

(Eq. 15) $$\gamma_{NO_2} = m \times \sqrt{[NEDA]} = \frac{4 \times K_{H(NO_2)} \times R \times T \times \sqrt{D_{NO_2}} \times \sqrt{k''} \times \sqrt{[NEDA]}}{\overline{v}},$$

(Eq. 16) $$k'' = \left(\frac{m \times \overline{v}}{4 \times K_{H(NO_2)} \times R \times T} \right)^2 \times \frac{1}{D_{NO_2}},$$

in which $K_{H(NO_2)}$ is the NO₂ Henry's law constant (1.6×10^{-2} M atm⁻¹ at 288 K, calculated using the expression from Squadrito and Postlethwait, 2009), $\overline{v}$ is the mean thermal molecular velocity (364 m s⁻¹ at 288 K), R is the gas constant (8.314 J mol⁻¹ K⁻¹), T the temperature and D_{NO_2} is the aqueous phase diffusion coefficient (1.1×10^{-5} cm² s⁻¹ at 288 K, Cheung et al., 2000, Komiyama and Inoue, 1980). From the slope of the plot shown in Fig. 25 a rate coefficient $k_{NO_2+NEDA} = (3.6 \pm 1.6) \times 10^6$ M⁻¹ s⁻¹ has been determined for the first time using equation (Eq. 16) for the recommended Gries-Saltzman solution (7g/l sulphanilamide and 84 g/l acetic acid). A similar value of k_{NO_2+NEDA} was also determined using higher concentrations of sulphanilamide (10 g/l) and acetic acid (158 g/l). Accordingly, it is proposed that the reaction mainly depends on the NEDA concentration.

In summary, based on the results of the kinetic study a limitation of gas phase diffusion and mass accommodation of NO₂ can be ruled out. The reaction between NO₂ and NEDA is fast, although the rates of the NO₂ reaction are relatively low caused by the low solubility of NO₂ in water. Thus, although the reaction is very fast, a high surface to volume ratio and a low gas flow rate/high reaction time is necessary to obtain quantitative uptake of NO₂ in the stripping coil of the NO₂ LOPAP instrument. The uptake of NO₂ is limited by the diffusion of NO₂ in the liquid phase and the reaction with NEDA occurs only in a very thin layer at the surface of the liquid phase. The thickness of the layer, for which NO₂ decrease to 1/e of its Henry's law surface concentration, i.e. the reacto diffusive length, can be calculated using the following equation

(Eq. 17) $$L = \sqrt{\frac{D_{lq}}{k'}},$$

where D_{lq} is the diffusion coefficient of NO₂ in water (see above) and k' is the pseudo first order rate constant of the reaction between NO₂ and NEDA. A value of 18 μm is calculated for the

recommended Griess-Saltzman solution, which is lower than the thickness of the liquid layer in the stripping coil (56 μm), further supporting the conclusion of a fast diffusion limited surface reaction. Based on these results, is concluded that the uptake is independent of the liquid flow, which can be changed in order to adjust the time response and the sensitivity of the instrument, without significantly changing other parameters, like for example the sampling efficiency.

4.3   Calibration

The LOPAP instrument shows a linear response with the NO_2 concentration for the entire measuring range (Fig. 26). Also for the calibration by liquid nitrite standards diluted in the Griess-Saltzman sampling solution a good linearity was obtained up to nitrite concentrations of 0.1 mg/l (Fig. 27). For higher nitrite concentrations non-linearity of the calibration was observed caused by losses, probably through the secondary reaction (R 32).

$$\text{absorbance} = 1.11 \times 10^{-05} \times [NO_2] \text{ pptv}$$
$$R^2 = 0.9999$$
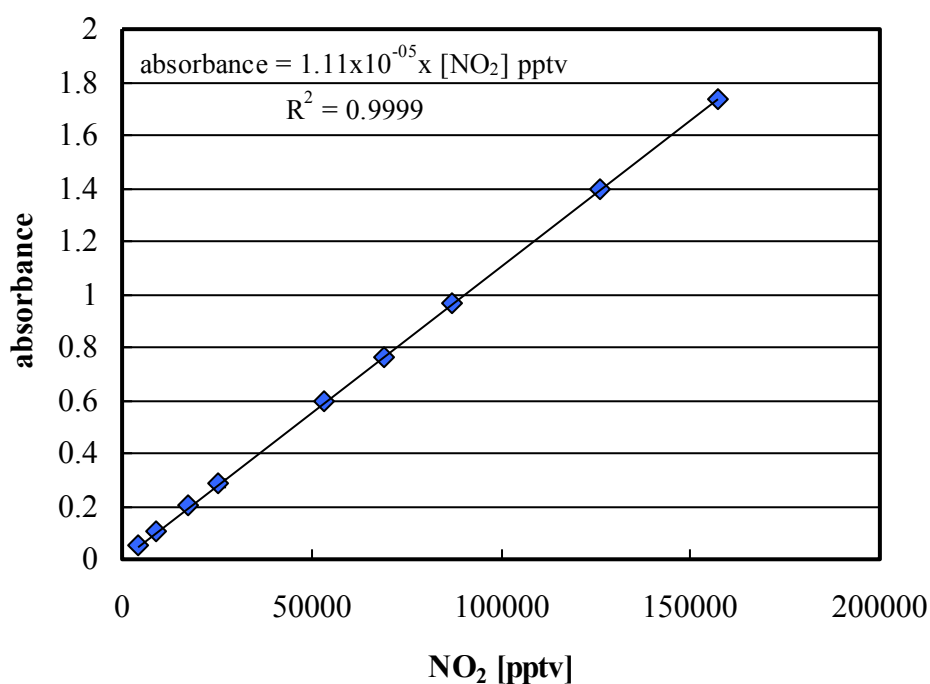
Fig. 26: NO_2 concentration dependency of the LOPAP signal using the recommended sampling solution (see Tab. 2) and instrument parameters (see Tab. 3, liquid flow = 0.35 ml/min).
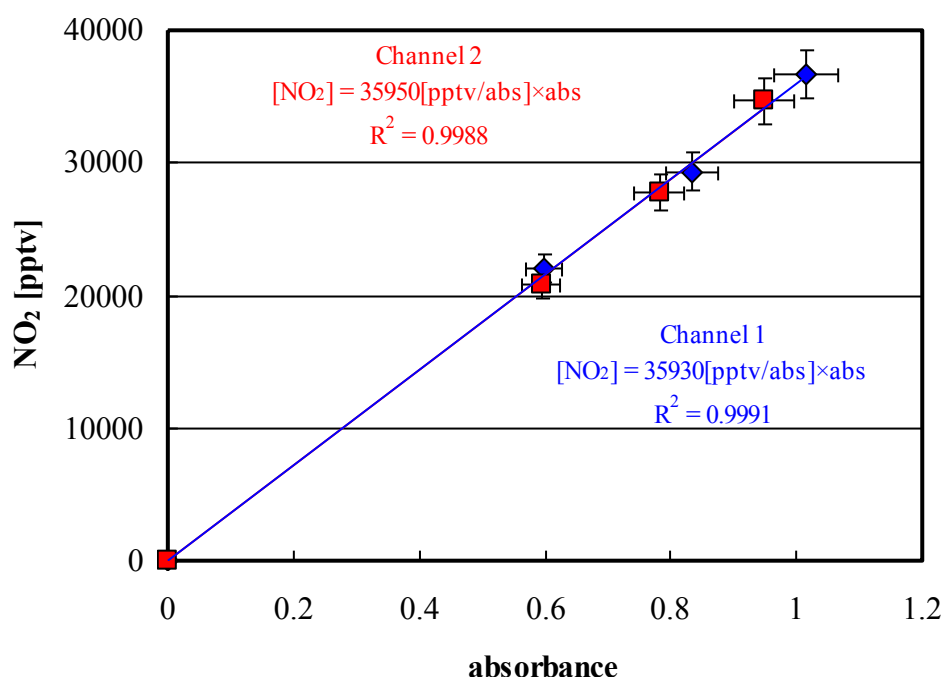
Fig. 27:   Calibration by liquid nitrite standards. Griess-Saltzman Reagent: 1 g/l NEDA, 5 g/l sulphanilamide, 84 g/l acetic acid, pH = 3, adjusted with NH_3. Air flow = 650 ml/min, liquid flow = 0.45 ml/min.

Caused by the linear response, the NO_2 instrument can be calibrated simply by a two point calibration (zero air + calibration) with commercial available nitrite standards (accuracy ±1 %) and by determination of the flow rates of the gas phase and of the stripping solution. This is a significant simplification in comparison with other NO_2 instruments, which usually are calibrated using NO_2 calibration gas mixtures. These mixtures are known to have a low long-term stability. In addition, significant deviations from the concentrations specified by manufacturer are often observed. Alternatively, more stable NO calibration gas mixtures and ozone titration is used for commercial NO_2 instruments, for which, however, an additional titration unit and an additional NO instrument are necessary.

4.4   Interferences

The present instrument is designed as a two channel instrument. In Channel 1, NO_2 and interferences are sampled, while in Channel 2 ideally only the interferences are measured under the assumption of a complete uptake of NO_2 in channel 1 and a small uptake of the interferences. The interferences are specified as the interference signal measured as NO_2 divided by the mixing ratio of the interfering compound in % (= 100 × signal NO_2 pptv/compound pptv). The

interferences are listed in Tab. 4, either as interference in Channel 1 as defined above, or as "real interference" after subtraction of Channel 2 from Channel 1. All values given in this section correspond to a gas flow rate of 0.5 l/min, a liquid flow rate of 0.4 ml/min and a temperature of 15 ^{o}C. It is important to note that in reality Channel 1 measures the sum of only 97 % of the NO_2 plus potential interferences, while in Channel 2, 3 % of the NO_2 plus interferences are determined. Assuming a small uptake of interfering compounds, their concentrations are almost constant in both coils, thus, the difference between the two channels corrected for the sampling efficiency of NO_2 and the loss in the $HONO/O_3$ scrubber gives a measure of the true NO_2 concentration.

4.4.1 HONO Interference

A well known interference for the Griess-Saltzman method is ambient HONO (Milani and Dasgupta, 2001), which is also formed during NO_2 detection as an intermediate in the Griess-Saltzman solution, reaction (R 31). Therefore an upstream stripping coil ("$HONO/O_3$ Scrubber") is placed in the NO_2 instrument, which is operated with a solution of sulphanilamide in acetic acid (sulphanilamide 10 g/l, potassium indigo-trisulphonate 0.6 g/l, acetic acid 158 g/l), see reactions (R 27) and (R 28). Acidic sulphanilamide solutions were already used as efficient HONO sampling solution (sampling efficiency >99 %) in the HONO-LOPAP instrument (Heland et al., 2001; Kleffmann et al., 2002; Kleffmann et al., 2006). The HONO interference was tested with a pure HONO source, which is explained in detail elsewhere (Kleffmann et al., 2004). Briefly, a nitrite solution (0.1 mg/l) is mixed with diluted sulphuric acid (H_2SO_4: 0.02 N) in a stripping coil which is operated under synthetic air (see Fig. 28). At low HONO concentrations, impurities by NO_x were found to be <1%.

With the use of the upstream "$HONO/O_3$ Scrubber", a minimum interference of 0.092 ± 0.090 % could be observed in Channel 1, which is in good agreement with the high sampling efficiency of HONO obtained for similar experimental conditions for the HONO-LOPAP instrument (sampling efficiency: 99.8 %). On the other hand, no interference could be observed in Channel 2, which can be explained by the high sampling efficiency of HONO in Channel 1 of the NO_2 instrument. The remaining real HONO interference of ca. 0.1 % represents even an upper limit, since the HONO source still could generate traces of NO_2. In addition, even if true, the HONO interference can be completely neglected for typical $HONO/NO_2$ ratios of ≤ 10 % in the atmosphere.
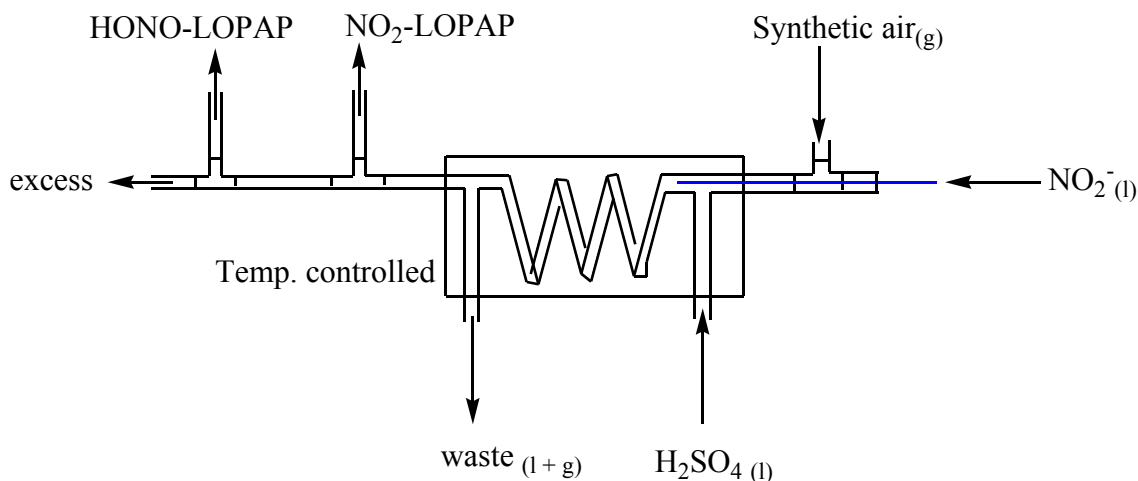
Fig. 28:   Scheme of the set up of the pure HONO source used for the HONO interference tests.

4.4.2   Ozone Interference

The ozone interference was tested with pure ozone mixtures, which were generated by the irradiation of pure O_2 with an Hg lamp (Pen-ray) and dilution with synthetic air. Without the HONO/O_3 scrubber, a relatively large ozone interference (ca. 1 %) could be observed in Channel 1 (see Fig. 29 and Fig. 31), which is explained by the oxidation of NEDA leading to a change in the absorption spectra of the Griess-Saltzman solution. In Channel 2 there is no signal due to complete uptake of ozone in Channel 1, so that the ozone interference could not be corrected by the two channel system. Initially, the value of 1 % seemed to be small; however, measurements in remote regions, in which the ozone concentration can be up to three orders of magnitude higher than those of NO_2, would be strongly affected by this ozone interference. Therefore, it was necessary to efficiently remove ozone through the addition of a suitable reagent to the HONO/O_3 scrubber solution.

Based on the iodometric method used for O_3 detection (Johnson et al., 2002), first tests have been done with the addition of potassium iodide (KI) to the HONO/O_3 scrubber solution. Even though there was a decrease of the O_3 interference with increasing KI concentration (see Fig. 29), this method was not successful, since iodine (I_2) formed in the reaction of KI with O_3, partly degassed from the HONO/O_3 scrubber leading to additional light absorption and interference in Channel 1 of the instrument. In addition, the uptake of NO_2 in the HONO/O_3 scrubber increased with increasing KI concentration leading to smaller sensitivity of the NO_2-LOPAP (see Fig. 30). Heterogeneous uptake of NO_2 has already been observed with halide ions in other studies

(Yabushita et al., 2009). Caused by these I_2 interferences and the significant loss of NO_2 in the scrubber solution, the use of KI as O_3 scrubber reagent is not recommended.
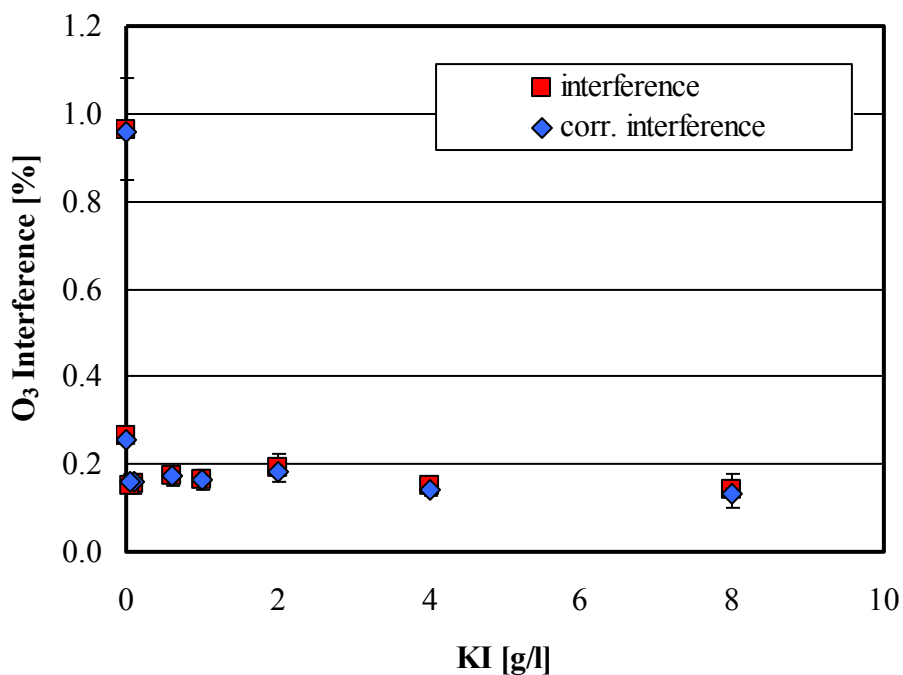
Fig. 29: O_3 interference as a function of KI concentration ($[O_3]$ = 180 ppbv, liquid flow = 0.4 ml/min).
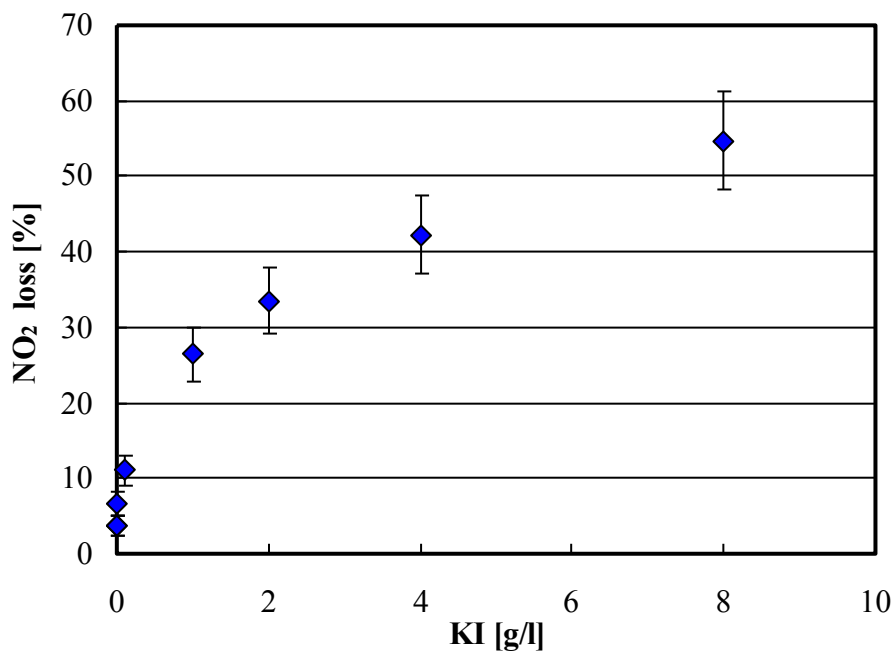
Fig. 30:   Loss of NO_2 in the HONO/O_3 scrubber as a function of [KI] ($[O_3]$ = 180 ppbv, liquid flow = 0.4 ml/min).

Alternatively, an Indigo solution has been used for quantitative detection of O_3 in aqueous solutions (Bader and Hoigné, 1981). Therefore, potassium Indigo-trisulphonate was chosen as scrubber solution and the ozone interference was tested as function of the Indigo concentration. A strong decrease of the O_3 interference with increasing Indigo concentration is observed (Fig. 31). With an Indigo concentration of 0.6 g/l an ozone interference of only 0.006 % was observed. This interference is so low that even in clean air regions with very large O_3/NO_2 ratios only small corrections are necessary. Similar to HONO, the ozone uptake in the $HONO/O_3$ scrubber is independent of the liquid flow, so that for the routine operation of the NO_2 instrument only small liquid flow rates (0.05 ml/min) of the scrubber solution are necessary.

As $HONO/O_3$ scrubber solution finally a mixture of sulphanilamide (10 g/l) and Indigo trisulphonate (0.6 g/l) in acetic acid (158 g/l) was selected. With this scrubber solution an uptake of NO_2 of only 4 % was determined, which is corrected during the data evaluation.
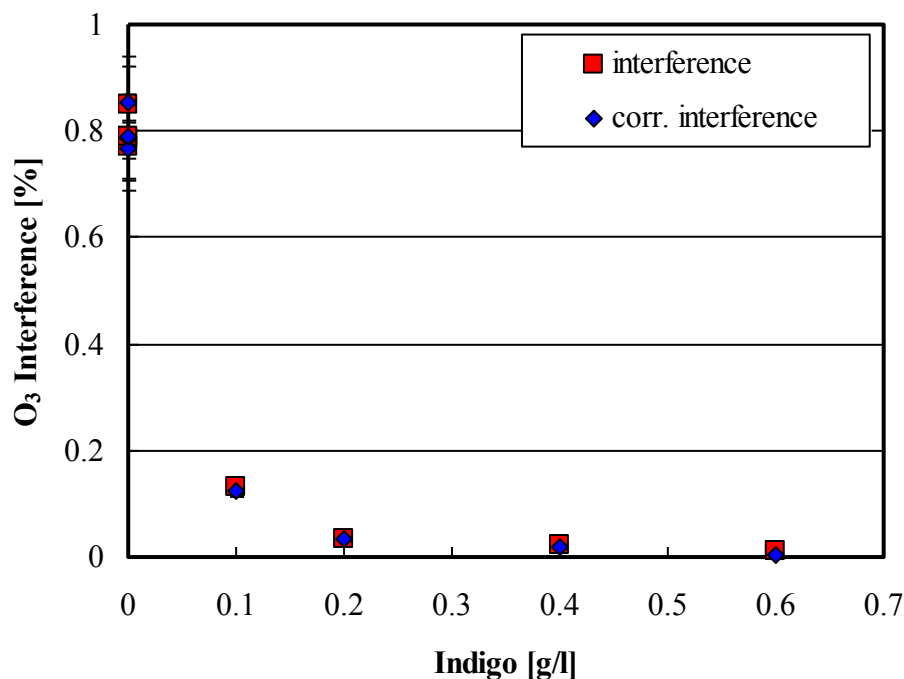
Fig. 31: O_3 interference as a function of Indigo concentration ($[O_3] = 240$ ppbv).

Beside HONO and O_3, further interferences were tested in the laboratory in a 1080 l photoreactor and are listed in Tab. 4. All interferences tested can be neglected under atmospheric conditions.

4.4.3   Glyoxal, Toluene, α-Pinene and n-Butane in the Presence of NO_x

During the smog chamber experiment (see section 4.5.2) the interferences against glyoxal (1.1 ppmv), toluene (0.64 ppmv), n-butane (0.56 ppmv) and α-pinene (0.43 ppmv) in the presence of NO_x (500 ppbv) were investigated. No interferences could be observed against hydrocarbon

under any conditions. The upper limits of the interferences of the LOPAP instrument are summarized in Tab. 4.

4.4.4 Hydrogen Peroxide (H_2O_2) and Propene ($NO_x + H_2O_2$) Interferences

The interference of H_2O_2 (19.3 ppmv) was also measured in the 1080 l photoreactor in a similar experiment than the one shown in section 4.5.2. Propene (2.78 ppmv) was injected when H_2O_2 and NO (340 ppbv) were already present under dark conditions. While no interference against propene could be observed, H_2O_2 showed a very small interference of (0.0044 ± 0.0002) %, which can be however neglected under atmospheric conditions (see Tab. 4).

4.4.5 Peroxyacetyl Nitrate (PAN) Interference

The PAN interference was also tested in the 1080 l photoreactor, in which PAN was generated using an illuminated mixture of hydrogen peroxide (H_2O_2), nitric oxide (NO), and propene in synthetic air. Caused by the low precision of the FTIR in this complex reaction mixture, only an upper limit the PAN interference of <0.5 % could be determined (see Tab. 4), i.e. the true PAN interference may be much lower. Even assuming a PAN interference of 0.5 % and a very high PAN/NO_2 ratios of up to 10, sometimes observed in the upper troposphere (Zhang et al., 2008), the correction of the NO_2 signal of the LOPAP instrument would be <5 %, which is still in between specified uncertainty (10 %) of the LOPAP instrument. For the future, the PAN interference should be more exactly quantified using a pure PAN source.

4.4.6 2-Nitro-toluene and 3-Methyl-2-Nitrophenol

Gas phase mixtures containing pure 2-nitrotoluene and 3-methyl-2-nitrophenol were generated by flushing 2.5 l/min synthetic air regulated by a flow controller, over liquid or solid samples, which were immersed in a temperature regulated water bath. Interferences against these nitroaromatic species were found to be non significant (see Tab. 4).

4.4.7 Summary of the Interference Results

After the elimination of the known, significant HONO and O_3 interferences by the use of the upstream "HONO/O_3-Scrubber", all tested interferences were found to be of minor importance under atmospheric conditions. In addition, even for those small interferences, which could be quantified (see Tab. 4), no signals were observed in the interference Channel 2 of the instrument.

Tab. 4:   Summary of the interferences tested for the NO$_2$-LOPAP instrument.

component	interference Ch1 [%]	real interference Ch1-Ch 2 [%]
ozone	0.0057±(0.0005)	0.0058±(0.0007)
H$_2$O$_2$	0.0044 ± 0.0002	0.0040 ± 0.0002
HONO	0.092 ± 0.090	0.088 ± 0.081
PAN	<0.48	<0.48
3-methyl-2-nitrophenol	<0.0006	<0.0006
2-nitrotoluene	<0.00001	<0.00001
glyoxal (+NO$_x$)	<0.11	<0.11
toluene (+NO$_x$)	<0.04	<0.04
α-pinene (+NO$_x$)	<0.06	<0.06
n-butane (+NO$_x$)	<0.04	<0.04
propene (+NO$_x$+H$_2$O$_2$)	<0.01	<0.01
Complex photosmog mixture (irradiation of NO$_x$, glyoxal, n-butane, α-pinene, toluene), NO$_2$ max. = 135 ppbv	deviation <4 ppbv (DL of the FTIR)	deviation <4 ppbv (DL of the FTIR)

Thus, the "real interference" was always of the same magnitude compared to the interference observed in Channel 1. This shows that Channel 2 is not necessary, at least for those interferences investigated. This conclusion is confirmed also by the measurements under even more complex conditions in the urban atmosphere and in photosmog experiments in the 1080 l photoreactor (see section 5). In these experiments, the signal in Channel 2 was always on average similar to the expected loss of NO$_2$ in Channel 1, caused by the sampling efficiency of still <100 %. Accordingly, also in the real atmosphere and in smog chamber experiments Channel 2 is not necessary and the instrument could be further simplified in the future, which is in contradiction to the HONO-LOPAP instrument, for which interferences in Channel 2 were found to be significant (e.g. Kleffmann and Wiesen, 2008). Reasons for the missing interferences may be:

a) other interferences are also removed in the "HONO/O$_3$ scrubber",

b) the Griess-Saltzman reaction is not sensitive to other trace species, for example PAN, which would interfere only under alkaline sampling conditions (Frenzel et al., 2000), which do not prevail in the LOPAP instrument,

c) all known reactions of NO_2 with other interfering trace species, like e.g. SO_2, activated aromatic species, alkenes, etc. are also only fast under alkaline conditions. In addition, these reactions lead to the formation of nitrite/HONO, which is also generated by the Griess-Saltzman reaction, see reaction (R 31) and thus will not interfere.

4.5 Validation of the New Instrument

4.5.1 Intercomparison in the Atmosphere

During the period March 10-13, 2007 an intercomparison campaign of the new NO_2-LOPAP instrument was carried out with a commercial chemiluminescence instrument (ECO-Physics: AL 770 ppt / PLC 760) at the University of Wuppertal. The commercial instrument was equipped with a photolytic converter for the selective detection of NO_2. For small to medium pollutant concentrations, good agreement with the DOAS technique was observed for this chemiluminescence instrument (Kurtenbach et al., 2001) and thus, high accuracy of this instrument is assumed for the experimental conditions applied. Only for very high pollutant concentrations, as they occur in traffic tunnels, at kerbside stations or in laboratory and smog chamber studies, this instrument exhibits negative interferences, which are caused by photochemical reactions in the photolytic converter (Kurtenbach et al., 2001; Kleffmann et al., 2001; Bejan et al., 2006b; Villena et al., 2012). However, for the relatively low pollutant concentrations occurring during the intercomparison campaign these interferences were neglected. The sampling site was on the balcony of the 5th floor of the main campus of the University of Wuppertal.

During all the period of the intercomparison, very good agreement was observed between both instruments in terms of absolute concentrations (see Fig. 32, Fig. 33 and Fig. 34) and temporal variation of the concentration (Fig. 33). Only for very fast variations of the NO_2 concentration, deviations were observed due to the smaller time resolution of the LOPAP instrument (e.g. Fig. 33, ca. 10:00 and ca. 12:15). It is well-known that due to the temporally shifted measurements of NO and NO_x with the one channel ECO Physics instrument, short term variations of pollutants often lead to unrealistic strong concentration peaks for this instrument. From a correlation plot of the 5 min averaged data a mean deviation between both instruments of only 2 % has been determined (Fig. 34), which is clearly within the errors of both methods. In conclusion, the LOPAP instrument could be successfully validated in the atmosphere under moderately polluted

conditions with the help of a commercial chemiluminescence instrument with photolytic converter.

The LOPAP instrument was used as a two channel system for the correction of unknown interferences during the intercomparison campaign. However, during the whole campaign, only a small signal in the interference channel (Channel 2) was observed, which corresponded exactly to the loss of NO_2 from Channel 1 caused by the sampling efficiency of the instrument. During this campaign the instrument had a sampling efficiency of (95 ± 1) % (old stripping coil) and an average value of the ratio Channel 2/Channel 1 of (4.7 ± 1.2) % was determined (see Fig. 35). Thus, in between the experimental errors no interferences could be observed in the real atmosphere.
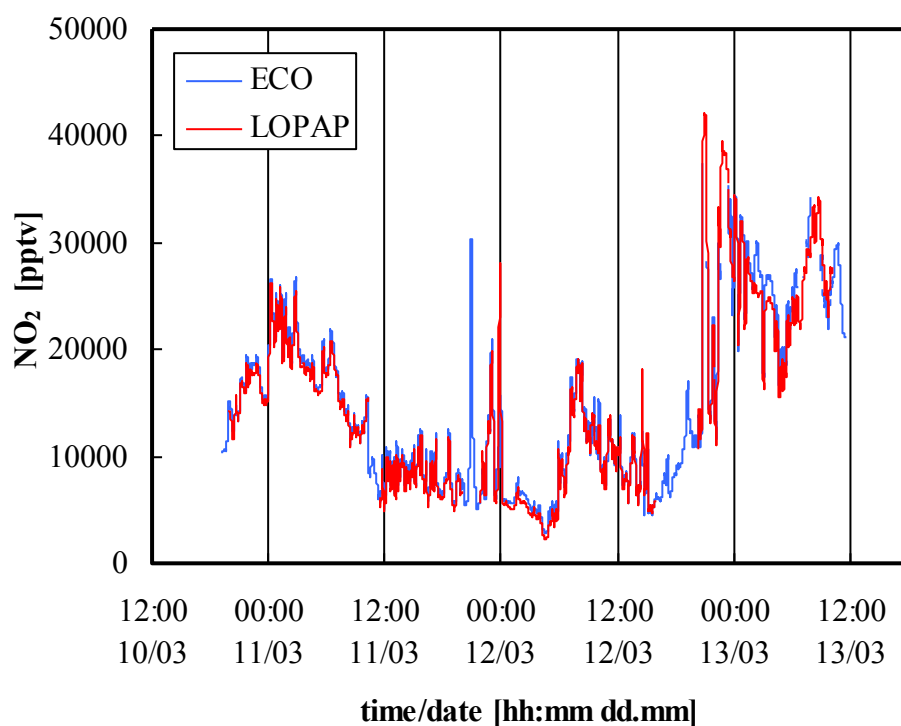
Fig. 32: NO_2 concentrations measured with the NO_2-LOPAP and the Eco-Physics instruments during the ambient intercomparison campaign at the University of Wuppertal.
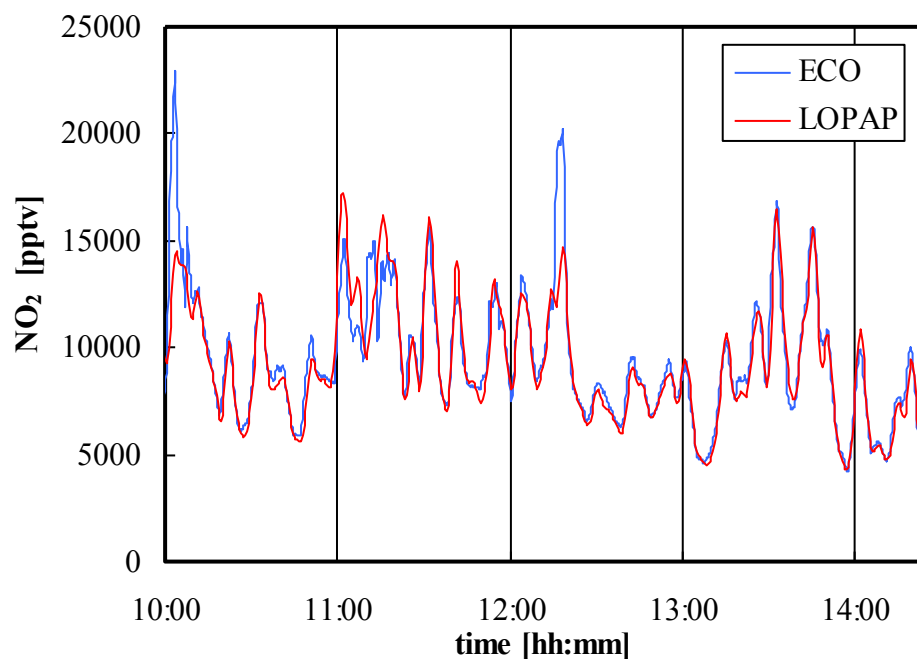
Fig. 33:   Selected time interval of the NO_2 concentrations measured with the NO_2-LOPAP and the Eco-Physics instruments during the ambient air intercomparison campaign at the University of Wuppertal.
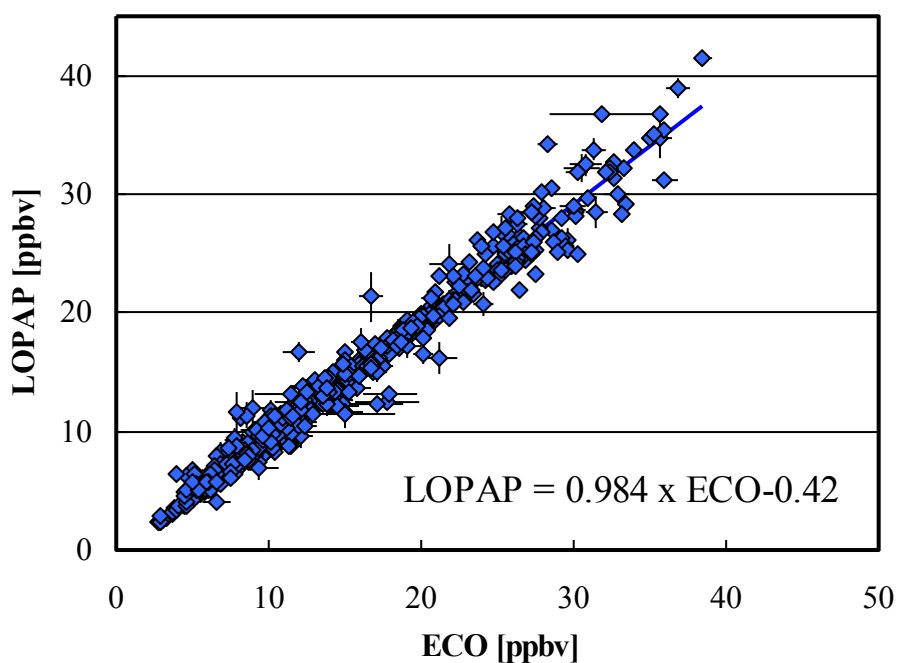
Fig. 34:   Correlation of all 5 min averaged NO_2 data of the NO_2-LOPAP against the Eco-Physics instrument. The error bars represent only the precision of the instruments. A weighted orthogonal regression analysis was used, for which the errors of both instruments were considered (Brauers and Finlayson-Pitts, 1997).
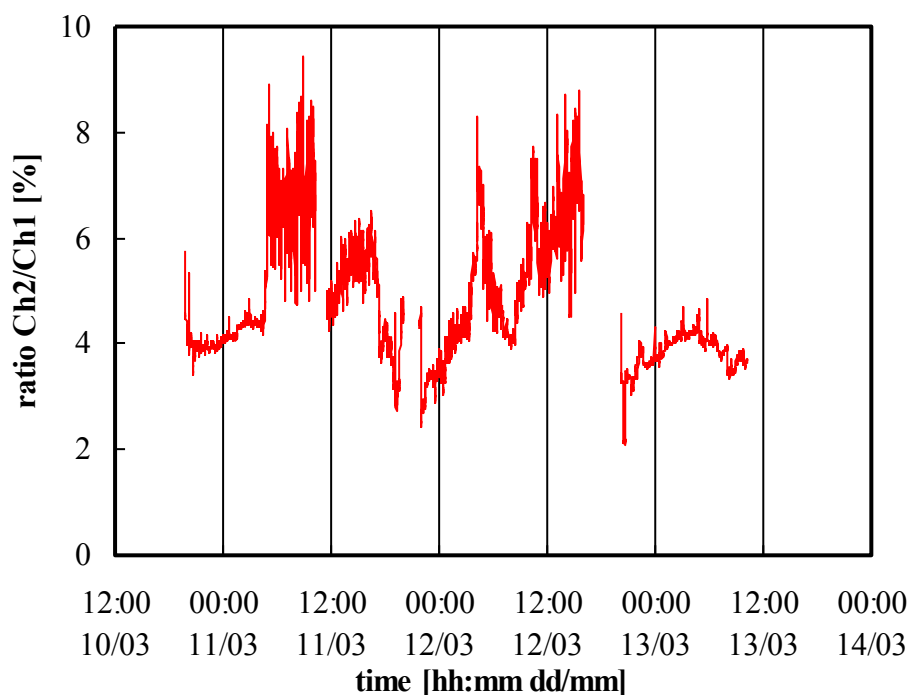
Fig. 35:   Ratio Ch2/Ch1 during the intercomparison campaign carried out on the balcony, of the main campus of the University of Wuppertal.

4.5.2   Intercomparison in a Complex Photosmog Experiment

To better understand the interferences of commercial chemiluminescence instruments mentioned in section 2.2.2 and to validate the new NO_2-LOPAP instrument, an intercomparison campaign with four NO_2 analysers (ECO, Ansyco blue-light, Luminol, LOPAP) and the FTIR technique was conducted under complex photo-smog conditions in the 1080 *l* photoreactor. The spectroscopic FTIR technique was used as a reference in these measurements, since sampling artefacts can be ruled out for this non-intrusive method. In addition, optical interferences by the overlap of absorption bands in this extremely complex mixture were excluded, since a known added amount of NO_2 at the end of such a photo-smog experiment could be quantified correctly using the FTIR.

An example of a photo-smog experiment is shown in Fig. 36, in which a complex volatile organic compound (VOC)/NO_x mixture was irradiated with UV/VIS light. In the experiment, NO (500 ppbv) with ~6 % impurities of NO_2, glyoxal (1.1 ppmv), toluene (0.64 ppmv), n-butane (0.56 ppmv) and α-pinene (0.43 ppmv) were introduced sequentially into a dark chamber. Before the lamps were switched on, a second NO injection (330 ppbv) was made to compensate for the dilution of the mixture, caused by the sample flow to the external instruments. The radical initiated degradation of the VOCs leads to the formation of O_3 and peroxy radicals (HO_2, RO_2), and further reaction with NO results in increasing levels of NO_2 in this photo-smog mixture.

When the reaction mixture was irradiated, the sample flow to all the external instruments was diluted by accurately known factors of 1.2 - 3.5 for certain periods to check for the linearity of the interferences affecting the different instruments (see grey shaded area in Fig. 36). Theoretically, the concentrations calculated in the photoreactor should not depend on the dilution ratio, when corrected for. In contrast to the external instruments, the FTIR measurements were not affected by the dilution tests.

Since hundreds of products including potential interfering photo-oxidants, like PAN, are formed during the irradiation, this complex photo-smog experiment is a good test to validate a new instrument under conditions that are even more complex and with higher pollution levels compared to the real atmosphere.
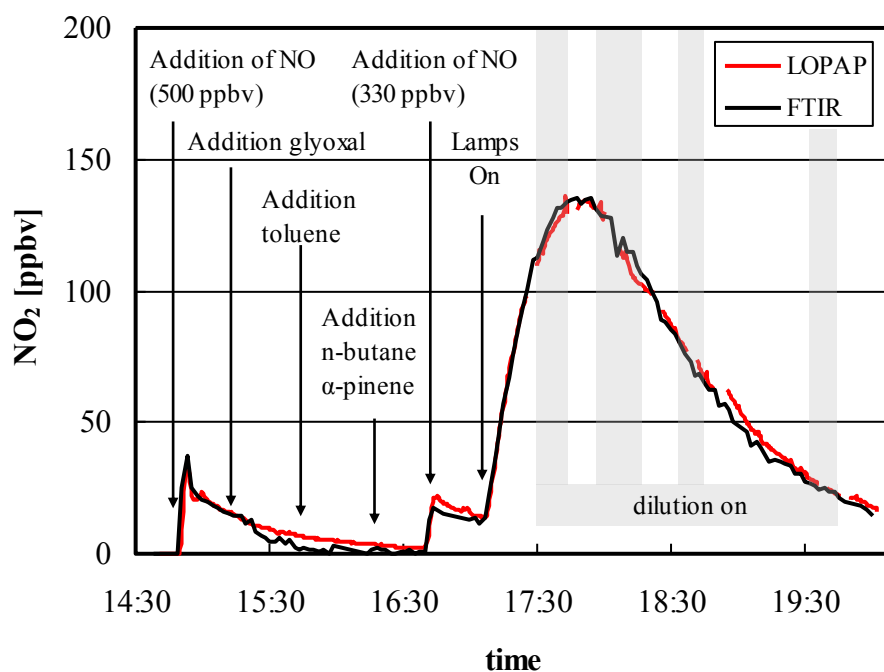
Fig. 36   Intercomparison of the NO$_2$-LOPAP instrument with FTIR spectrometry during a complex photo-smog experiment. The grey shaded area indicate the periods, when the sample air of all the external instruments was diluted with synthetic air by factors of between 1.2-3.5, which was considered for the concentration calculations.

In contrast to the chemiluminescence instruments (see section 4.6.1) the LOPAP instrument showed excellent agreement with the FTIR technique (see Fig. 36) with an average deviation of 4 % (see Fig. 37). Lower concentrations were observed for the FTIR technique compared to the LOPAP instrument only while adding glyoxal (Fig. 36). However, since glyoxal does not react with NO$_2$ in the dark and since the LOPAP signal remained unchanged in the presence of glyoxal, this difference can be explained by optical interferences of the FTIR instrument

resulting from the overlap of absorption bands from glyoxal and NO_2. These interferences accounted for max. 5 ppbv, which is close to the precision of the FTIR instrument. In addition, the optical interference decreased with time because of the continuous dilution of the reaction mixture and thus, did not influence the accuracy of the FTIR during the photo-smog phase of the experiment.

$$LOPAP = 0.96 \times FTIR + 2.5 \text{ ppbv}$$
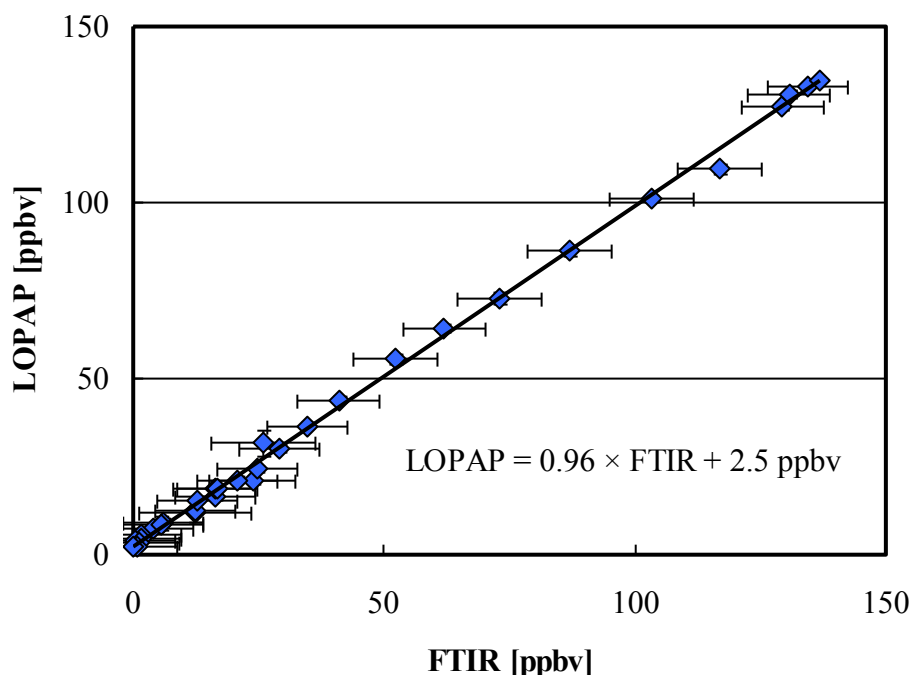
Fig. 37: Correlation of all LOPAP and FTIR NO_2 data during the complex photo-smog experiment, shown in Fig. 3. The error bars only represent the precision of both instruments.

In addition to the general good agreement with the FTIR technique, no changes of the corrected measurement signal of the LOPAP instrument occurred during the dilution tests. Accordingly, a significant interference can be excluded for the LOPAP instrument even for this very complex reaction mixture. This is supported by the fact that an average value of the ratio Channel 2 / Channel 1 of (9 ± 1.4) % was determined (see Fig. 38), which corresponds to the loss of NO_2 in Channel 1 considering that during the experiment the sampling efficiency of the stripping coil was (91 ± 1) % due to it was used an air flow of 700 ml/min. Thus, since no interferences were observed in Channel 2 of the instrument neither during the smog-chamber experiments (see Fig. 38), nor in the atmosphere (see section 4.5.1), an even simpler one-channel set-up could be used in the future.

Based on the results of the intercomparison exercises presented above, the new LOPAP is not only suitable for atmospheric applications but also for complex smog-chamber experiments, where commercial NO_2 instruments have severe problems.
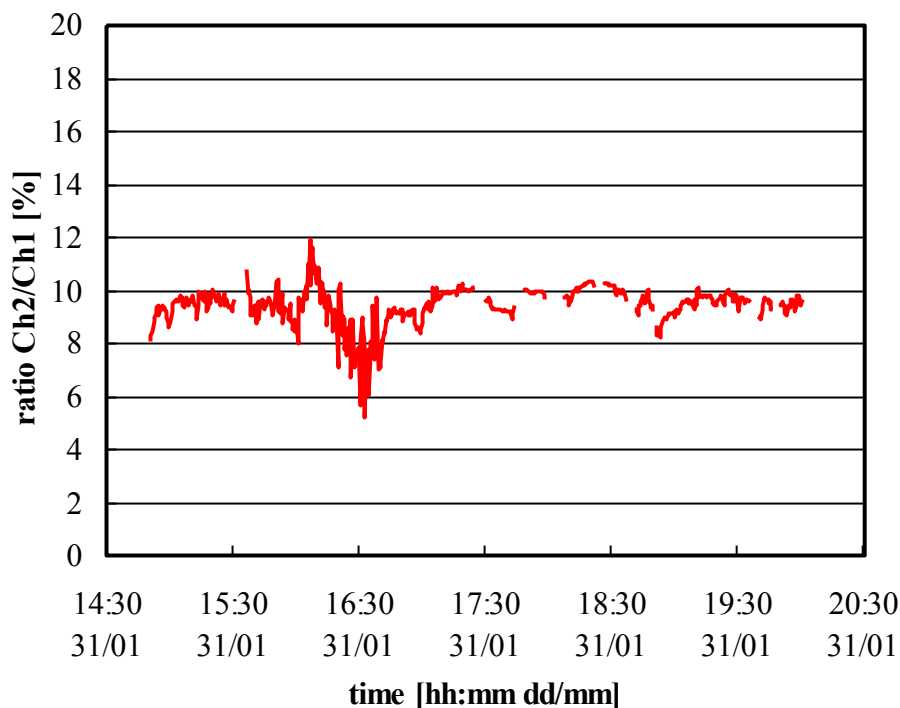
Fig. 38:   Relative interferences measured in Channel 2 of the LOPAP instrument.

4.6   Uncertainties of Commercial NO_2 Instruments

4.6.1   Smog Chamber

Whereas excellent agreement was obtained between the NO_2 measurements performed with the LOPAP and FTIR techniques, substantial deviations were observed for the other NO_2 instruments used (see Fig. 39).

For the Luminol instrument lower NO_2 concentrations could be initially observed when adding high NO concentrations (500 ppbv) (Fig. 39, first addition of NO). This is due to the quenching of the chemiluminescence of the luminol by NO, which decreases the sensitivity of the instrument (Kleffmann et al., 2004). This phenomenon was also observed for high concentrations of nitroaromatic species in another recent study (Bejan et al., 2006b). Since the quenching efficiency of different trace gases is not well known, the Luminol technique should not be used for smog-chamber experiments, at least when ppmv levels of trace gases are used.

Deviations also occurred for the Luminol instrument in comparison with the FTIR during the photo-smog period. In contrast to the Ansyco blue light and ECO instruments, the Luminol

technique suffered from positive interferences during the course of the photo-smog experiment. To the end of the experiment the NO_2 data of the Luminol instrument was more than two times higher than the FTIR data. These interferences may be explained by photo-chemical formation of ozone and different PAN like species (peroxyacylnitrates) (Fehsenfeld et al., 1990). Under the very alkaline sampling conditions prevailing in the Luminol instrument, it is well known that PAN and other peroxyacylnitrates decompose (Frenzel et al., 2000). The observed positive interferences of the Luminol technique showed a clear non-linear behaviour, which decreased with increasing dilution of the sample (see Fig. 39, dilution on). In contrast, for interferences, which increase linearly with the concentration of the interfering species, the dilution tests should not affect the calculated concentrations in the chamber.
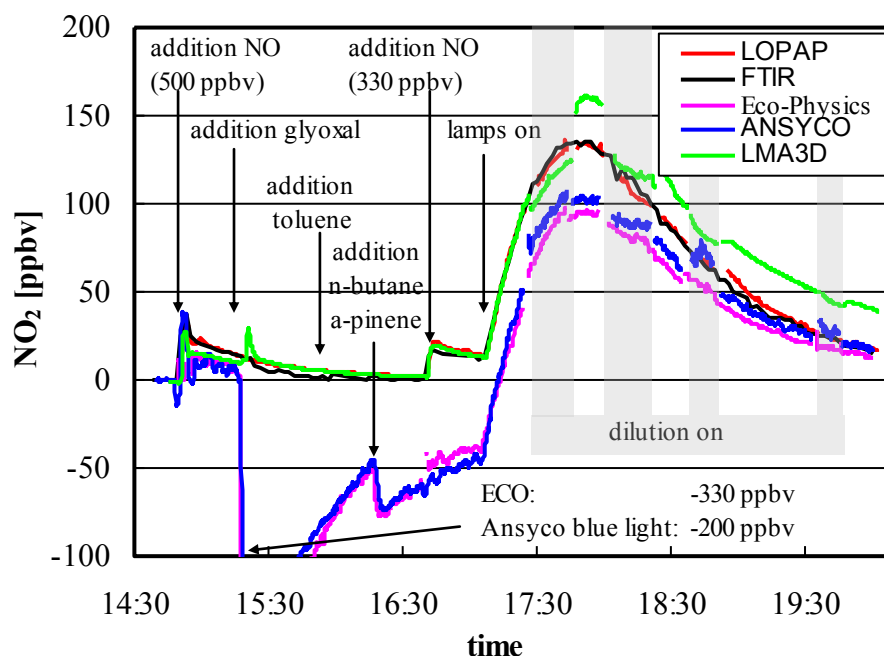
Fig. 39:   Intercomparison of three commercial NO_2 instruments and the new NO_2-LOPAP instrument with FTIR spectrometry during a complex photo-smog experiment. The grey shaded area indicate the periods, when the sample air of all the external instruments was diluted with synthetic air by factors of between 1.2-3.5, which was considered for the concentration calculations.

For both chemiluminescence instruments with photolytic converters (ECO and Ansyco blue light) strong negative interferences were observed when adding glyoxal to the chamber. As in the tunnel study mentioned before (see section 2.2.2.2), artificial negative concentrations were registered for the ECO and Ansyco blue light instruments reaching -330 ppbv and -200 ppbv, respectively (see Fig. 39). To understand these negative interferences the photo-chemistry of glyoxal has to be considered, which produces formyl radicals (HCO) at wavelengths <420 nm:

(R 34) $(HCO)_2 + h\nu$ $\longrightarrow$ 2 HCO,
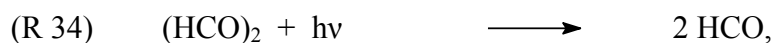
which further react with molecular oxygen leading to the formation of HO_2 radicals:

(R 35) $HCO + O_2$ $\longrightarrow$ $HO_2 + CO$.

It is well known that peroxyradicals (HO_2, RO_2) efficiently convert NO into NO_2:

(R 36) $HO_2 (RO_2) + NO$ $\longrightarrow$ $OH (RO) + NO_2$.
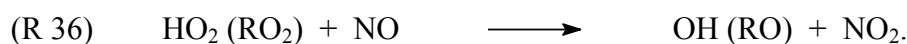
For the high glyoxal concentrations used, the NO concentration in the NO_x channels of both instruments is significantly reduced via reaction (R 36). The apparent negative concentrations can be explained with the low NO_2/NO_x ratio at the beginning of the experiment and the high loss of NO through reaction (R 36). This results in the measured NO concentration without converter (NO channel) being higher than that with converter (NO_x channel).

To confirm the explanation of the negative interferences observed in the photo-smog experiment, the deviations of both instruments compared to the FTIR data during the dark period were plotted against the product of [NO]×[glyoxal]. Highly linear correlations were obtained for both chemiluminescence instruments (see Fig. 40).
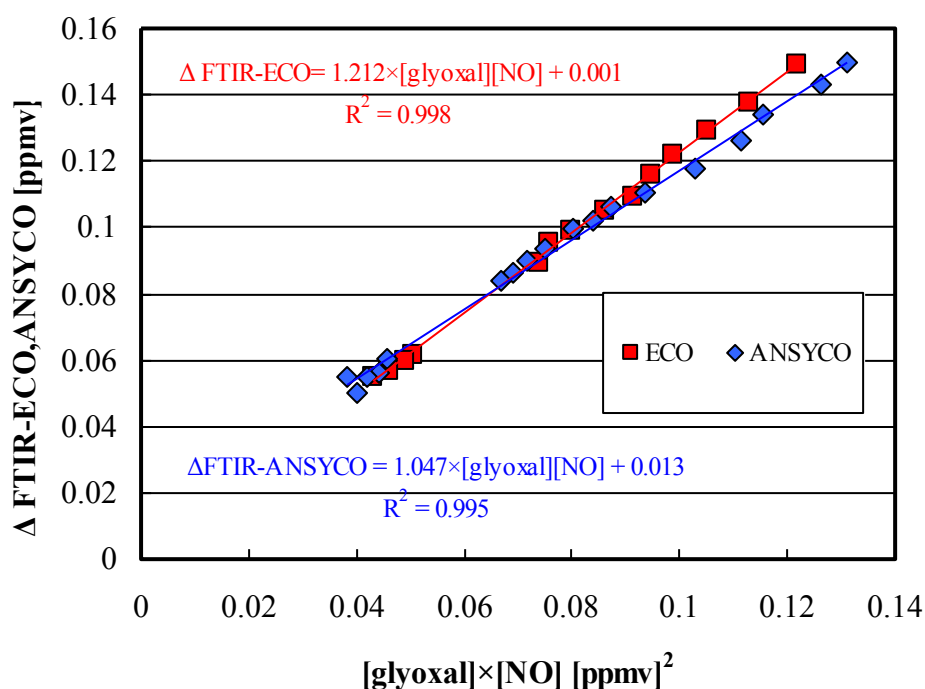
Fig. 40:   Negative interferences of the chemiluminescence instruments with photolytic converter as a function of the product of the glyoxal and the NO concentrations.

Since reactions (R 34) and (R 35) follow first-order and pseudo first-order kinetics, respectively, it can be expected that the HO_2 concentration in the converter will scale linearly with glyoxal concentration considering that HO_2 self reactions are not significant under these conditions due to high NO levels present. In this case, the negative interference, which is explained here by NO loss through reaction (R 36), follows second order kinetics and will be proportional to $[NO] \times [HO_2]$ and $[NO] \times [glyoxal]$, as observed. As a consequence of these non-linear negative interferences, the NO_2 level given by both instruments was not observed to increase during the second addition of NO at ~16:50 local time (LT) (see Fig. 39), in contrast to the other instruments, for which the impurities of NO_2 in the NO could be correctly quantified. This is caused by the increasing NO level leading to increasing negative interferences by reaction (R 36), which compensates the increased NO_2 level in the chamber.

Another interesting feature of the intercomparison was the enhancement of the negative interferences of both chemiluminescence instruments after the addition of n-butane and α-pinene (see Fig. 39). Both VOCs do not photolyse in the spectral range of both photolytic converters and thus, will themselves not form the peroxyradicals necessary to convert NO by reaction (R 36). However, since OH radicals are formed from glyoxal photolysis via reactions (R 34)-(R 36), peroxyradicals (RO_2) will be formed by the OH initiated degradation of n-butane and α-pinene ("R-H"):

(R 37)   R-H + OH $\longrightarrow$ R + H_2O,

(R 38)   R + O_2 $\longrightarrow$ RO_2.

The RO_2 radicals will further reduce the NO level in the photolytic converter by reaction (R 36). Hence, photo-induced radical chemistry, well known from atmospheric chemistry textbooks, takes place in the photolytic converters, depending on the admitted VOCs, so that NO_2 data using these instruments are inaccurate for highly polluted conditions such as can prevail in street canyons, tunnels and smog chambers. However, because of the second order reaction kinetics, these negative interferences are not expected to be of significant importance in the less polluted atmosphere (see for example, Fig. 5, between 0:00-4:00 LT, and Fig. 32).

During the course of the experiment a continuous reduction of the negative interferences of the chemiluminescence instruments with photolytic converter (Ansyco blue light und ECO) was observed. This is due to the continuous dilution of the reaction mixture, which results from the addition of synthetic air to replenish the gas sample flow to the external instruments and the second order reaction kinetics of the interferences (see above). The non-linear behaviour of these interferences was also reflected by the data in instances where the reaction mixture was diluted

for the external instruments leading to smaller interferences (see Fig. 39, Ansyco blue light and ECO: dilution on).

Generally, negative interferences were larger for the ECO compared to the Ansyco blue light instrument. This can be explained by the broader spectral range (320-420 nm) of the Xenon lamp used in the photolytic converter of the ECO instrument compared to the blue light converter (λ_{max} = 395 $\pm$ 10 nm), which is optimised for the photolysis of only NO_2. In addition, the residence time in the blue-light converter is much shorter compared to the Xenon lamp converter. Thus, in the case of the ECO instrument, more photons are absorbed by glyoxal in the photolytic converter leading to higher radical yields. In addition, caused by the different spectral range applied, it can be expected that in the atmosphere, photolysis of more photo-labile species will lead to larger radical production in a photolytic converter containing a xenon lamp compared to one using a blue light converter. Thus, if photolytic converters are used for the chemiluminescence technique, it is recommended to use blue light converters, although these instruments will still suffer from negative interferences for high pollution levels (see Fig. 39 and Fig. 41).

4.6.2 Street Canyon

Based on the interferences observed in the smog chamber, a field campaign was performed to investigate whether the negative interferences are also of importance in the real atmosphere. This second intercomparison campaign was carried out in the period of May 7-27, 2008 at the *Loher Kreuz* on *Friedrich Engels Allee (B7)*, a main busy street in Wuppertal. The measurements took place in the former trailer laboratory of the *Landesamt für Natur, Umwelt und Verbraucherschutz Nordrhein-Westfalen* (hereafter LANUV), which is now administrated by the University of Wuppertal.

The main goal of this second intercomparison was to demonstrate that the negative interferences observed for photolytic converters (see section 2.2.2.2 b) can also be of importance in the open urban atmosphere. Hence two chemiluminescence instruments (ECO and Ansyco blue light) were compared to the NO_2-LOPAP in a street canyon in Wuppertal for the first two days of the campaign when sunny conditions prevailed. In addition, this intercomparison was also aimed to quantify typical positive interferences of the chemiluminescence instrument with molybdenum converter (Ansyco Mo), which is routinely used at this site. The LOPAP instrument was used as reference because of the excellent agreement with the FTIR technique under complex conditions in a smog chamber, for which the other instruments showed strong interferences (see section 4.5.2). All instruments were calibrated by the same calibration mixtures to ensure that the differences observed are only caused by interferences and the precision errors.

For the early night and during the morning rush hour, higher NO_2 levels were observed (see Fig. 41a), for which the differences between the instruments used were largest. In contrast, during late night-time when the NO_2 levels were lower, better agreement was obtained. For a more quantitative evaluation the 30 min average data of all chemiluminescence instruments were plotted against the corresponding LOPAP data. As expected, both instruments with photolytic converters showed smaller NO_2 levels compared to the LOPAP, which was more distinct for the ECO Physics with Xenon lamp converter (about 30 % deviation) compared to the Ansyco with blue light converter (about 7 %, see Fig. 41 b and c). While the correlation of Ansyco to the LOPAP was excellent ($r^2 = 0.99$), a lower correlation was observed for the ECO Physics ($r^2 = 0.86$), which is caused by the one channel design of this instrument, for which fast variations of the trace gas levels lead to artificial noise. The higher negative interferences of the ECO Physics are explained by the broader spectral range of the Xenon lamp converter compared to the blue light converter, for which much more photolabile species will form interfering peroxy radicals (for details, see section 4.6.1). Thus, although the extent of the negative interferences of the photolytic converters was much lower compared to the tunnel measurements and no negative NO_2 data was obtained, the NO_2 concentration was still significantly underestimated in the open atmosphere.

In contrast, for the chemiluminescence instrument with molybdenum converter (Ansyco Mo) slightly higher concentrations compared to the LOPAP were observed. However, the small differences of about 5 % were close to the precision errors of both instruments. Such small differences can only be explained by the absence of significant NO_y species, which is in contrast to the results from a study in Santiago de Chile (see section 2.2.2.2a). However, since the measurements in the street canyon were close to the main NO_x emission source, it can be expected that only emitted NO_y species play an important role here. The data shown in section 2.2.2.2a was collected at an urban background site on the open campus of the University of Santiago de Chile, for which secondary photochemical formation of NO_y species is more important, also with respect to the much higher photochemical activity in Santiago de Chile compared to Germany.

The slightly higher NO_2 levels from the chemiluminescence instrument compared to the LOPAP can be well explained by NO_y emissions from vehicles, for which mainly nitrous acid (HONO) is expected. Since the typical emission ratio of HONO is ~1 % of NO_x (Kurtenbach et al., 2001), and since the average NO_x concentration was ca. two times higher than NO_2 during the intercomparison, a positive interferences by HONO of only ~2 % is expected for the molybdenum converter instrument.
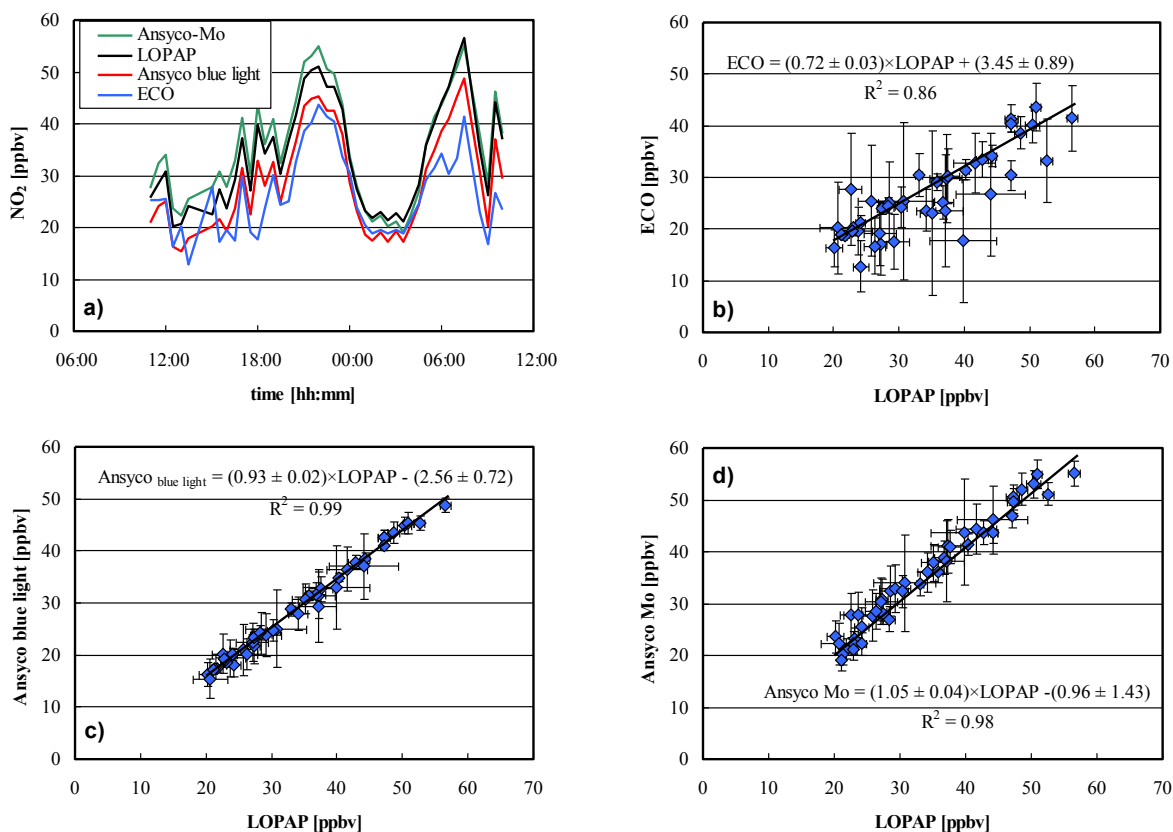
Fig. 41: a) NO$_2$ concentrations measured by different instruments in a street canyon; b)-d) correlation plots of the different chemiluminescence instruments against the LOPAP data, which was used as reference here (see text). A weighted orthogonal regression analysis was used, for which the errors of both instruments were considered (Brauers and Finlayson-Pitts, 1997).

The results from the street canyon show that chemiluminescence instruments with molybdenum converters can provide even more accurate NO$_2$ data compared to instruments with photolytic converters under certain condition, i.e. for measurements close to emission sources, e.g. in kerbside or tunnel studies. For these conditions, instruments with photolytic converters show much stronger, negative interferences, which were not yet considered. For example, if only two chemiluminescence instruments with molybdenum and photolytic converter were used in the street canyon (e.g. ECO and Ansyco Mo), the differences would have been explained by the well known positive NO$_y$ interferences from the molybdenum converter and not by the yet unknown but more important negative interferences of photolytic converters.

During this campaign, for all LOPAP data a small signal arose in the interference Channel 2 (see Fig. 42). On average a small value of (3.2 ± 0.6) % was calculated for the ratio Channel 1/Channel 2. This can be explained in terms of the sampling efficiency of the new stripping coil used, which has a sampling efficiency of 97 %. Thus, the observed signal in Channel 2 is the

NO$_2$ that is not collected in Channel 1 and hence, as was explained above for the first campaign using the old stripping coil, there are no interferences affecting the instrument at this kerbside monitoring station.
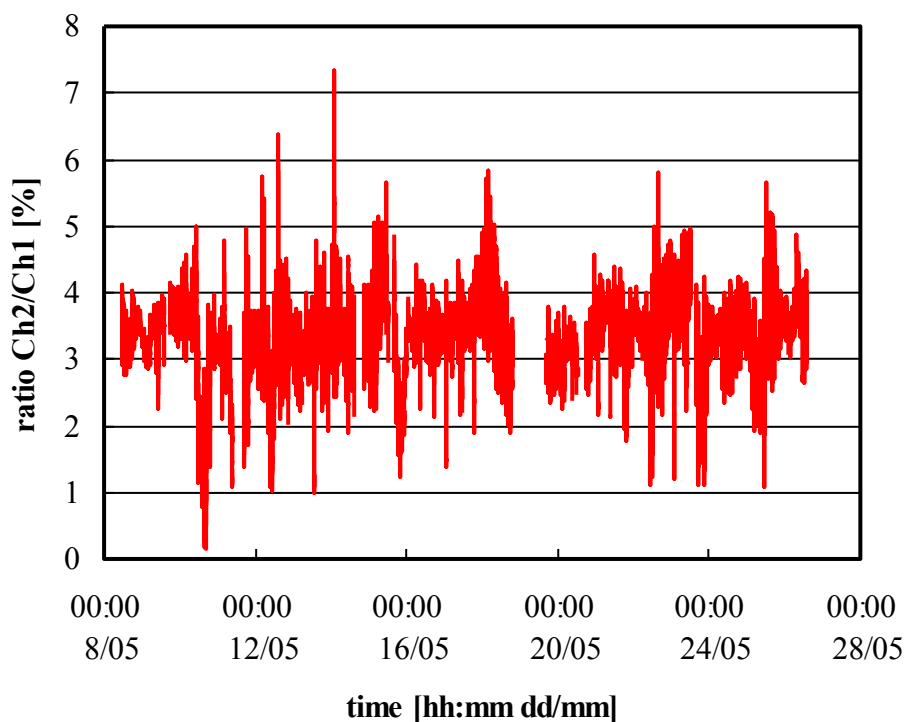
Fig. 42:   Ratio Channel 2/Channel 1 during the intercomparison campaign carried out in a busy street in Wuppertal city.

4.6.3   Concluding Remarks

In the present study, commercial NO$_2$ chemiluminescence instruments have shown strong interferences compared to spectroscopic techniques under certain conditions. Accordingly, if data from these instruments are used, e.g. in chemical models, model-measurement deviation may be also caused by the uncertainties in the NO$_2$ measurement data. Therefore, critical evaluation of the data from each type of NO$_2$ instruments for any measurement condition is required. For example, at urban kerbside stations for which chemiluminescence instruments are generally used, the NO$_2$ level may be strongly underestimated if instruments with photolytic converters are used, whereas it will be overestimated for those using molybdenum converters. Whereas the positive interferences of molybdenum converters by NO$_y$ species are a well known problem (Dunlea et al., 2007 and references therein), the negative interferences of photolytic converters have not yet been discussed in the literature in detail. If an intercomparison of these

two types of instruments is carried out under heavily polluted atmospheric conditions; one might argue that instruments with photolytic converter would provide better data than those with molybdenum converter. However, under these conditions, the negative deviations of the photolytic converters can be even much stronger than the positive interferences by the NO_y species for the molybdenum converters. For example, if the NO_x level at a kerbside station originates only from local direct vehicle emissions, a small NO_y fraction, resulting mainly from direct emissions of nitrous acid (HONO), is expected. Since the typical emission ratio of HONO is ~1 % of NO_x (Kurtenbach et al., 2001), only positive interferences of ~2 % are expected for molybdenum converter instruments for a NO_2/NO_x ratio of 15 %. In contrast, for photolytic converter instruments, even negative NO_2 concentrations can result for high pollution levels, thus the error could be up to 100 %.

On the other hand, for urban background, rural or remote measurement stations the NO_y and PAN fractions can be significant compared to the NO_2 level, for which the Luminol technique and the chemiluminescence instruments with molybdenum converters would be more affected.

Thus, the use of selective NO_2 instruments, like for example DOAS, LIF, cavity ring down or the new NO_2-LOPAP technique, are recommended for the detection of NO_2 in the atmosphere.

5   Application of the NO$_2$-LOPAP

5.1   Direct NO$_2$ Emissions from Mobile Vehicle Sources

During the last 20 years, NO$_x$ emissions have decreased considerably, being the road transport sector that contributes to about 40 % to the total emissions of NO$_x$ in Europe (Vestreng et al., 2009) and in Germany to about 60 % (Tappe et al., 2008). On the other hand, urban NO$_2$ concentrations tend to keep unchanged or even have been observed to increase (Carslaw, 2005; AQEG, 2007).

Nitrogen dioxide (NO$_2$) is a harmful trace gas (see section 2.1.5) and a precursor of tropospheric O$_3$. For these reasons, the European union, as well as Environmental Protection Agency (EPA) in USA, have established a legislative framework to improve the protection of the human health and the environment against several pollutants, among them nitrogen dioxide. As already explained in section 2.1.5, the EU countries have to meet two new air quality limits for NO$_2$: the one hour average concentration of 200 $\mu g/m^3$ (~100 ppbv) and the annual average concentration of 40 $\mu g/m^3$ (~20 ppbv). These two new limits came into effect on January 1, 2010, however, in many urban areas the annual air quality standard of NO$_2$ is often exceeded (Keuken et al., 2009), which is explained by secondary chemistry of the atmosphere, but also by increasing direct NO$_2$ emissions (see section 2.1).

As was explained in section 2.1.3, NO and NO$_2$ are formed directly by combustion processes. Once NO is released to the atmosphere it is partly converted to NO$_2$ by O$_3$ or peroxy radicals (RO$_2$):

(R 39)   NO + O$_3$ (RO$_2$) $\longrightarrow$ NO$_2$ + O$_2$ (RO),

and NO$_2$ further photolyses to NO:

(R 40)   NO$_2$ + hν $\longrightarrow$ NO + O(^{3}P).

Under the assumption that RO$_2$ photochemistry is negligible and that the background concentration of O$_3$ is constant (Clapp and Jenkin, 2001), then the concentration of O$_x$ is defined as:

(Eq. 18)   NO$_2$ + O$_3$ = O$_x$.

The different trends of NO$_x$ and NO$_2$ described above may have different reasons. It can be explained by an increase of the direct emissions of NO$_2$ and on the other hand also by an increase of the secondary (indirect) formation of NO$_2$ by (R 39). To determine the fraction of primarily emitted NO$_2$, Clapp and Jenkin (2001) proposed to plot O$_x$ against NO$_x$ for urban

measurement sites. The slope of the plot gives the primary emitted NO$_2$/NO$_x$ ratio and the intercept yields the background level of O$_3$. The directly emitted NO$_2$ (primary) is obtained by the product of the NO$_2$/NO$_x$ ratio (slope) with the NO$_x$ concentration. The difference between the measured NO$_2$ (total) and the resulting primarily emitted NO$_2$ (direct) gives the secondarily formed NO$_2$ (indirect). For kerbside measurements of NO, NO$_2$ and O$_3$ during the morning rush hours, the background concentration of O$_3$ can be assumed to be nearly constant. In addition, the RO$_2$ chemistry in the atmosphere is negligible and the NO$_x$ variation is large at that time of the day. Therefore, measurement data from this time interval provide the best linear O$_x$ to NO$_x$ correlation.

To investigate this important topic for the city of Wuppertal, measurements of NO Mo converter (Ansyco "blue light"), NO$_2$ (LOPAP) and O$_3$ (Environnemental 41M) were carried out in a busy street in Wuppertal during May 8-27, 2008 (see details in section 3.4.2) in order to determine the fraction of direct and indirect traffic emissions of NO$_2$. In Fig. 43 30 min averaged NO, NO$_2$ and O$_3$ profiles during May 8, 2008 are depicted for the monitoring station. A typical rush hour peak for NO and NO$_2$ is observed during the morning (5:00-8:30 hour). The decay of the O$_3$ concentration at this time can be explained in terms of the oxidation of NO by O$_3$ by reaction (R 39) to produce secondary NO$_2$ (indirect).
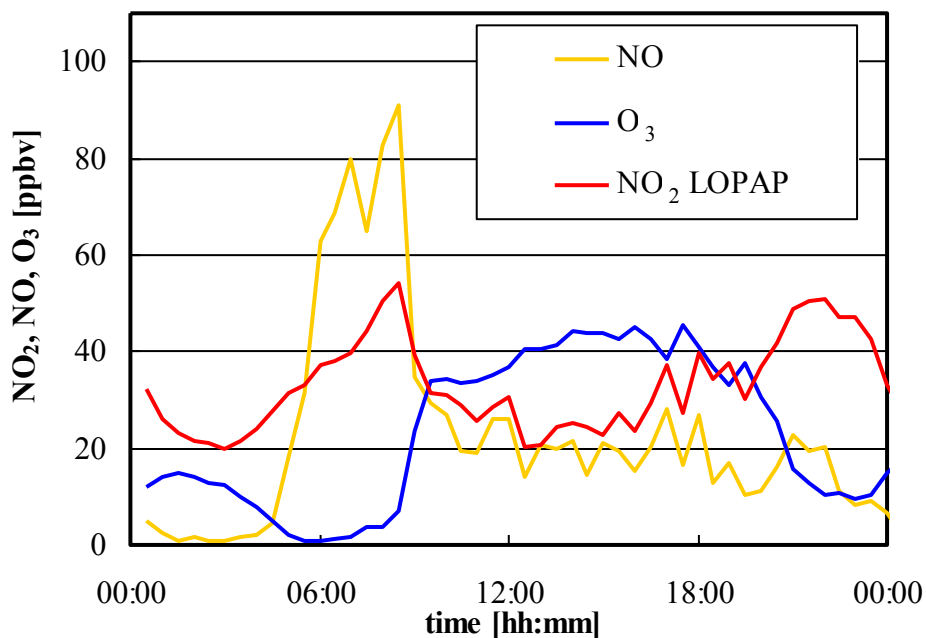
Fig. 43: Example of diurnal NO, NO$_2$ and O$_3$ profiles (30 min average) at the monitoring station at the Friedrich-Engels Allee, on May 8, 2008.

In Fig. 44 the correlation between O$_x$ and NO$_x$ is shown for the time interval 5:00-8:30 on May 8, 2008. The linear regression yields a primary emitted NO$_2$/NO$_x$ ratio of (0.13 ± 0.001) and a

background O$_3$ concentration of (34 ± 5) ppbv. The average NO$_2$/NO$_x$ ratio determined for the period May 8-17 2008 was (0.12 ± 0.01), which is in good agreement with values measured at this station during the year 2009 by Elsner (2010), but is much higher than the value of (0.04 ± 0.01), which was determined by Lörzer (2002) for the year 1997 in a tunnel study (see Fig. 45). When using the NO$_2$ data from the chemiluminescence instrument with molybdenum converter, which is routinely operated at that station, an average NO$_2$/NO$_x$ ratio of (0.15 ± 0.02) was determined, which is slightly higher than the value determined by the LOPAP instrument. The difference is explained by the NO$_y$ interferences of the chemiluminescence instrument.

The high NO$_2$/NO$_x$ emission ratio determined at a kerbside monitoring station supports the idea that one reason for the stagnating NO$_2$ concentrations during the last decades is due to increasing direct NO$_2$ emissions and is in good agreement with other reported NO$_2$/NO$_x$ ratios around the world (see Fig. 45) (Keuken et al., 2009; Elsner, 2010; Anttila et al., 2011; Carslaw et al., 2011a; Villena et al., 2011).
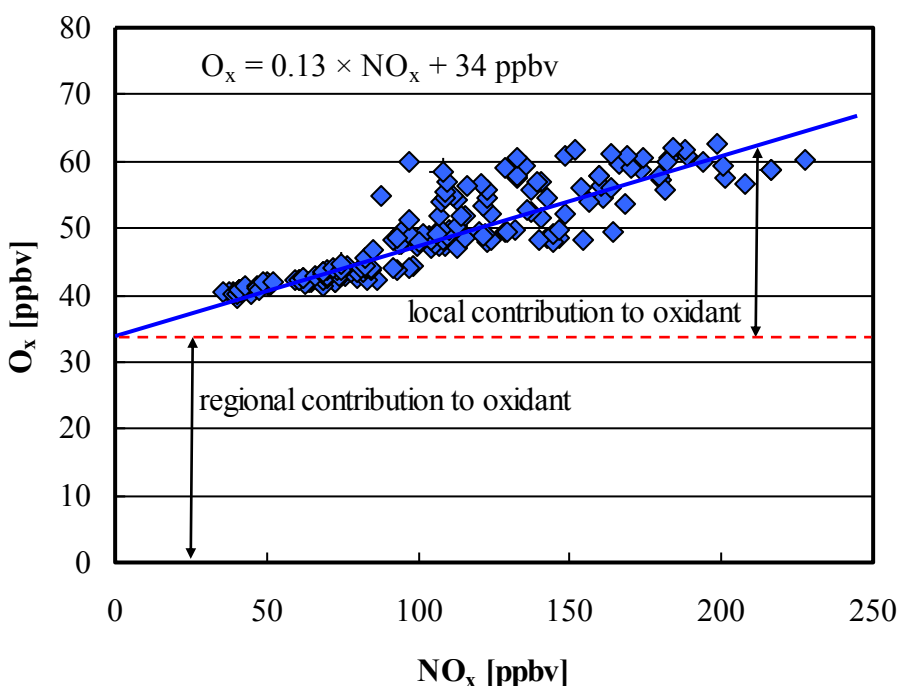
Fig. 44:   Plot of O$_x$ (NO$_2$ + O$_3$) against NO$_x$ (NO$_2$ + NO) during the rush hour (5:00-8:30 h) on May 8, 2008 at the kerbside monitoring station (1 min averages).
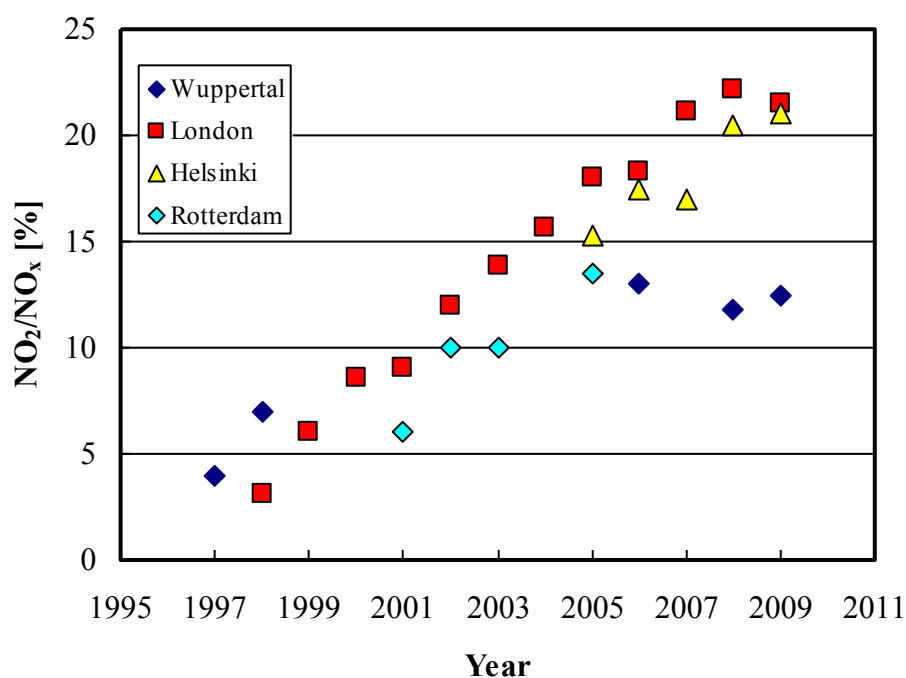
Fig. 45: NO$_2$/NO$_x$ ratio for London (Carslaw et al., 2011a), Helsinski (Anttila et al., 2011), Rotterdam (Keuken et al., 2009) compared with the trend in Wuppertal (1997-1998: Lörzer, 2002; 2006: Kurtenbach, 2012; 2008: this thesis; 2009: Elsner, 2010).

The increasing trend of the ratio of directly emitted NO$_2$/NO$_x$ can be explained by the trend of the composition of the vehicle fleet in Germany. During the last years the percentage of diesel engines has increased. Modern diesel engines are known to emit higher fractions of NO$_2$ of up to 50 % (AQEG, 2007 and references therein). Reasons for these high emissions are at least in part the use of oxidation catalysts, which are aimed to reduce VOC emissions, but also to increase the fraction of NO$_2$ for regeneration of particle filters, on which the collected soot is oxidized by the NO$_2$ formed.

Another reason for the stagnating NO$_2$ concentrations at urban kerbside stations is the secondary formation of NO$_2$ by reaction (R 39). To study the contribution of secondary NO$_2$ formation to the observed NO$_2$ levels in Wuppertal, the contribution of the direct NO$_2$ emissions was calculated by multiplying the average NO$_2$/NO$_x$ emission ratio with the measured NO$_x$ values. The indirect NO$_2$ was obtained by subtraction of the primary NO$_2$ from the measured NO$_2$ LOPAP values. The total, direct and indirect NO$_2$ levels obtained are plotted in Fig. 46 together with the new EU limit value (~20 ppbv). Two important conclusions can be drawn:

a) the NO$_2$ limit value of 20 ppbv was exceeded almost all the time.
b) the indirect NO$_2$ is of much higher importance compared to the direct NO$_2$ and is already exceeding the 20 ppbv limit most of the time.

From Fig. 46 it is concluded that not only primary emissions of NO$_2$ should be reduced, but it is also necessary to pay attention to the secondary formation of NO$_2$. For this purpose also the background O$_3$ concentrations should be controlled, which is however a global problem, that cannot be easily solved. Thus, the only way to reach the new EU limit value for NO$_2$ is to further strongly reduce total NO$_x$ emissions, in order to reduce secondary NO$_2$ formation through reaction (R 39). Only when the urban NO$_x$ concentrations can be reduced close to the ozone background levels, the 20 ppbv limit value can be reached.
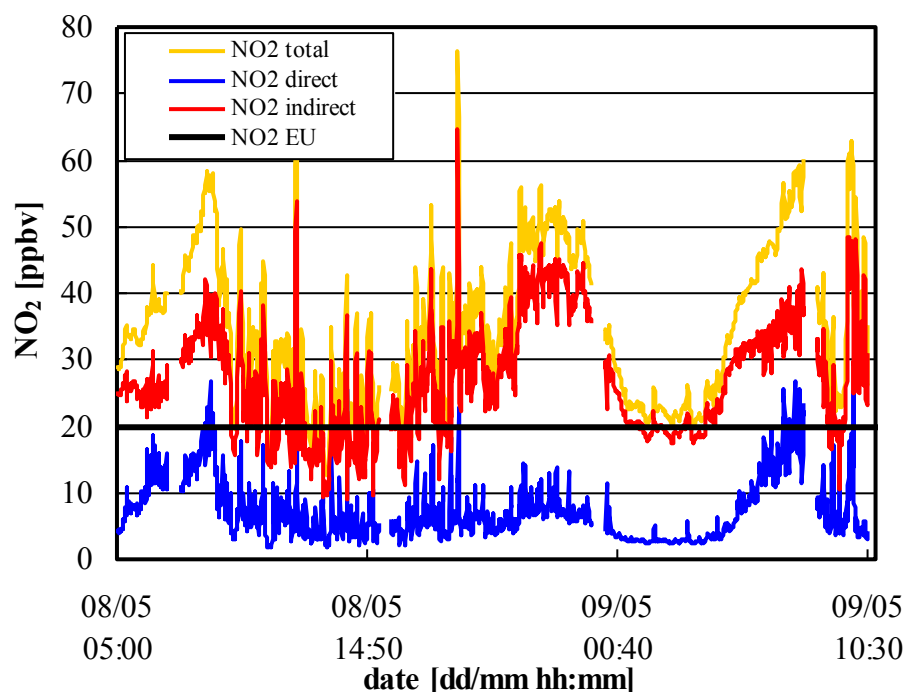
Fig. 46:   Determination of the direct, indirect and total NO$_2$ concentrations (1 min average) during May 8-9, 2008.

5.2   NO$_2$ Formation in the Photolysis of 2-Nitro-Toluene

In 2006, Bejan et al. observed a new source of HONO based on the photolysis of a series of ortho-nitrophenols (2-nitrophenol, 3-methyl-2-nitrophenol, 4-methyl-2-nitrophenol and 5-methyl-2-nitrophenol). In that study the formation of NO$_2$ and its possible participation in the HONO formation, through its photosensitized conversion to HONO on organic surfaces (George et al., 2005; Stemmler et al., 2006; 2007), was ruled out because NO$_2$ was not detected in the experiments. At that time a luminol NO$_2$ instrument (Unisearch, LMA3D) was used, which suffered from a significant reduction of its sensitivity in the presence of the ppmv levels of nitrophenols used. Thus, during the experiments the instrument was calibrated in the presence of the nitrophenols. However, a possible non linearity of the instrument at very low NO$_2$ levels was not investigated, leading to a high uncertainty of the upper limit NO$_2$ yield obtained. The Eco-Physics instrument (PLC 760) with photolytic converter could not be used during these experiments, caused by the significant negative interferences in the photolytic converter in the presence of the photo-labile nitrophenols, which can be explained in terms of similar reactions than those postulated in section 4.6.

In order to test the new NO$_2$-LOPAP under such difficult conditions, a number of experiments was performed with 2-nitrotoluene, the photolysis of which is another potential HONO source. The photolysis of 2 nitrotoluene (2-NT) was studied in the glass flow reactor shown in Fig. 9, where a gas phase mixture of 2-NT was generated by flushing 2.5 l/min pure synthetic air over a liquid sample of nitrotoluene, which was immersed in a temperature regulated water bath. The gas containing the 2-NT was passed through the photoreactor of borosilicate glass, which has 50 mm id., 80 cm length and a surface to volume ratio (S/V) of 0.75 cm^{-1}. The photoreactor was placed in an aluminium housing, where six UV/VIS lamps (Phillips TL/05, 20 W, 300-500 nm, λ_{max}= 370 nm) were installed symmetrically around the photoreactor and could be operated individually. With all six lamps in operation a J(NO$_2$) value of 0.016 s^{-1} is obtained, which is ca. two times higher compared to noontime conditions in Europe. During the experiment a HONO-LOPAP was also used, which is explained in detail elsewhere (Heland et al., 2001; Kleffmann et al., 2002). The concentration of 2-NT was determined using a FTIR spectrometer coupled to a 10 l White type multiple reflection cell (see section 3.2.2 and Fig. 9).

In Fig. 47 a typical experiment is shown. Only a small blank HONO and NO$_2$ formation was observed in the reactor when only flushed with pure synthetic air. In contrast, ppbv levels of NO$_2$ and HONO were formed when ppmv levels of 2-NT were irradiated.
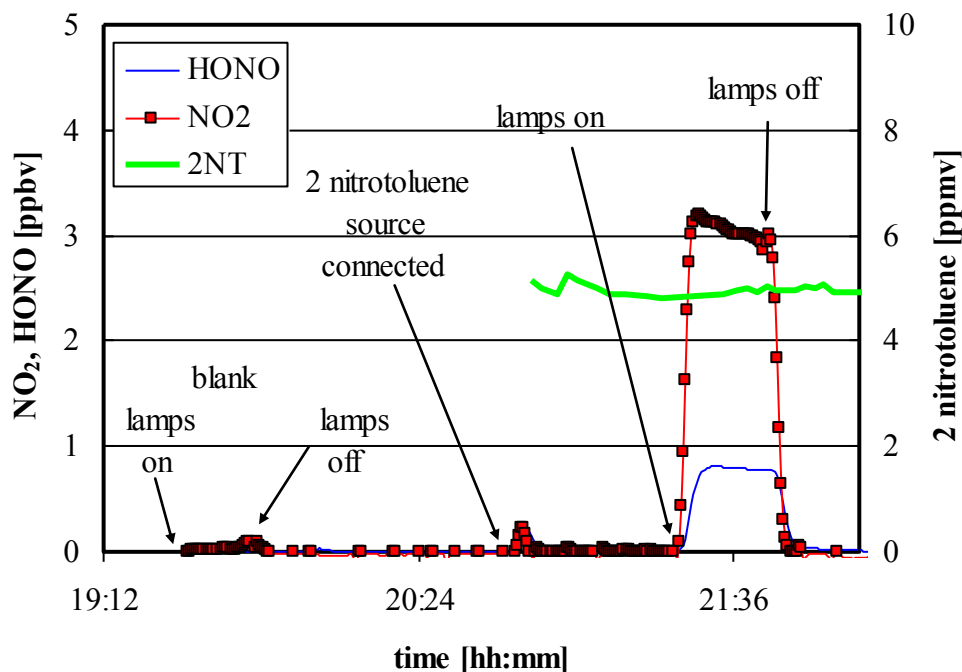
Fig. 47: NO$_2$ formation together with HONO formation during irradiation of the empty reactor flushed with synthetic air (blank) and during the irradiation of 2 nitrotoluene (2-NT) in synthetic air.

A linear correlation between the photolytic formation of NO$_2$ and HONO and the 2-NT concentration was observed (see Fig. 48), which can be explained by a gas phase photolysis of 2-NT.

The influence of the light intensity on the NO$_2$ and HONO formation during the photolysis of 2-NT was also studied by the variation of the number of lamps used. A linear correlation between NO$_2$ and HONO formation and the light intensity was observed (see Fig. 49), clearly confirming the photochemical origin of NO$_2$ and HONO. However, since higher NO$_2$ levels were observed compared to HONO, a possible secondary HONO formation by heterogeneous photosensitized conversion NO$_2$ (George et al., 2005; Stemmler et al., 2006; 2007) may still be possible. Further studies using also mixtures of NO$_2$ and 2-NT are necessary to identify the HONO formation mechanism.
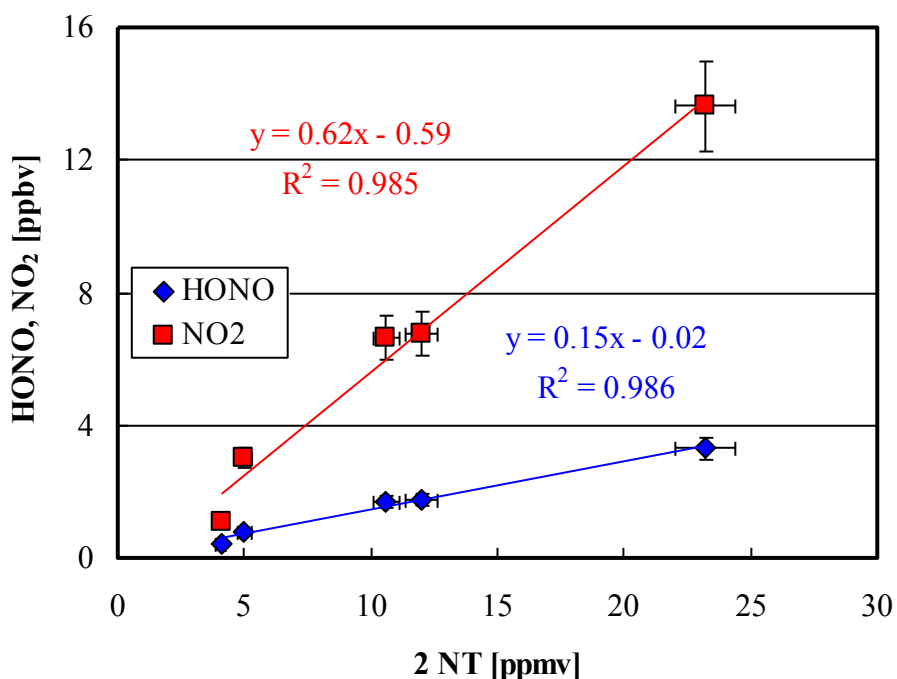
Fig. 48:   NO$_2$ and HONO formation as a function of 2-nitrotoluene (2-NT) concentration during photolysis experiments.

As the processes studied show first order kinetics, the formation of NO$_2$ and HONO can be quantified by photolysis frequencies, which can be calculated by:

(Eq. 19) $\ln\left([2-NT]_t / [2-NT]_0\right) = -J_{2-NT \rightarrow NO_2(HONO)} \times t,$

where $[2\text{-NT}]_0$ is the initial concentration of 2-NT, and $[2\text{-NT}]_t$ is the concentration of 2-NT at time t. $[2\text{-NT}]_t$ is determined by the difference between initial concentration of 2-NT and the concentration of either NO$_2$ or HONO. $J_{2\text{-NT} \rightarrow NO_2(HONO)}$ is the photolysis frequencies of 2-NT for either NO$_2$ or HONO formation and t is the reaction time that can be determined knowing the volume of the flow tube and the gas flow rate. From the HONO and NO$_2$ formation observed, values of $J_{2\text{-NT} \rightarrow NO_2} = 2 \times 10^{-5}$ s^{-1} and $J_{2\text{-NT} \rightarrow HONO} = 5 \times 10^{-6}$ s^{-1} were determined by equation (Eq. 19). This photolysis frequency of 2-NT determined in this study for HONO formation is one order of magnitude lower compared with the photolysis frequencies determined by Bejan et al. (2006b) for different Nirophenols (e.g. $J_{3M2NP \rightarrow HONO} = 4.4 \times 10^{-5}$ s^{-1}, 3M2NP= 3-methyl-2-nitro phenol).
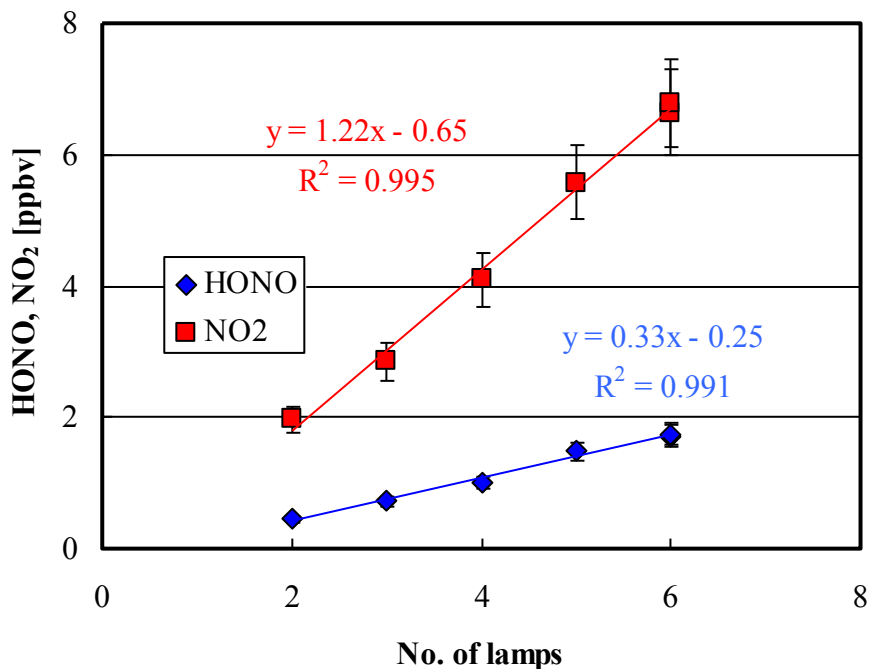
Fig. 49: NO$_2$ and HONO formation during photolysis of 2 nitro-toluene (2-NT) in the photo-flow reactor as a function of the number of lamps.

In order to determine the average quantum yield (ϕ_i) for the formation of NO$_2$ and HONO, i.e. the fraction of NO$_2$ and HONO formed per photon absorbed, the upper limit photolysis frequency of 2-NT (J_{max}) should be known, which is the theoretically possible maximum photolysis frequency of 2-NT assuming a quantum yield of one. J_{max} can be determined by the cross section of 2 NT (σ_λ), the actinic flux (F_λ) of the lamps used and the wavelength interval $\Delta\lambda$ that depends on the resolution of the actinic flux data (see (Eq. 20)):

(Eq. 20) $\quad J_{max} = \sum F_\lambda \times \sigma_\lambda \times \varphi \times \Delta\lambda.$

The quantum yields for the individual channels ϕ_i i.e. for HONO and NO$_2$ formation, are determined by:

(Eq. 21) $\quad \varphi_i = \dfrac{J_i}{J_{max}}.$

Values of $\phi_{NO_2} = 2.2 \times 10^{-3}$ and $\phi_{HONO} = 5 \times 10^{-4}$ were determined.

Atmospheric implications

For an estimate of the potential homogeneous NO$_2$ and HONO formation by photolysis of ortho substituted alkyl-nitroaromatics in the atmosphere, it was assumed that all these species show similar HONO and NO$_2$ formation compared to 2-NT studied. In addition, a concentration of 1 ppbv has been assumed as an upper limit for urban conditions. Assuming first order kinetics and constant nitroaromatic level ([2NT]) the rate of HONO and NO$_2$ formation in the atmosphere can be calculated, if the photolysis frequency is known:

(Eq. 22) $$\frac{\Delta[Xi]}{\Delta t} = J_{2NT \rightarrow X_i} \times [2NT],$$

where X$_i$ is either HONO or NO$_2$. Using the quantum yield determined for 2-NT and the atmospheric actinic flux (zenith angle = 50°), production rates of 71 pptv/h of NO$_2$ and 18 pptv/h of HONO were determined. In the case of HONO, this production is even smaller than the rate calculated for 3-methyl-2-nitrophenol (100 pptv/h; Bejan et al., 2006b). Since typical daytime HONO formations rates of some ppbv/h are observed for the heavily polluted atmosphere (Ren et al., 2003; Elshorbany et al., 2009), photolysis of alkyl-substituted nitroaromatics is not expected to be a major photolytic HONO source in the atmosphere.

6   Conclusion

A new instrument for the sensitive measurement of NO_2 by wet sampling and photometric detection has been developed and successfully tested. The instrument shows a linear response with a measurement range from the detection limit up to 300 ppbv, which can be calibrated absolutely by commercial nitrite standards. The instrument has a detection limit of 2 pptv for a time resolution of 3 min, which can be further reduced to <1 pptv for lower time resolution. Known interferences against O_3 and HONO were successfully suppressed by an additional scrubber for both gases. All other interferences tested can be neglected, both, in the atmosphere but also under complex conditions in a smog chamber.

The instrument was validated by intercomparison with a commercial chemiluminescence instrument with photolytic NO_2 converter in an urban atmosphere and with the FTIR technique in a smog chamber. Excellent agreement was obtained under all conditions applied. In contrast, for other commercial instruments used under complex conditions in a smog chamber and at an urban kerbside station, significant interferences were observed, which are discussed in detail.

Two applications under complex heavily polluted conditions were studied with the new NO_2-LOPAP instrument, for which commercial instruments show strong interferences.

At an urban kerbside station a NO_2/NO_x ratio from direct vehicle emissions of 12 % was determined. This value was much larger in comparison with the value of 4 % determined in 1997, which is explained by the increasing fraction of modern diesel vehicles. A high contribution of secondary NO_2 formation to urban NO_2 levels was observed indicating that present EU limit values for NO_2 can only be reached when NO_x emissions are further reduced in the future.

In addition, the photolysis of 2 nitro-toluene was studied, which is a potential photolytic HONO source in the atmosphere. In contrast to former studies on nitrophenols, significant NO_2 formation was observed besides HONO formation. The NO_2 formation observed may have a significant impact on the HONO formation mechanism. Further studies also on the photolysis of nitrophenols using the new NO_2-LOPAP instrument are necessary in the future.

7   References

Adema, E. H.: Ozone interference in the determination of nitrogen dioxide by a modified manual Saltzman method, Anal. Chem., 51, 1002-1006, 1979.

Alfassi, Z. B., Huie, R. E., and Neta, P.: Substituent effects on the rates of one-electron oxidation of phenols by the radicals ClO_2, NO_2, and SO_3^-, J. Phys. Chem., 90, 4156-4158, 1986.

Alvarez, R., Weilenmann, M., and Favez, J. Y.: Evidence of increased mass fraction of NO_2 within real-world NO_x emissions of modern light vehicles-derived from a reliable online measuring method, Atmos. Environ., 42, 4699-4707, 2008.

Ammann, M., Rössler, E., Strekowski, R., and George, C.: Nitrogen dioxide multiphase chemistry: uptake kinetics on aqueous solutions containing phenolic compounds, Phys. Chem. Chem. Phys., 7, 2513-2518, 2005.

Anttila, P., Tuovinen, J. P., and Niemi, J. V.: Primary NO_2 emissions and their role in the development of NO_2 concentrations in a traffic environment, Atmos. Environ., 45, 986-992, 2011.

AQEG, 2004: Nitrogen Dioxide in the United Kingdom. Report of the UK Air Quality Expert Group, AQEG. Prepared for the department for environment food and rural affairs, the Scottish executive, the Welsh assembly and the department of the environment in Northern Ireland. Defra Publications, London, 2004.

AQEG, 2007: Trends in primary nitrogen dioxide in the UK. Report of the UK Air Quality Expert Group, AQEG. Prepared for the department for environment food and rural affairs, the Scottish executive, the Welsh assembly and the department of the environment in northern Ireland. Defra Publications, London, 2007.

Bader, H., and Hoigné, J.: Determination of ozone in water by the indigo method, Water Res., 15, 449-456, 1981.

Barnes, I., Becker, K. H., and Mihalopoulos, N.: An FT-IR product study of the photo-oxidation of dimethyl disulfide, J. Atmos. Chem., 18, 267-289, 1994.

Baumgardner, R. E., Clark, T. A., and Stevens, R.: Comparison of instrumental methods to measure nitrogen dioxide, Environ. Sci. Technol., 9, 67-69, 1975.

References

Bejan, I.: "Investigations on the gas phase atmospheric chemistry of nitrophenols and catechols", PhD thesis, University of Wuppertal, Germany, 2006a.

Bejan, I., Abd El Aal, Y., Barnes, I., Benter, T., Bohn, B., Wiesen, P., and Kleffmann, J.: The photolysis of ortho-nitrophenols: A new gas phase source of HONO, Phys. Chem. Chem. Phys., 8, 2028 - 2035, 2006b.

Bennett, A. N. C.: Researches on nitrous oxide, J. Phys. Chem., 34, 1137-1157, 1929.

Berden, G., Peeters, R., and Meijer, G.: Cavity ring-down spectroscopy: Experimental schemes and applications, Int. Rev. Phys. Chem., 19, 565-607, 2000.

Biermann, H. W., Tuazon, E. C., Winer, A. M., Wallington T. J., and Pitts, J. N.: Simultaneous absolute measurements of gaseous nitrogen species in urban ambient air by long pathlength infrared and ultraviolet-visible spectroscopy, Atmos. Environ., 22, 1545-1554, 1988.

Brasseur, G. P., Orlando, J. J., and Tyndall, G.: Atmospheric chemistry and global change, Oxford University Press, New York, 1999.

Bratton, A. C., and Marshall, E. K.: A new coupling component for sulphanilamide determination, J. Biol. Chem., 128, 537-550, 1939.

Brauers, T., and Finlayson-Pitts, B. J.: Analysis of relative rate measurements, Int. J. Chem. Kinet., 29, 665-672, 1997.

Brown, S. S.: Absorption spectroscopy in high-finesse cavities for atmospheric studies, Chem. Rev., 2003, 103, 5219-5238, 2003.

Brunekreef, B.: NO_2: The gas that won't go away, Clin. Exp. Allergy, 31, 1170-1172, 2001.

Burling, I: R., Yokelson, R. J., Griffith, D. W. T., Johnson, T. J., Veres, P., Roberts, J. M., Warnecke, C., Urbanski, S. P., Reardon, J., Weise, D. R., Hao, W. M., and Gouw, J. de.: Laboratory measurements of trace gas emissions from biomass burning of fuel types from the southeastern and southwestern United States, Atmos. Chem. Phys., 10, 11115-11130, 2010.

Carslaw, D. C.: Evidence of an increasing NO_2/NO_x emissions ratio from road traffic emissions, Atmos. Environ., 39, 4793-4802, 2005.

Carslaw, D. C., and Beevers, S. D.: New directions: Should road vehicle emissions legislation consider primary NO_2?, Atmos. Environ., 38, 1233-1234, 2004.

References

Carslaw, D. C., and Beevers, S. D.: Estimations of road vehicle primary NO_2 exhaust emission fractions using monitoring data in London, Atmos. Environ., 39, 167-177, 2005a.

Carslaw, D. C., and Beevers, S. D.: Development of an urban inventory for road transport emissions of NO_2 and comparison with estimates derived from ambient measurements, Atmos. Environ., 39, 2049-2049, 2005b.

Carslaw, D. C., Beevers, S. D., and Bell, M. C.: Risks of exceeding the hourly EU limit value for nitrogen dioxide resulting from increased road transport emissions of primary nitrogen dioxide, Atmos. Environ., 41, 2073-2082, 2007.

Carslaw, D. C., and Carslaw, N.: Detecting and characterising small changes in urban nitrogen dioxide concentrations, Atmos. Environ., 41, 4723-4733, 2007.

Carslaw, D. C., Beevers, S. D., Westmoreland, E., Williams, M., Tate, J., Murrels, T., Stedman, J., Li, Y., Grice, S., Kent, A., and Tsagatakis, I.: Trends in NO_x and NO_2 emissions and ambient measurements in the UK, Report, http://uk-air.defra.gov.uk/reports/cat05/1108251149_110718_AQ0724_Final_report.pdf, Version: July 2011a, last access August 2012

Carslaw, D. C., Beevers, S. D., Tate, J., Westmoreland, E., Williams, M. L.: Recent evidence concerning higher NO_x emissions from passenger cars and light duty vehicles, Atmos. Environ., 45, 7053-7063, 2011b.

Cheung, J. L., Li, Y. Q., Boniface, J., Shi, Q., Davidovits, P., Worsnop, D. R., Jayne, J. T., and Kolb, C. E.: Heterogeneous interactions of NO_2 with aqueous surfaces, J. Phys. Chem. A, 104, 2655-2662, 2000.

Clapp, L. J., and Jenkin, M. E.: Analysis of the relationship between ambient levels of O_3, NO_2, and NO as a function of NO_x in the UK, Atmos. Environ., 35, 6391-6405, 2001.

Crutzen, P. J.: The role of NO and NO_2 in the chemistry of the troposphere and stratosphere, Ann. Rev. Earth Planet. Sci., 7, 443-472, 1979.

Dari-Salisburgo, C., Di Carlo, P., Giammaria, F., Kajii, Y., and D'Altorio, A.: Laser induced fluorescence for NO_2 measurements: Observations at a central Italy background site, Atmos. Environ., 43, 970-977, 2009.

Day, D. A., Wooldridge, P. J., Dillon, M. B., Thornton, J. A., and Cohen, R. C.: A thermal dissociation laser-induced fluorescence instrument for in situ detection of NO_2, peroxy nitrates, alkyl nitrates, and HNO_3, J. Geophys. Res., 107, D6, doi: 10.129/2001JD000779, 2002.

Dean, A. M. and Bozzelli, J. W.: Combustion chemistry of nitrogen, in Gas-Phase Combustion Chemistry, edited by Gardiner, W. C. Jr., Springer-Verlag New York Inc., 2000.

Delfino, R. J., Staimer, N., Tjoa, T., Gillen, D., Kleinman, M. T., Sioutas, C., and Cooper, D.: Personal and ambient air pollution exposures and lung function decrements in children with asthma, Environ. Health Persp., 116, 550-558, 2008.

Demerjian, K. L.: A review of national monitoring networks in North America, Atmos. Environ., 34, 1861-1884, 2000.

Dunlea, E. J., Herndon, S. C., Nelson, D. D., Volkamer, R. M., San Martini, F., Sheehy, P.M., Zahniser, M. S., Shorter, J. H., Wormhoudt, J. C., Lamb, B. K., Allwine, E. J., Gaffney, J. S, Marley, N. A., Grutter, M., Marquez, C., Blanco, S., Cardenas, B., Retama, A., Ramos Villegas, C. R., Kolb, C. E., Molina, L. T., and Molina, M. J.: Evaluation of nitrogen dioxide chemiluminescence monitors in a polluted urban environment, Atmos. Chem. Phys., 7, 2691-2704, 2007.

Eckert, P, and Rakowski, S.: Pollutant Formation in Combustion Engines Development edited by Merker, G.P., Schwarz, C., and Teichmann, R.,Springer-Verlag Berlin Heidelberg, 2012.

EEA Report, Air Pollution in Europe 1990-2004. European environment agency. Report 2/2007. ISSN 1725-9177, Copenhagen, Denmark, 2007.

Elshorbany, Y. F., Kurtenbach, R., Wiesen, P., Lissi, E., Rubio, M., Villena, G., Gramsch, E., Rickard, A, R., Pilling, M. J., and Kleffmann, J.: Oxidation capacity of the city air of Santiago, Chile, Atmos. Chem. Phys., 9, 2257-2273, 2009.

Elsner, V.: Untersuchung des NO_2/NO_x-Verhältnisses an der Messstation Wuppertal, Friedrich-Engels-Allee, im Zeitraum 2006 bis 2009, Master Thesis, University of Wuppertal, Germany, 2010.

EPA 456/F-99-006R: Technical Bulletin: Nitrogen oxides (NOx), Why and How they are controlled, USA, November 1999.

References

EPA 600/R-08/071: Integrated science assessment for oxides of nitrogen – Health criteria, USA, July 2008.

EU Directive 96/62/EC. On ambient air quality assessment and management (the framework directive). From the official Journal of the European Communities 21.11.1996. En Series, L296/55, 27 September, 1996.

EU Directive 98/69/EC. Relating to measures to be taken against air pollution by emissions from motor vehicles and amending Council Directive 70/220/EEC. From the official Journal of the European Communities, 28.12.1998. En Series, L350/1, 13 October, 1998.

EU Directive 99/30/EC. Relating to limit values for sulphur dioxide, nitrogen dioxide and oxides of nitrogen, particulate matter and lead in ambient air (The First Daughter Directive). From the official Journal of the European Communities 29.06.1999. En Series, L163/41, 22 April, 1999.

EU Directive 99/96/EC. On the approximation of the laws of the Member states relating to measures to be taken against the emission of gaseous and particulate pollutants from compression ignition engines for use in vehicles, and the emission of gaseous pollutants from positive ignition engines fuelled with natural gas or liquefied petroleum gas for use in vehicles and amending Council Directive 88/77/EEC. From the official Journal of the European Communities, 13.12.1999. En Series, L 44/1, 13 December 1999.

European Standard, EN 14211: Ambient air quality - Standard method for the measurement of the concentration of nitrogen dioxide and nitrogen monoxide by chemiluminescence, 2005.

Fehsenfeld, F. C., Drummond, J. W., Roychowdhury, U. K., Galvin, P. J., Williams, E. J., Buhr, M. P., Parrish, D. D., Hübler, G., Langford, A. O., Calvert, J. G., Ridley, B. A., Grahek, F., Heikes, B. G., Kok, G. L., Shetter, J. D., Walega, J. G., Elsworth, C. M., Norton, R. B., Fahey, D. W., Murphy, P. C., Hovermale, C., Mohnen, V. A., Demerjian, K. L., Mackay, G. I., and Schiff, H. I.: Intercomparison of NO_2 measurement techniques, J. Geophys. Res., 95, D4, 3579-3597, 1990.

Finlayson-Pitts, B. J., and Pitts J. N. Jr.: Chemistry of the upper and lower atmosphere: Theory, Experiments and Applications, Academic Press: New York, 2000.

Flanagan, R. C., and Seinfeld, J. H.: Fundamentals of air pollution engineering, Prentice Hall, Inc, New Jersey, USA, 1988.

Fogg, P.; Details and measurement of factors determining the uptake of gases by water, in Chemicals in the Atmosphere: solubility, sources and reactivity, Edited by Fogg, P. and Sangster, J., John Wiley and Sons, England, 2003.

Fong, C., and Brune, W. H.: A laser induced fluorescence instrument for measuring tropospheric NO_2, Rev. Sci. Instrum., 68, 4253-4262, 1997.

Fontjin, A., Sabadell, A. J., and Ronco, R. J.: Homogeneous chemiluminescence measurement of nitric oxide with ozone, Anal. Chem., 42, 575-579, 1970.

Frenzel, A., Kutsuna, S., Takeuchi, K., and Ibusuki, T.: Solubility and reactivity of Peroxyacetyl Nitrate (PAN) in dilute aqueous solutions and in sulphuric acid, Atmos. Environ., 34, 3641-3644, 2000.

Fried, A., and Richter, D.: Infrared absorption spectroscopy. In: Analytical Techniques for Atmospheric Measurements, D. E. Heard (editor), Blackwell Publishing, Oxford, 2006.

Fuchs, H., Dubé, W. P., Lerner, B. M., Wagner, N. L., Williams, E. J., and Brown, S. S.: A sensitive and versatile detector for atmospheric NO_2 and NO_x based on blue diode laser cavity ring-down spectroscopy, Environ. Sci. Technol., 43, 7831-7836, 2009.

Fuchs, H., Ball, S. M., Bohn, B., Brauers, T., Cohen, R. C., Dorn, H.-P., Dubé, W. P., Fry, J. L., Häseler, R., Heitmann, U., Jones, R. L., Kleffmann, J., Mentel, T. F., Müsgen, P., Rohrer, F., Rollins, A. W., Ruth, A. A., Kiendler-Scharr, A., Schlosser, E., Shillings, A. J. L., Tillmann, R., Varma, R. M., Venables, D. S., Villena Tapia, G., Wahner, A., Wegener, R., Wooldridge, P. J., and Brown, S. S.: Intercomparison of measurements of NO_2 concentrations in the atmosphere simulation chamber SAPHIR during the NO3Comp campaign, Atmos. Meas. Tech., 3, 21-37, 2010.

Garnica, R. M., Appel, M. F., Eagan, L., McKeachie, J. R., and Benter, Th.: A REMPI method for the ultrasensitive detection of NO and NO_2 using atmospheric pressure laser ionization mass spectrometry, Anal. Chem, 72, 5639-5646, 2000.

Gauderman, W. J., Avol, E., Gilliland, F., Vora, H., Thomas, D., Berhane, K., McConnell, R., Kuenzli, N., Lurmann, F., Rappaport, E., Margolis, H., Bates, D., and Peters, J.: The effect of air pollution on lung development from 10 to 18 years of age, New Engl. J. Med., 351, 1057-1067, 2004.

George, L. A., and O´Brien, R. J.: Prototype FAGE determination of NO_2, J. Atmos. Chem., 12, 195-209, 1991.

George, C., Strekowski, R., Kleffmann, J., Stemmler, K., and Ammann, M.: Photoenhanced uptake of gaseous NO_2 on solid organic compounds: a photochemical source of HONO?, Faraday Discuss., 130, 195-210, 2005.

Gherman, T., Venables, D., Vaughan, S., Orphal, J., and Ruth, A.: Incoherent broadband cavity-enhanced absorption spectroscopy in the near-ultraviolet application to HONO and NO_2, Environ. Sci. Technol., 42, 890-895, 2008.

Grasshoff, K., Ehrhardt, M., and Kremling, K.: Methods of Seawater Analysis, 2nd ed., Verlag Chemie: Weinheim, p 140, 1983.

Grice, S., Stedman, J., Kent, A., Hobson, M., Norris, J., Abbott, J., and Cooke, S.: Recent trends and projections of primary NO_2 emissions in Europe, Atmos. Environ., 43, 2154-2167, 2009.

Griess, P.: Bemerkungen zu der Abhandlung der HH. Weselsky und Benedikt „Ueber einige Azoverbindungen", Ber. Dtsch. Chem. Ges., 12, 426-428, 1879.

Gregory, G. L., Hoell, J. M., Carroll, M. A., Ridley, B. A., Davis, D. D., Bradshaw, J., Rodgers, M. O., Sandholm, S. T., Schiff, H. I., Hastie, D. R., Karecki, D. R., Mackay, G. I., Harris, G. W., Torres, A. L., and Fried, A.: An intercomparison of airborne nitrogen dioxide instruments, J. Geophys. Res., 95, 10103-10127, 1990.

Goyal, S. K.: Comparison of two manual methods of nitrogen dioxide determination in ambient air, Environ. Monit. Assess., 89, 305-314, 2003.

Harder, J. W., Williams, E. J., Baumann, K., and Fehsenfeld, F. C.: Ground-based comparison of NO_2, H_2O, and O_3 measured by long-path and in situ techniques during the 1993 tropospheric OH photochemistry experiment, J. Geophys. Res., 102, D5, 6227-6243, 1997.

Hargrove, J., Wang, L., Muyskens, K., Muyskens, M., Medina, D., Zaide, S., and Zhang, I.: Cavity ring-down spectroscopy of ambient NO_2 with quantification and elimination of interferences, Environ. Sci. Technol., 40, 7868-7873, 2006.

Harwood, E. A., Hopkins, P. B., and Sigurdsson, S. T.: Chemical synthesis of cross-link lesions found in nitrous acid treated DNA: A general method for the preparation of N2-substituted 2´-deoxyguanosines, J. Org. Chem., 65, 2959-2964, 2000.

References

Hauser, T. R., and Shy, C. M.: Position paper: NO_x measurement, Environ. Sci. Technol., 6, 890-894, 1972.

Heland, J., Kleffmann, J., Kurtenbach, R., and Wiesen P.: A new instrument to measure gaseous nitrous acid (HONO) in the atmosphere, Environ. Sci. Technol., 35, 3207-3212, 2001.

Herndon, S. C., Shorter, J. H., Zahniser, M., Nelson, D. D., Jayne, J. J., Brown, R. C., Miake-Lye, R. C., Waitz, I., Silva, P., Lanni, T., Demerjian, K., and Kolb, C.: NO and NO_2 emission ratios measured from in-use commercial aircraft during taxi and takeoff, Environ. Sci. Technol, 38, 6078-6084, 2004.

Heywood, J. B.: Internal combustion engine fundamentals, McGraw-Hill, Inc., New York, USA, 1988.

Holloway, A. M., and Wayne, R.: Atmospheric chemistry, RSC publishing, Cambridge, UK, 2010.

Horii, C. V., Munger, J. W., Wofsy, S. C., Zahniser, M., Nelson, D., McManus, J. B.: Fluxes of nitrogen oxides over a temperate deciduous forest, J. Geophys. Res., 109, D08305, doi:10.1029/2003JD004326, 2004.

Huygens, C., and Lanting R. W.: Short communications on the Saltzman factor, Atmos. Environ., 9, 1027-1029, 1975.

IPCC: Climate change 2007: The physical science basis, Cambridge University Press, 2007, http://www.ipcc.ch/publications_and_data/publications_ipcc_fourth_assessment_report_wg1_report_the_physical_science_basis.htm, last access: 29 June 2011.

Ivanov, V. M.: The 125th Anniversary of the Griess reagent, J. Anal. Chem., 59, 1002-1005, 2004.

Jacobs, M. B.: Chemical Analysis, Vol. X, The chemical analysis of air pollutants, Chapter 10, Interscience publishers, Inc., New York, 1960.

Jacobs, M. B., and Hochheiser, S.: Continuous sampling and ultramicrodetermination of nitrogen dioxide in air, Anal. Chem., 30, 426-428, 1958.

Jarvis, D. L., Leaderer, B. D., Chinn, S., and Burney, P. G.: Indoor nitrous acid and respiratory symptoms and lung function in adults, Thorax, 60, 474-479, 2005.

Jenkin, M. E., Utembe, S. R., and Derwent, R. G.: Modelling the impact of elevated primary NO_2 and HONO emissions on regional scale oxidant formation in the UK, Atmos. Environ., 42, 323-336, 2008.

Jimenez, J. L., Mcrae, G. J., Nelson, D. D., Zahniser, M. S., and Kolb, C. E.: Remote sensing of NO and NO2 emissions from heavy-duty diesel trucks using tunable diode lasers, Environ. Sci. Technol., 34, 2380-2387, 2000.

Johnson, B. J., Oltmans, S. J., Vömel, H., Smit, H. G. J., Deshler, T., and Kröger, C.: Electrochemical concentration cell (ECC) ozonesonde pump efficiency measurements and tests on the sensitivity to ozone of buffered and unbuffered ECC sensor cathode solutions, J. Geophys. Res., 107, D19, 4393-4411, 2002.

Jones, A. E., Wolff, E. W., Ames, D., Bauguitte, S. J.-B., Clemitshaw, K. C., Flemming, Z., Mills, G. P., Saiz- Lopez, A., Salmon, R. A., Sturges, W. T., and Worton, D. R.: The multi-seasonal NO_y budget in coastal Antarctica and its link with surface snow and ice core nitrate: results from the CHABLIS campaign, Atmos. Chem. Phys., 11, 9271-9285, 2011.

Kebabian, P. L., Herndon, S. C., and Freedman, A.: Detection of nitrogen dioxide by cavity attenuated phase shift spectroscopy, Anal. Chem., 77, 724-728, 2005.

Kebabian, P. L., Wood, E. C., Herndon, S. C., and Freedman, A.: A practical alternative to chemiluminescence-based detection of nitrogen dioxide: Cavity Attenuated Phase Shift Spectroscopy, Environ. Sci. Technol., 42, 6040-6045, 2008.

Kelly, T. J., Spicer, C. W., and Ward, G. F.: An assessment of the luminol chemiluminescence technique for measurement of NO_2 in ambient air, Atmos. Environ., 24A, 2397-2403, 1990.

Keuken, M., Roemer, M., and van den Elshout, S.: Trend Analysis of Urban NO_2 Concentrations and the Importance of Direct NO_2 Emissions versus Ozone/NO_x Equilibrium, Atmos. Environ., 43, 4780-4783, 2009.

Kleffmann, J., Heland, J., Kurtenbach, R., Lörzer, J. C., Wiesen, P., Ammann M., Gutzwiller, L., Rodenas, M., Garcia, M. Pons, Wirtz, K, Scheer, V., and Vogt, R.: HONO emissions from a diesel engine, Proceedings of the 94th Annual Conference and Exhibition of the Journal of the Air & Waste Management Association, paper 239, 2001.

References

Kleffmann, J., Heland, J., Kurtenbach, R., Lörzer, J. C., and Wiesen, P.: A new instrument (LOPAP) for the detection of nitrous acid (HONO), Environ. Sci. Pollut. Res., 9 (special issue 4), 48-54, 2002.

Kleffmann, J., Benter, T., and Wiesen, P.: Heterogeneous reaction of nitric acid with nitric oxide on glass surfaces under simulated atmospheric conditions, J. Phys. Chem. A, 108, 5793-5799, 2004.

Kleffmann, J., Lörzer, J. C., Wiesen, P., Kern, C., Trick, S., Volkamer, R., Rodenas, M., and Wirtz, K: Intercomparisons of the DOAS and LOPAP techniques for the detection of nitrous acid (HONO) in the atmosphere, Atmos. Environ., 40, 3640-3652, 2006.

Kleffmann J., Gavriloaiei, T., Elshorbany, Y., Ródenas, M., and Wiesen, P.: Detection of nitric acid (HNO_3) in the atmosphere using the LOPAP technique, J. Atmos. Chem., 58, 131-149, 2007.

Kleffmann, J., and Wiesen, P.: Technical note: Quantification of interferences of wet chemical HONO LOPAP measurements under simulated polar conditions, Atmos. Chem. Phys., 8, 6813-6822, 2008.

Kley, D., and McFarland M.: Chemiluminescence detector for NO and NO_2, Atmos. Tech., 12, 63-69, 1980.

Kolb, C.E., Worsnop, D. R., Zahniser, M. S., Davidovits, P., Keyser, L. F., Leu, M. T., Molina, M. J., Hanson, D. R., and Ravishankara, A. R.: Laboratory studies of atmospheric heterogeneous chemistry. In Progress and problems in atmospheric chemistry, (J. R. Barker, Ed.), Chap.18, Advances series in physical chemistry, Vol. 3, World scientific, Singapore, 1995.

Komiyama, H., and Inoue, H.: Absorption of nitrogen oxides into water, Chem. Eng. Sci., 35, 154-161, 1980.

Kurtenbach, R., Becker, K. H., Gomes, J. A. G., Kleffmann, J., Lörzer, J. C., Spittler, M., Wiesen, P., Ackermann, R., Geyer, A., and Platt, U.: Investigation of emissions and heterogeneous formation of HONO in a road traffic tunnel, Atmos. Environ., 35, 3385-3394, 2001.

References

Kurtenbach, R., Becker, K. H., Bruckmann, P., Kleffmann, J., Niedojadlo, A., and Wiesen, P: Das innerstädtische „Stickstoffdioxid (NO$_2$)-Problem", Welchen Einfluss haben direkte Verkehrsemissionen?, Gefahrstoffe Reinhaltung der Luft, 69, 146-149, 2009.

Kurtenbach, R., Kleffmann, J., Niedojadlo, A., and Wiesen, P.: Primary NO$_2$ emissions and their impact on air quality in traffic environments in Europe, Environ. Sci. Eur., 2012, submitted.

Langridge, J. M., Laurila, T., Watt, R. S., Jones, R. L., Kaminski, C. F., and Hult, J.: Cavity enhanced absorption spectroscopy of multiple trace gas species using a supercontinuum radiation source, Opt. Express, 16, 10179-10188, 2008.

Leighton, P. A.: Photochemistry of air pollution, Physical Chemistry, A Series of Monographs, Academic Press, New York, USA, 1961.

Li, Y. Q., Demerjian, K. L., Zahniser, M. S., Nelson, D. D., McManus, J. B., and Herndon, S. C.: Measurement of formaldehyde, nitrogen dioxide, and sulfur dioxide at Whiteface mountain using a dual tunable laser system, J. Geophys. Res., 109, D16S08, 2004.

Lissianski, V. V., Zamansky, V. M., and Gardiner, W. C. Jr.: Combustion chemistry modeling, in Gas-Phase Combustion Chemistry, edited by Gardiner, W. C. Jr., Springer-Verlag New York Inc., 2000.

Lörzer, J. C.: Messung ausgewählter Abgaskomponenten in einem Verkehrstunnel zur Bestimmung von Emisionsfaktoren, Dissertation Bergische Universität-Gesamthochschule, Wuppertal, 2002.

Lyshkow, N. A.: A rapid and sensitive colorimetric reagent for nitrogen dioxide in air, JAPCA, 15, 481-484, 1965.

McAllister, S., Chen, J. Y., and Fernandez-Pello, A. C.: Fundamentals of Combustion Processes, Chapter 9, Springer, USA, 2011.

Margeson, J. H., and Fuerst, R. G.: Evaluation of a continuous colorimetric method for measurement of nitrogen dioxide in ambient air, Report No. 650/4-75-022, Environmental Protection Agency, http://hero.epa.gov/index.cfm?action=search.view&reference_id=34197, US, 1975, last access 19 December 2011.

Margeson, J. H., Fuerst, R. G., Constant, P. C., Sharp, M. C., and Scheil, G. W.: Evaluation and collaborative testing of a continuous colorimetric method for measurement of nitrogen

References

dioxide in ambient air, Calibration in air monitoring, ASTM STP 598, American society for testing materials, 144-155, 1976.

Matsumi, Y., Murakami, S., Kono, M., and Takahashi, K.: High-sensitivity instrument for measuring atmospheric NO_2, Anal. Chem., 73, 5485-5493, 2001.

Matsumoto J., Hirokawa J., Akimoto H., and Kajii Y.: Direct measurement of NO_2 in the marine atmosphere by laser-induced fluorescence technique, Atmos. Environ., 35, 2803-2814, 2001.

Matsumoto, J., Kosugi, N., Nishiyama, A., Isozaki, R., Sadanaga, Y., Kato, S., Bandow, H., and Kajii, Y.: Examination on photostationary state of NO_x in the urban atmosphere in Japan, Atmos. Environ., 40, 3230-3239, 2006.

Mazurenka, M. I., Fawcett, B. L., Elks, J. M. F., Shallcross, D. E., and Orr-Ewing, A. J.: 410-nm diode laser cavity ring-down spectroscopy for trace detection of NO_2, Chem. Phys. Lett., 367, 1-9, 2003.

McAllister, S., Chen, J. Y., and Fernandez-Pello, C.: Fundamentals of combustion processes, Springer, New York, 2011.

McKeachie, J. R., Van der Veer, W. E., Short, L. C., Garnica, R. M., Appel, M. F., and Benter, T.: Selective ultra-trace detection of NO and NO_2 in complex gas mixtures using broad-bandwidth REMPI mass spectrometry, Analyst, 126, 1221-1228, 2001.

McKelvy, M. L.: Infrared spectroscopy: Introduction. In: Encyclopedia of analytical chemistry, John Wiley & Sons Ltd, UK; 2000.

Mentel, Th. F., Bleilebens, D., and Wahner, A.: A study of nighttime nitrogen oxide oxidation in a large reaction chamber - The fate of NO_2, N_2O_5, HNO_3, and O_3 at different humidities, Atmos. Environ., 30, 4007-4020, 1996.

Milani, M. R., and Dasgupta, P. K.: Measurement of nitrogen dioxide and nitrous acid using gas-permeable liquid core waveguides, Anal. Chim. Acta, 431, 169-180, 2001.

Miller, J. A., and Bowman, C. T.: Kinetic modelling of the reduction of nitric oxide in combustion products by isocyanic acid, Int. J. Chem. Kinet., 23, 289-313, 1991.

Mol, W. J. A., Van Hooydonk, P. R., and De Leeuw, F. A. A. M.: European exchange of monitoring information and state of the air quality in 2006. European Topic Centre on Air and

Climate Change (ETC / ACC). European Environment Agency, The Netherlands. Technical paper 2008/1, 2008.

Molina, M. J., Molina, L. T., and Kolb, C. E.: Gas-phase and heterogeneous chemical kinetics of the troposphere and stratosphere, Annu. Rev. Phys. Chem., 47, 327-367, 1996.

Möller, D.: Chemistry of the climate system, Walter de Gruyter GmbH & Co. HG, Berlin, Germany, 2010.

Monks, P. S.: Gas phase radical chemistry in the troposphere, Chem. Soc. Rev., 34, 376-395, 2005.

Murphy, D. M., and Fahey, D. W.: Mathematical treatment of the wall loss of a trace species in denuder and catalytic-converter tubes, Anal. Chem., 59 (23), 2753-2759, 1987.

Nafstad, P., Haheim, L. L., Oftedal, B., Gram, F., Holme, I., Hjermann, I., and Leren, P.: Lung cancer and air pollution: a 27 year follow up of 16,029 Norwegian men, Thorax, 58, 1071-1076, 2003.

Nelson, D. D., Zahniser, M. S., McManus, J. B., Kolb, C. E., and Jimenez, J. L.:A tunable diode lasr system for the remote sensing of on-road vehicle emissions, Appl. Phys. B, 67, 433-441, 1998.

Nyberg, F., Gustavsson, P., Järup, L., Bellander, T., Berglind, N., Jakobsson, R., and Pershagen, G.: Urban air pollution and lung cancer in Stockholm, Epidemiology, 11, 487-495, 2000.

Oftedal, B., Brunekreef, B., Nystad, W., Madsen, C., Walker, S. E., and Nafstad, P.: Residential outdoor air pollution and lung function in schoolchildren, Epidemiology, 19, 129-137, 2008.

Osthoff, H. D., Brown, S. S., Ryerson, T. B., Fortin, T. J., Lerner, B. M., Williams, E. J., Pettersson, A., Baynard, T., Dubé, W. P., Ciciora, S. J., and Ravishankara, A. R.: Measurement of atmospheric NO_2 by pulsed cavity ring-down spectroscopy, J. Geophys. Res., 111, D12305, 2006.

Patty, F. A., and Petty, G. M.: Nitrite field method for the determination of oxides of nitrogen, J. Ind. Hyg. Toxicol., 25, 361-365, 1943.

Peters, A., Liu, E., Verrier, R. L., Schwartz, J., Gold, D. R., Mittleman, M., Baliff, J., Oh, J. A., Allen, G., Monahan, K., and Dockery, D. W.: Air pollution and incidence of cardiac arrhythmia, Epidemiology, 11, 11-17, 2000.

Peters, S.: Entwicklung und Erprobung eines Messgerätes für den selektiven Nachweis von Ozon (O₃) in der Atmosphäre, Diplom arbeit, Bergische Universität Wuppertal, Deutschland,, 2011.

Pitts, J. N. Jr., Grosjean, D., Cauwenberghe, K. V., Schmid, J. P., and Fitz, D. R.: Photooxidation of aliphatic amines under simulated atmospheric conditions: Formation of nitrosamines, amides, and photochemical oxidant, Environ. Sci. Technol., 12, 946-953, 1978.

Plane, J. M. C., and Smith, N.: Atmospheric monitoring by differential optical absorption spectroscopy. In: Advances in spectroscopy, Vol. 24, Edited by Clarck, R. J. H., and Hester, R. E., John Wiley and Sons, England, 1995.

Plane, J. M. C., and Saiz-Lopez, A.: UV-Visible Differential Optical Absorption Spectroscopy (DOAS), In: Analytical Techniques for Atmospheric Measurements, D. E. Heard (editor), Blackwell Publishing, Oxford, 2006.

Platt, U., Perner, D., and Pätz, W.: Simultaneous measurement of atmospheric CH₂O, O₃ and NO₂ by differential optical absorption, J. Geophys. Res., 84, 6329-6335, 1979.

Platt, U.: Differential Optical Absorption Spectroscopy (DOAS) in Air monitoring by spectroscopic techniques, Chemical Analysis, Vol. 127, edited by J. D. Winefordner, John Wiley & Sons, Inc., USA, 1994.

Platt, U., and Stutz, J.: Differential Optical Absorption Spectroscopy: principles and applications, Springer Verlag, Berlin-Heidelberg, Germany, 2008,

Pryor, W. A., and Lightsey, J. W.: Mechanisms of nitrogen dioxide reactions: Initiation of lipid peroxidation and the production of nitrous acid, Science, 214, 435-437, 1981.

Purdue, L. J., Dudley, J. E., Clemens, J. B., and Thompson, R. J.: Reinvestigation of the Jacobs-Hochheiser procedure for determining nitrogen dioxide in ambient air, Environ. Sci. Technol., 6, 152-154, 1972.

Ramazan, K. A., Syomin, D., and Finlayson-Pitts, B. J.: The photochemical production of HONO during the heterogeneous hydrolysis of NO₂, Phys. Chem. Chem. Phys., 6, 3836-3843, 2004.

Raheem, A. M. O. A., Adekola, F. A., and Obioh, I. O.: The seasonal variation of the concentrations of ozone, sulphur dioxide, and nitrogen oxides in two Nigerian cities, Environ. Model. Assess., 14, 497-509, 2009.

References

Ren, X., Harder, H., Martinez, M., Lesher, R. L., Oliger, A, Simpas, J. B, Brune, W. H., Schwab, J. J, Demerjian, K. L., He, Y., Zhou, X., and Gao, H.: OH and HO_2 Chemistry in the Urban Atmosphere of New York City, Atmos. Environ., **37**, 3639-3651, 2003.

Ridley, B. A., and Howlett, L. C.: An instrument for nitric oxide measurements in the stratosphere, Rev. Sci. Instrum., 45, 742-746, 1974.

Roberts, J. M., and Bertman, S. B.: The thermal decomposition of peroxyacetic nitric anhydride (PAN) and peroxymethacrylic nitric anhydride (MPAN), Int. J. Chem. Kinet., 24, 297-307, 1992.

Roberts, J. M.: PAN and related compounds, in: Volatile organic compounds in the atmosphere, edited by: Koppmann, R., Blackwell publishing Ltd., 221-268, 2007.

Rohrer, F., Bohn, B., Brauers, T., Brüning, D., Johnen, F.-J., Wahner, A., and Kleffmann, J.: Characterisation of the photolytic HONO-source in the atmosphere simulation chamber SAPHIR, Atmos. Chem. Phys., 5, 2189-2201, 2005.

Saltzman, B. E.: Colorimetric microdetermination of nitrogen dioxide in the atmosphere, Anal. Chem., 26, 1949-1955, 1954.

Saltzman, B. E.: Modified nitrogen dioxide reagent for recording air analyzers, Anal. Chem., 32, 135-136, 1960.

Saltzman, B. E., and Mendenhall, A. L.: Desing parameters and performance of a miniaturized colorimetric recording air analyzers, Anal. Chem., 36, 1300-1304, 1964.

Samoli, E., Aga, E., Touloumi, G., Nisiotis, K., Forsberg, B., Lefranc, A., Pekkanen, J., Wojtyniak, B., Schindler, C., Niciu, E., Brunstein, R., Dodic Fikfak, M., Schwartz, J., and Katsouyanni, K.: Short-term effects of nitrogen dioxide on mortality: an analysis within the APHEA project, Eur. Respir. J., 27, 1129-1137, 2006.

Schiff, H. I., Hastie, D. R., Mackay, G. I., Iguchi, T., and Ridley, B. A.: Tunable diode laser systems for measuring trace gases in tropospheric air, Environ. Sci. Technol., 17, 352A-364A, 1983.

Schiff, H. I., Karecki, D. R., Harris, G. W., Hastie, D. R., and Mackay, G. I.: A tunable diode laser system for aircraft measurements of trace gases, J. Geophys. Res., 95, 10147-10153, 1990.

References

Schiff, H. I.: Ground based measurements of atmospheric gases by spectroscopic methods, Ber. Bunsenges. Phys. Chem., 96, 296-306, 1992.

Schiff, H. I., Mackay, G. I., and Bechara, J., The use of tunable diode laser absorption spectroscopy for atmospheric measurements, in: Air monitoring by spectroscopic techniques, John Wiley & Sons, Inc., New York, Vol. 127, 1994.

Schnelle, K. B., and Brown, C. A.: Air pollution control technology handbook, CRC Press, USA, 2002.

Seinfeld, J. H., and Pandis, S. N.: Atmospheric chemistry and physics: From air pollution to climate change, 2nd edition, John Wiley & Sons, Inc., New Jersey, 2006.

Shinn, M. B.: Colorimetric method for determination of nitrite, Ind. Eng. Chem., 8, 33-35, 1941.

Spicer, C. W., Billick, I. H., and Yangagisawa, Y.: Nitrous acid interference with passive NO_2 measurement methods and the impact on indoor NO_2 data, Indoor Air, 11, 156-161, 2001.

Spittler, M.: Untersuchungen zur troposphärischen oxidation von Limonen: Produktanalysen, Aerosolbildung und Photolyse von Produkten, PhD Thesis, University of Wuppertal, Germany, 2001.

Squadrito, G. L., and Postlethwait, E. M.: On the hydrophobicity of nitrogen dioxide: Could there be a "lens" effect for NO_2 reaction kinetics?, Nitric Oxide, 21, 104-109, 2009.

Steinbacher, M., Zellweger, C., Schwarzenbach, B., Bugmann, S., Buchmann, B., Ordóñez, C. Prevot, A. S. H., and Hueglin, C.: Nitrogen oxide measurements at rural sites in Switzerland: Bias of conventional measurement techniques, J. Geophys. Res., 112, D11307, doi: 10.1029/2006JD007971, 2007.

Stemmler, K., Ammann, M., Donders, C., Kleffmann, J., and George, C.: Photosensitized reduction of nitrogen dioxide on humic acid as a source of nitrous acid, Nature, 440, 195-198, 2006.

Stemmler, K., Ndour, M., Elshorbany, Y., Kleffmann, J., D´Anna, B., George, C., Bohn, B., and Ammann, M.: Light induced conversion of nitrogen dioxide into nitrous acid on submicron humic acid aerosol, Atmos. Chem. Phys., 7, 4237-4248, 2007.

Stutz, J., and Platt, U.: Improving long-path differential optical absorption spectroscopy with a quartz-fiber mode mixer, Appl. Optics, 36, 1105-1115, 1997.

Sutton, J. A., and Fleming, J. W.: Towards accurate kinetic modeling of prompt NO formation in hydrocarbon flames via the NCN pathway, Combust. Flame, 154, 630-636, 2008.

Tappe, M., Friedrich, A., Höpfner, U., and Knörr, W.: Berechnung der direkten Emissionen des Straßenverkehrs in Deutschland im Zeitraum 1995 bis 2010, Umweltforschungsplan des Bundesministeriums für Umwelt, Naturschutz und Reaktorsicherheit − Luftreinhaltung, Forschungsbericht 2008, 05 06 095 UBA-FB 96-087, Texte 73 / 96 (http://www.umweltbundesamt.de).

Thomas, M. D., MacLeod, J. A., Robbins, R. C., Goettelman, R. C., Eldridge, R. W., and Rogers, L. H., Automatic apparatus for determination of nitric oxide and nitrogen dioxide in the atmosphere, Anal. Chem., 28, 1810-1816, 1956.

Thornton, J. A., Wooldridge, P. J., and Cohen, R. C.: Atmospheric NO_2: In situ Laser-Induced Fluorescence detection at parts per trillion mixing ratios, Anal. Chem., 72, 528-539, 2000.

Thornton, J. A., Wooldridge, P. J., Cohen, R. C., Williams, E. J., Hereid, D., Fehsenfeld, F. C., Stutz, J., and Alicke, B.: Comparison of in situ and long path measurements of NO_2 in urban plumes, J. Geophys. Res., 108, D4496, 2003.

Treadwell, F. P., and Hall, W. T.: Analytical Chemistry, Vol. II, John Wiley & Sons, Inc., London, 1955.

Van Strien, R. T., Gent, J. F., Belanger, K., Triche, E., Bracken, M. B., and Leaderer, B. P.: Exposure to NO_2 and nitrous acid and respiratory symptoms in the first year of life, Epidemiology, 15(4), 471-478, 2004.

Vasudev, R., Usachev, A., and Dunsford, W. R.: Detection of toxic compounds by cavity ring-down spectroscopy, Environ. Sci. Technol., 33, 1936-1939, 1999.

Vestreng, V., Ntziachristos L., Semb, A., Reis, S., Isaksen I. S. A., and Tarrasón L.: Evolution of NO_x emissions in Europe with focus on road transport control measures, Atmos. Chem. Phys., 9, 1503-1520, 2009.

Villena, G., I. Bejan, R. Kurtenbach, P. Wiesen and J. Kleffmann: Interferences of commercial NO_2 instruments in the urban atmosphere and in a smog-chamber, Atmos. Meas. Tech., 5, 149-159, 2012.

References

Villena, G., Kleffmann, J., Kurtenbach, R., Wiesen, P., Lissi, E., Rubio, M. A., Croxatto, G., and Rappenglück, B.: Vertical gradients of HONO, NO_x and O_3 in Santiago de Chile, Atmos. Environ., 45, 3867-3873, 2011.

Wallace, J. M., Hobbs, P. V.: Atmospheric science: An introductory survey, Elsevier Inc., Canada, 2006.

Wang, T., Wei, X. L., Ding, A. J., Poon, C. N., Lam, K. S., Li, Y. S., Chan, L. Y., and Anson, M.: Increasing surface ozone concentrations in the background atmosphere of southern China, 1994-2007, Atmos. Chem. Phys., 9, 6217-6227, 2009.

Warnatz, J., Maas, U., and Dibble, R. W.: Combustion: Physical and Chemical Fundamentals, Modelling and Simulation, Experiments, pollutant formation., 4th edition, Springer, Germany, 2006

Warneck, P.: Chemistry of the natural atmosphere, Second edition, Vol. 71, International geophysics series, Academic press, USA, 2000.

Wendel, G. J., Stedman, D. H., and Cantrell, C. A.: Luminol-based nitrogen dioxide detector, Anal. Chem., 55, 937-940, 1983.

Winer, A. M., Peters, J. W., Smith, J. P., and Pitts, J. N. Jr.: Response of commercial chemiluminescence NO-NO_x analyzers to other nitrogen-containing compounds, Environ. Sci. Technol., 8, 1118-1121, 1974.

Williams, M. L., and Carslaw, D. C.: New directions: Science and policy - Out of step on NO_x and NO_2?, Atmos. Environ., 45, 3911-3912, 2011.

Wu, T., Zhao, W., Chen, W., Zhang, W., and Gao, X.: Incoherent broadband enhanced absorption spectroscopy for in situ measurements of NO_2 with a blue light emitting diode, Appl. Phys. B, 94, 85-94, 2009.

Wurzenberger, J. C. and Tatschl, R.: Exhaust aftertreatment in combustion engines development, Springer Verlag, Germany, Berlin Heidelberg, 2012.

Yabushita, A., Enami, S., Sakamoto, Y., Kawasaki, M., Hoffmann, M. R., and Colussi, A. J.: Anion-catalyzed dissolution of NO_2 on aqueous microdroplets, J. Phys. Chem. A, 113, 4844-4848, 2009.

References

Yao, W., Byrne, R. H., and Waterbury, R. D.: Determination of nanomolar concentrations of nitrite and nitrate in natural waters using long path length absorbance spectroscopy, Environ. Sci. Technol., 32, 2646-2649, 1998.

Zhang, L., Jacob, D. J., Boersma, K. F., Jaffe, D. A., Olson, J. R., Bowman, K. W., Worden, J. R., Thompson, A. M., Avery, M. A., Cohen, R. C., Dibb, J. E., Flock, F. M., Fuelberg, H. E., Guey, L. G., McMillan, W. W., Singh, H. B, and Weinheimer, A. J.:Transpecific transport of ozone pollution and the effect of recent Asian emission increases on air quality in North America:an integrated analysis using satellite, aircraft, ozonesonde, and surface observations, Atmos. Chem. Phys., 8, 6117-6136, 2008.